Maneuver Load Controls, Analysis and Design for Flexible Aircraft

A thesis submitted to
The PhD school of Aerospace, Naval and Quality Engineering
of
Università degli Studi di Napoli

Federico II

by

Nicola Paletta

In partial fulfillment of the requirements
for
the degree of Doctor of Philosophy
in
Aerospace Engineering

School Coordinator: Chiar.mo Prof. Antonio Moccia

Tutor: Chiar.mo Prof. Leonardo Lecce

Supervisor: Ing. Modesto Pecora

Alla mia famiglia

TABLE OF CONTENTS

List of Figures

List of Tables

List of Acronyms

AF	Alleviation Factor
AoA	Angle of Attack
CAS	Calibrated Air Speed
DLM	Doublet Lattice Method
EAS	Equivalent Air Speed
FBW	Fly-By-Wire
FEM	Finite Element Method
FCS	Feed-back Control System
FW	Front Wing
GAG	Ground-Air-Ground
GM	Gain Margin
HALE	High Altitude and Long Endurance
HAPD	High Altitude Performance Demonstrator
HM	Hinge Moment
IM	Interface Mesh
JWB1	Joined-Wing Baseline 1
KCAS	Calibrated Air Speed in knots
KEAS	Equivalent Air Speed in knots
KTAS	True Air Speed in knots
LAS	Load Alleviation System
LCRS	Load Coordinate Reference Systems
LFF	Load Factor Feedback
LRA	Load Reference Axis
LVR	Laboratorio Volante di Ricerca
MCRS	Main Coordinate Reference Systems
MIMO	Multi Input – Multi Output
MLC	Maneuver Load Control
MTOW	Max Take-Off Weight
OEW	Operative Empty Weight
PID	Proportional Integral Derivative
PM	Phase Margin
RW	Rear Wing
SISO	Single Input – Single Output
TAS	True Air Speed
WCS	Wing Control Station

List of Symbols

α	=	Angle of Attack
δ	=	Elevator Deflection
β	=	Load Alleviation Control Surface Deflection
ρ	=	Air Density
V	=	Aircraft Velocity
q	=	Dynamic Pressure
S_w	=	Reference Wing Surface
c_r	=	Aeroelastic Reference Chord
C_Z	=	Aerodynamic Force Coefficient along z direction
C_m	=	Aerodynamic Pitching Moment Coefficient
G	=	Control Function
n_z	=	Vertical Load Factor
$\ddot{\theta}$	=	Pitch Acceleration
ϕ_i^x	=	Generic modal amplitude due to mode i along x-direction
ϕ_i^y	=	Generic modal amplitude due to mode i along y-direction
ϕ_i^z	=	Generic modal amplitude due to mode i along z-direction
q_i	=	Generalized degree of freedom associated with mode i
$\underline{q}$	=	Vector of Generalized degrees of freedom
$\underline{u}_a$	=	Vector of Local displacements evaluated on the aerodynamic boxes
$\underline{u}_{st}$	=	Vector of Local displacements evaluated on Interchange Data Grids (IDGs)
$\underline{\underline{\Theta}}_{a,st}$	=	Interpolation Matrix
$\underline{F}_a$	=	Forces evaluated on the aerodynamic boxes
$\underline{F}_{st}$	=	Forces evaluated on IDGs
$\underline{\underline{\tilde{P}}}$	=	Quasi-steady aerodynamic pressure

$\underline{\underline{Q}}$	=	Generalized Aerodynamic Forces
m	=	Generalized Masses
S	=	Shear
M	=	Bending Moment
T	=	Torsion
V_S	=	Stalling Speed
V_A	=	Design Maneuvering Speed
V_C	=	Design Cruising Speed
V_D	=	Design Dive Speed
$C_{n'}$	=	Local (strip) Lift Coefficient
$C_{m'}$	=	Local (strip) Moment Coefficient
T_d	=	Rise Time
$S(s)$	=	Sensitivity Function
$G_C(s)$	=	Controller Transfer Function
$G_P(s)$	=	Plant Transfer Function
$C(s)$	=	Closed-Loop System Transfer Function
H_p	=	Pressure Altitude
f_c	=	Cumulative Frequency
$(f_c)_p$	=	Cumulative Frequency (Maximum Peak per Flight cumulative frequency curve)
M_p	=	Wing root bending (Maximum Peak per Flight cumulative frequency curve)
D	=	Damage.

1. Introduction

Several aircraft manufacturers have for many years conducted research in the area of active controls, that are becoming increasingly important in the design of modern aircraft. Nowadays active control systems drive the constructing architecture and the configuration of the whole aircraft by affecting operative mission feasibility and flight performances. Thus the adoption of active control systems plays an essential role since the early stages of design.

The choice to equip an airplane with active controls modifies the design philosophy approach also from a certification viewpoint. The vehicle must be able to take on board a set of equipments such as

- Sensors aimed at measuring what has to be observed or controlled;
- On-board computers;
- Fly-By-Wire (FBW) controls;
- Electro-mechanic and/or electro-hydraulic actuators;
- Classic or advanced aerodynamic controls (control surfaces, control jets, etc.).

All these kinds of equipments together with their on-board integration systems are nowadays subjects of research and development in order to optimize the automatic control efficiency and at the same time their reliability. Active controls must have a level of safety equivalent to that of conventional design.

In this context an automatic system aimed at reducing structural loads can be conceived. This kind of system is generally called Load Alleviation System (LAS) and involves systems for gust and/or maneuver load control.

Over the last few decades, several kinds of load alleviation systems have been studied and installed on aircraft. These load alleviation systems are mainly aimed at gust-alleviation for improved ride comfort, e.g. Boeing 747, Lockheed L-1011 Tristar. The alleviation is accomplished by means of an active wing bending damping, which alleviates structural fatigue loads on the one hand, and lowers pitch attitude variation and vertical accelerations in the cabin on the other [1]-[3]. A recent survey by Hecker and Hahn [4] showed that a Gust Load Alleviation System (GLAS) directed towards the reduction of vertical accelerations due

to turbulence can yield to an undesired overcompensation of structural loads, which can be avoided only by appealing on an optimized tuning of the GLAS: the simulation results from the authors showed good performance also for structural load alleviation although this was not the purpose of that system.

The present work is focused on a different objective that can be achieved with a Load Alleviation system: to obtain a reduction in internal wing loads for enhanced performance (such as an aerodynamic efficiency increase due to a wing Aspect-Ratio augmentation or higher maneuver limit load factors for high performance aircraft), structural fatigue life extension, or Operative Empty Weight (OEW) reduction. The main difference with the above cited gust load alleviation systems is that the performance improvement is accomplished if the maximum vertical load factor attained during the non-alleviated maneuver is kept constant whether the LAS is switched on.

Aircraft Wing Structure is generally maneuver-load or gust-load critical depending on whether the airplane is a high-performance (such as a fighter or a military unmanned air vehicle) or a commercial transport. In the case of a high performance aircraft the improving of ride comfort is not a concern, whereas a method aimed at reducing directly internal structural loads due to maneuvers can be of great significance. In other words, since the wing weight is essentially function of the bending moment acting near the wing root, an effective load alleviation system must be able to reduce the bending by means of a redistribution of the aerodynamic load during a maneuver by acting on aerodynamic controls in an automatic manner. The whole process becomes relevant for high performance aircraft if the alleviated maneuver is performed at the same vertical load factor as that attained in case of LAS switched off.

Structural weight reduction (part of the Operative Empty Weight, OEW) obtained with Load Alleviation systems that keep the vertical load factor unvaried allows more payload and/or fuel to be carried since the Max Take-Off Weight (MTOW) does not vary. In opposite, by keeping the MTOW and the OEW constant, the LAS allows obtaining higher maneuver load factors with the same values of maximum wing bending, thus leading to better maneuver performance.

Nevertheless the weight reduction is not the unique benefit to be gained from the adoption of a LAS. This system can allow increasing the wing span length and, at the same time,

keeping the same structural weight. The resulting higher wing aspect ratio (and thus less induced drag) leads to a reduction in fuel consumption and thus in the opportunity to carry greater pay-loads. An other benefit can be the possibility to embark more fuel for increased wing internal volume. In both cases, less fuel consumption and major wing volume capability result in an autonomy increase, a relevant advantage especially for some commercial transports. An active control system for Load Alleviation has been developed by Lockheed-California Company for a long range version of the L-1011 Tristar. This system permits the use of an extended wing span with minimum structural changes. It is presented and the criteria to which it is designed are described in [5]-[7]. In particular the Maneuver Load Control (MLC) has the dominant requirement to minimize the overall structural penalty associated with the extended span. The MLC system accomplishes this by deflecting the outboard ailerons symmetrically, in response to accelerometer signals, to redistribute the wing loads during maneuvers. This effect of moving the center of pressure inboard for a longitudinal maneuver is illustrated in Fig. 1.

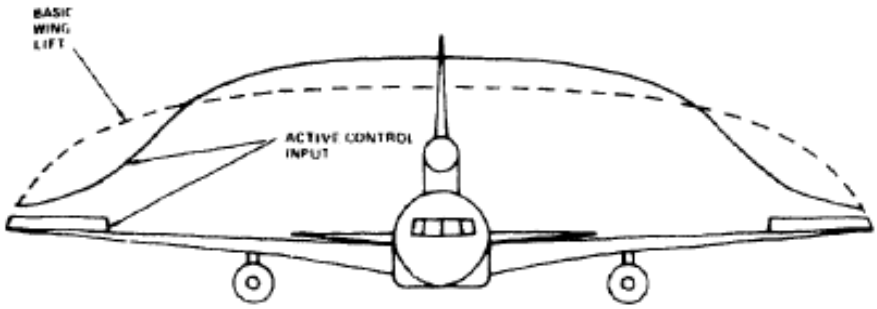

Fig. 1: Load Redistribution with Maneuver Load Control.

Fig. 2 shows the in flight measurements in terms of bending moment, shear, and torsion versus load factor for an outer wing station obtained during pull-up and push over maneuver tests with the MLC on and off. A linear regression line is shown for both sets of data.

The predicted 1.6 g incremental load from system-off to system-on is shown with the measured results and indicates the system to be somewhat more effective than predicted. The measured aileron angles versus load factor data indicate that the aileron gain was within 3 percent of the nominal gain of 8.67 degrees per g. The data generated during the NASA ACEE program substantiated the analytical methods used to develop the MLC system.

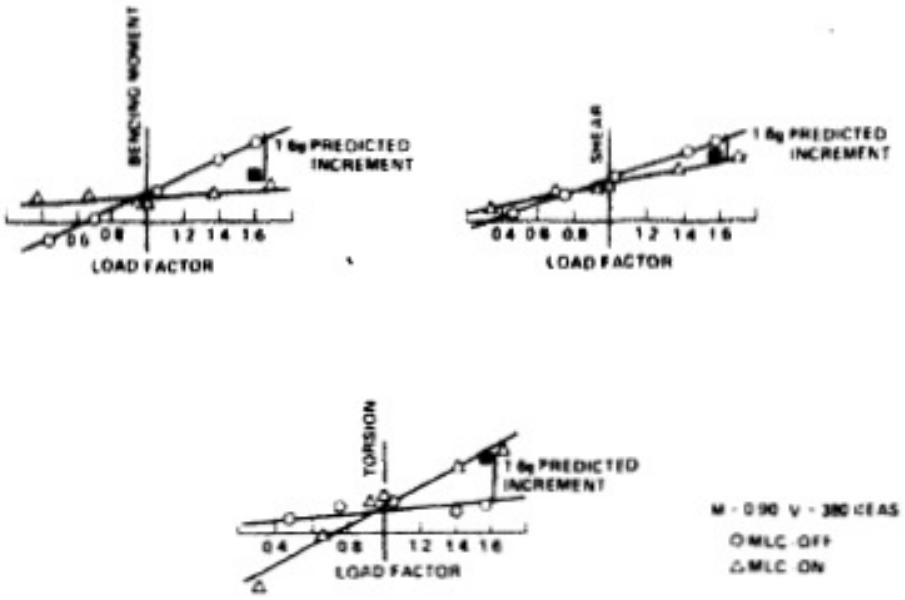

Fig. 2: Bending Moment, Shear, and Torsion vs Load Factor (Typical Outer Wing Station).

Fig. 3 illustrates the typical variation for critical design conditions of outer wing stress with load factor for a MLC system that uses outboard aileron versus the variation for an airplane designed without the MLC system. The slope of the curve of load or stress versus load factor for an airplane without a MLC is greater than for an airplane with MLC. Actually, all MLC systems will saturate (reach the maximum aileron authority limit) below the ultimate load or load factor. The effect of this saturation is also illustrated.

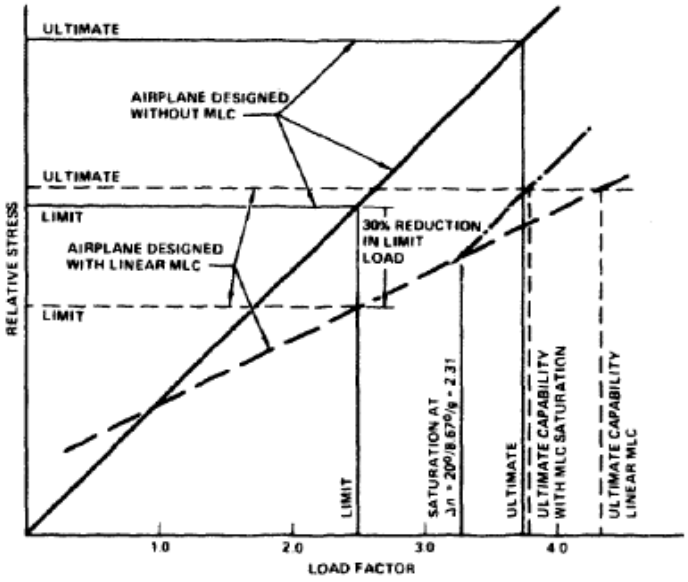

Fig. 3: Typical Effect of MLC on Ultimate Maneuver Load Capability.

The weight reduction associated with the adoption of a MLC system together with the wing span augmentation leads to a decrease of the wing stiffness in terms of flexural and torsional frequency diminution. This phenomenon causes smaller flutter and divergence speeds. Thus, if the project is critical from an aeroelastic viewpoint, the adoption of a flutter suppression system becomes necessary, although it limits at the same time the potentiality of a MLC system.

The major limit of this kind of systems is related to the certification requirements when they have to be installed on commercial transport aircraft. The MLC in-flight availability must be sufficient to assure the same safety as a conventional airplane, thus it is necessary to perform extensive RAMS analyses and to strongly increase the redundancy level of each sub-system related to the MLC one. This process generally leads to a considerable augmentation of design costs and then of direct and indirect operating costs, often making its adoption inconvenient.

For high-performance aircraft, such as fighters or military unmanned air vehicles, the certification requirements are much less restrictive, thus the adoption of an MLC system become significant and worthy of being studied and eventually adopted.

Other several surveys highlighted the advantages achievable with active control systems [8],[9] on fighter and/or transport applications: Reference [8], developed under NASA SST Program, reported a structural weight saving of about 1000-2000 lb (referring to NASA SCAT-15F concept) derived from a 5-9% reduction of wing root bending moment. Kurzhals [9] pointed out that active control systems are a useful means to reduce structural weight as well as to decrease direct operational costs related to fuel consumption (15% reduction in wing weight meant 2-3% reduction in direct operational costs) and to enhance fatigue life.

A fully active maneuver and gust load reduction system has been developed and flight tested and finally has been incorporated on the Lockheed C-5A at present. This system was developed for the specific purpose of providing a significant wing fatigue life improvement through reduction of maneuver and gust-induced incremental wing bending moments.

The Active Lift Distribution Control System (ALDCS) provides symmetric aileron and inboard elevator deflections as a function of vertical acceleration, pitch rate, control column position, and airspeed/Mach number. Surface command signals are generated by the ALDCS computer and are fed through the existing primary servoactuator system.

Fig. 4 and Fig. 5, extracted from [10], show the ALCDS System Components and the simplified block diagram of the system.

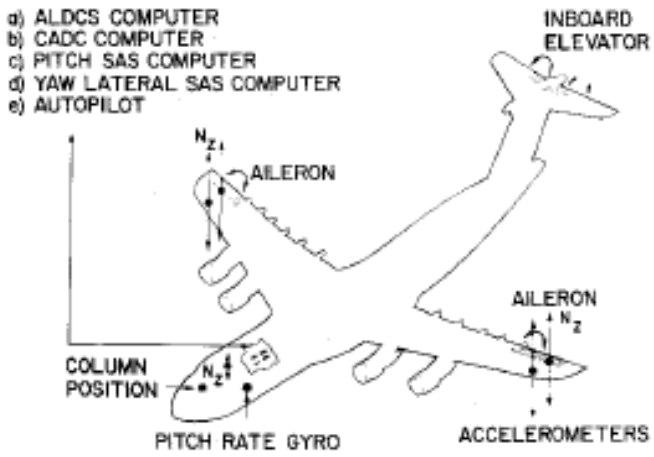

Fig. 4: ALCDS System Components.

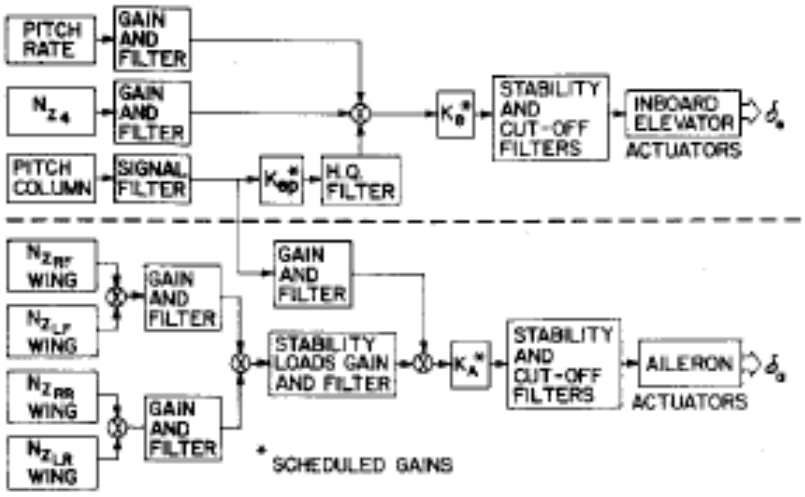

Fig. 5: ALCDS Simplified Block Diagram.

Numerical and flight test results showed that maneuver and gust incremental wing stresses were reduced to approximately 20-30% with a 1.25 life improvement factor.

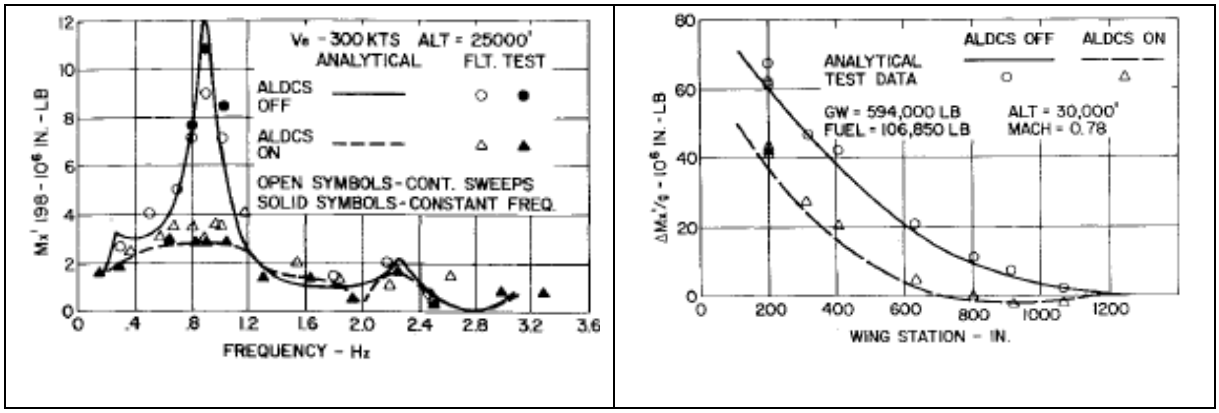

Fig. 6: Wing Bending response and Spanwise Bending Moment.

The forward displacement of the center of pressure associated with the use of a LAS in the case of positive swept wing, causes the deterioration of the longitudinal stability of aircraft. Thus the integration of the LASs with other navigation and control systems has to be foresee from the early stages of design in order to prevent flight mechanics and aeroelastic performance deterioration.

Recent research work by Caplin, Ray and Joshi [11] was aimed at setting up a design methodology for a robust damage-mitigating control that could achieve structural durability without loss of aircraft performance. Besides the aeroservoelastic model, the damage-mitigating control by Caplin, Ray and Joshi included a fatigue crack damage model. The authors pointed to the fact that it would be advisable to consider such a model during the early stage of design in order to allow the structural engineers and the control system engineers to simultaneously converge to their individual goals.

Work conducted by NASA [12] from May 1977 through June 1979 reports a net airplane Operative Empty Weight reduction equivalent to 2.5% of the wing structural box weight due to a maneuver bending moment alleviation performed by symmetrically deflecting the outboard ailerons.

Moreover, in the first 90's, NASA conducted a series of experiments on an F-111A modified with a mission adaptive wing having a supercritical airfoil with continuously variable smooth camber [13].

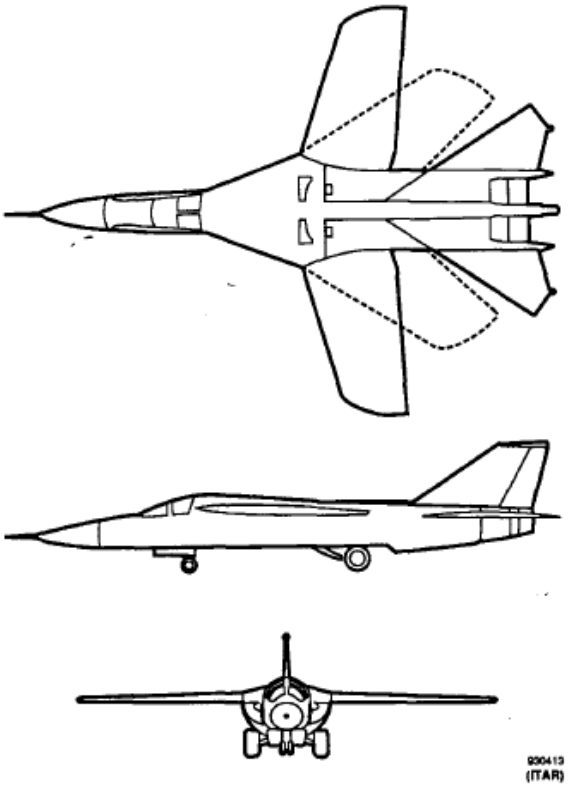

Fig. 7: Three viewes of the General Dynamics F-111A.

The transonic fighter-bomber aircraft was fitted with a MLC system that implements a technique to reduce the inboard bending moments in the wing by shifting the spanwise load distribution inboard as load factor increases. The system modifies the spanwise camber distribution by automatic commanding flap position as a function of flap positions, true air speed, Mach number, dynamic pressure, normal acceleration and wing sweep position. Flight test data were registered at various Mach numbers, dynamic pressures and Reynolds numbers. The main result was an increase of more than 1.0 g in load factor with no increase in root wing bending moment.

That being stated, the driving idea of this survey is to perform a Load Alleviation by means of a symmetrical actuation of the ailerons or other dedicated control surfaces located close to the wing tip in order to rearrange the aerodynamic loads. As discussed so far, this way to proceed is not new, but the purpose of this work is to offer a practical approach to quantify the Load Alleviation during longitudinal maneuvers by taking into account the aircraft flexibility and to drive the design and the analysis of the active control architecture, control laws, actuators and sensors to be adopted.

Furthermore the estimation of the main benefit associated with the load control system on a civil aircraft is performed: the fatigue life improvement resulting from such a system is the most important aspect to be studied for strategic and economic reasons.

The entire work is made of four parts:

1. The first one deals with symmetric balanced maneuvers, providing a method to evaluate the load alleviation effectiveness in an effortless and linear manner.

2. The second part is focused on the estimation of the control surface effectiveness when it is used as load alleviator. Results showed in this section are obtained by means of open-loop calculations only.

3. The third part of the work is a conceptual design of a MLC system for longitudinal maneuver. The system, when switched on, is able to minimize the bending moment augmentation in a wing station near the wing root during an unsteady maneuver. The maneuver is performed by following a desired vertical load factor law by deflecting elevators, starting from the trim equilibrium in level flight. The system observes load factor and structural bending through accelerometers and calibrated strain sensors and sends signals to a computer that symmetrically actuates ailerons for reducing the structural bending and elevators for compensating the perturbation to the longitudinal equilibrium.

4. The fourth part is focused on the estimation of the fatigue life extension of a structural joint (wing lower skin-stringer) located close to the wing root. Analyses are carried-out for a business jet responding to the Part 25 of the EASA Certification Specification for two kinds of mission: short and long range.

All numerical analyses are performed always by taking into account the flexibility of the case-study aircraft.

2. Load Alleviation in symmetric balanced maneuvers. Application to a Joined Wing Unmanned Aircraft

The present section of the thesis has been published by Journal of Aircraft, Vol. 47, No. 6, November-December 2010 [14].

A method of alleviating wing structural load of a flexible aircraft during a symmetric balanced maneuver is presented. An application on the Unmanned Aircraft in development at CIRA, HAPD (High-Altitude-Performance-Demonstrator), characterized by a Joined-Wing configuration is illustrated.

This Load Alleviation technique enables a desired value of the bending moment on a fixed wing control station to be obtained. The load reduction is achieved by means of a symmetrical actuation of the ailerons or other dedicated control surfaces located close to the wing tip in order to rearrange the aerodynamic loads, but always by keeping the vertical load factor constant in order to preserve the maneuvering performance.

The main hypotheses are: significant aeroelastic effects, linear behavior of aerodynamics and structure and unvarying tensor of inertia under structural deflections. The purpose of the work is to offer a practical approach to quantify the Load Alleviation during longitudinal balanced maneuvers taking into account aeroelastic effects, in a relatively effortless and linear manner even if it is applied to an aircraft in an unconventional Joined-Wing configuration

HAPD is a scaled performance demonstrator of a 80m-wing span High-Altitude & Long Endurance Unmanned Aircraft in a Joined-Wing configuration. The advantages in terms of performance, fatigue life extension and weight reduction can be achieved from the integration of an on board load alleviation system.

The results show that the attainable value of load alleviation in terms of bending moment reduction at the wing root is 37%. Moreover the test-case analyses show that the maximum value of the alleviation increases with respect to the dynamic pressure although the load distribution varies because of significant aeroelastic effects.

2.1.Introduction to Joined-Wing Configurations

Many research efforts have been focused on HALE UAV over the past few decades, encompassing different aircraft configurations [20]-[22], different concepts (Aircrafts and/or Airships [22][23]) and/or power systems [23]. The advantages and areas of application of such platforms were widely discussed [24]: they can act as artificial satellites, thus allowing the same potentiality of use, but at a smaller cost due to their self-launch capability and reusability.

Because of weight restrictions, High altitude and Long Endurance Aircraft are typically characterized by a high aspect ratio flying wing configuration. The high flexibility of this configuration makes the linear theories not relevant for the aeroelastic analysis.

Patil, Hodges and Cesnik [25] presented the results of a low-order, high-fidelity nonlinear aeroelastic analysis on a high aspect ratio flying wing configuration, which showed how the large deflections experienced lead to significant changes in the aeroelastic behavior of the wing, in particular, changes in the natural frequencies as a function of the tip displacement, ergo changes on the flutter speed.

Patil and Hodges [26] developed a complete nonlinear theoretical methodology for the flight dynamic analysis of a highly flexible flying wing configuration, demonstrating that both the flight dynamic modes and the flexible modes change significantly with respect to those predicted with a linear analysis. The same methodology was used by Raghavan and Patil [27] to study additional trim cases and lateral flight dynamics. The nonlinear gust response was also investigated by Patil [28], both in the time domain and in the frequency domain.

Shearer and Cesnik [29] proposed a modified version of a strain-based approach developed earlier by Cesnik et al., to model the high-aspect-ratio lifting surfaces, and concluded that linearized approaches can be used to study simple symmetric maneuvers whereas nonlinear structural modeling is essential when studying asymmetric maneuvers.

Notwithstanding this, Patil applied the nonlinear aeroelastic methodology developed in the previous works to a joined wing configuration too [30], coming to the conclusion that nonlinear analysis results were close to the linear analysis results, due to the fact that such a configuration is much stiffer than a similar single wing: the structural nonlinearities for the joined wing configuration were quite negligible.

Concerning the many advantages of Joined Wing configuration if compared to conventional configurations, Wolkovitch [31] highlighted lighter structural weight, less induced drag and a synergistic predisposition to new technologies (for example the use of composite materials and laminar flow airfoils). In addition Wolkovitch himself and other authors [32][32],[33] outlined how even in the preliminary design phase an integrated methodology involving weight estimation techniques, structural analyses and aeroservoelastic design is mandatory if a reliable design is pursued. A brief consideration of the non-negligible importance of the junctions stiffness on the aeroelastic behavior or about the impact of the redundant configuration on the Load Evaluation process [33] are ideal examples of this.

The same remarks were made by Frediani et al.[34],[35], who were engaged in an Italian national project (during the period 2000-2002), and who focused on the analysis of the PrandtlPlane configuration, a very efficient joined wing configuration derived from Prandtl intuition. Multidisciplinary preliminary design studies conducted by Frediani and his colleagues took into account aerodynamic efficiency, maneuverability, structure sizing and aeroelastic phenomena, such as flutter. The aeroelastic aspect was taken into account in a multilevel structural optimization process aimed at the preliminary wing box weight estimation [36],[37].

As explained previously, the Joined-Wing configuration is a valid alternative to a flying wing configuration for solar powered High altitude and Long Endurance vehicles, not only for its higher structural stiffness and its larger solar array area but also for the possibility to rely solely on linear analysis [30], thus resulting in a cheaper design process.

Demasi and Livne performed aeroelastic analysis on a Joined-Wing configuration by means of a non linear Updated Lagrangian Formulation for the structural part [38],[39], and their results demonstrated a significant influence of structural nonlinearities on divergence and flutter.

Nevertheless in this work the extent of the structural deformations experienced during balanced maneuver analyses, ergo the extent of geometric structural nonlinearities result in a negligible influence on the quasi-steady aerodynamic pressure calculations.

For all the above considerations, it is believed that for such an unconventional airplane a practical approach which is capable of quantifying the Load alleviation, to identify

performance targets of endurance, operational costs and payload embarking capability could be a valuable tool especially during the early stages of design.

2.2.Methodology

Within the hypothesis of linear aerodynamics, aircraft lift and pitch moment can be broken down into their unit aerodynamic contributions due to “Zero Effect”, angle of attack, and unit deflections of all the control surfaces involved during the maneuver. The so called “Zero Effect” represents the aerodynamics acting on the airplane at zero angle of attack without any control surface deflection: it is due to airfoil camber, viscosity and other non negligible sources of non-linearity (i.e. strong compressibility effects such as shock waves, etc.).

Among all the internal load characteristics acting on the wing, the principal Bending Moment M has been chosen as the load characteristic to be reduced because it commonly drives the design of the main wing structure. The principal bending moment is the so-called “out-of-plane bending”, to be precise that acting along the streamwise direction (on a Joined-Wing aircraft the in-plane bending assumes comparable values).

The second hypothesis of the survey consists in having small structural displacements, resulting in an unvarying tensor of inertia. This hypothesis is generally valid for conventional aircraft and also for high aspect-ratio aircraft having such a main structural typology that leads to relatively small wing displacements under limit loads. Under such hypotheses the principal bending moment (M_{EQ}) acting on a generic wing section is broken down as follows:

$$M_{EQ} = M_0 + M_\alpha \alpha + \sum_{i=1}^{N} M_{\delta i} \delta_i + M_{n_z=1} n_z \,, \tag{1}$$

where M_0, M_α, $M_{\delta i}$, $M_{n_z=1}$ are the Bending Moment Derivatives, each one representing the bending moment at a generic wing section due to each unit aerodynamic and inertial contribution.

Since a symmetric deflection of the ailerons or of another dedicated control surface modifies the aircraft longitudinal balance, the equations of longitudinal equilibrium with Load Alleviation have to be rewritten. The goal is to develop a method that allows the attainment of

a desired reduction of the principal Bending Moment in a specified Wing Control Station (WCS).

The equilibrium equations in quasi-steady symmetric maneuver without Load Alleviation have to fulfill the following requirements:

1) Zero resultant aircraft normal force (z-direction);

2) Zero resultant aircraft pitching moment;

The aircraft has two degrees of freedom or dependent variables: the angle of attack and the elevator deflection. Starting from the longitudinal balance equation system for a rigid aircraft

$$\begin{cases} C_{Z_\alpha}\alpha + C_{Z_\delta}\delta = \dfrac{n_z W}{S_w q} - C_{Z_0} \\ C_{m_\alpha}\alpha + C_{m_\delta}\delta = -C_{m_0} \end{cases}, \tag{2}$$

the symmetric balanced maneuver parameters, the angle of attack and the elevator deflection, are known since the limit vertical load factor, the aircraft velocity, the altitude, the Mach number, the center of gravity and the aircraft weight are defined.

The system of equations (2) is basically valid also for a flexible aircraft. In this latter case, the Aerodynamic Derivatives must be evaluated taking into account the aircraft flexibility. The Aerodynamic Moment Derivatives are calculated with the respect to the center of gravity and they are firstly dependent on its position.

Defining an Alleviation Factor (AF) as

$$M_{IMP} = (1 - AF)\, M_{EQ}, \tag{3}$$

the desired value of the Bending Moment M_{IMP} acting on the WCS may be calculated.

The longitudinal balanced condition with Load Alleviation is accomplished by solving the following system of equations obtained by adding two new equations to the system (2) and by imposing a desired value of AF (and consequently of M_{IMP}).

$$\begin{cases} C_{Z_\alpha}\alpha + C_{Z_\delta}\delta + C_{Z_\beta}\beta & = \dfrac{n_z Mg}{S_w q} - C_{Z_0} \\ C_{m_\alpha}\alpha + C_{m_\delta}\delta + C_{m_\beta}\beta & = -C_{m_0} \\ M_\alpha\alpha + M_\delta\delta + M_\beta\beta & = M_{IMP} - M_{n_z=1}n_z - M_0 \\ \beta - n_z G = 0 & \end{cases}, \tag{4}$$

where β is the deflection of the wing control surface used as load alleviator.

The fourth equation of the system (4) is uncoupled from the others and it represents a linearized relationship between the Load Alleviation control surface deflection and the limit vertical load factor. The unknown function G

$$G = f\left(WCS\ location, q, n_z, AF, Mach\ number\right), \tag{5}$$

can provide a preliminary indication for the design of a control system aimed at controlling the load alleviator in real time during an unsteady longitudinal maneuver; G is a first estimation of the gain to be used in a SISO (Single Input - Single Output) system in order to feedback the vertical load factor (output) to the load alleviator deflection (input). Since the aeroelastic model of a generic airplane is available, from extensive calculations it is possible to build a data-base with the values of the function G with the respect to flight parameters, WCS and desired level of alleviation in order to use it as a controller gains data-base. The engineering of the control system lies beyond the scope of the work presented in this section.

2.3.Application to a Joined-Wing Aircraft

This study has been performed within a research project aimed at the preliminary design of a High Altitude Performance Demonstrator (HAPD) aimed at performing aerodynamic, structural, flying control experimental tests and performance demonstration [40].

The joined-wing configuration is a good compromise between high lift, low flexibility and low weight. A potential disadvantage is an increased complexity in the design process. Such a configuration is structurally redundant, resulting in internal forces that depend upon the stiffness distribution. In addition the stiffness of wing junctions has a great influence on the aeroelastic behavior both in terms of divergence and flutter speeds. For these reasons an integrated methodology able to combine the aeroelastic and the structural aspects has been developed at CIRA [33].

The configuration consists of a Front Wing (FW), including an unswept inner part, an outer part with a negative sweep angle and a winglet tip, and a Rear Wing (RW) with negative sweep and dihedral angles.

The RW gives additional support to the FW by changing the aerodynamic load distribution and by affecting the wing weight and the structural stiffness distribution. The RW support allows the reduction of FW bending moments and consequently its structural weight. The junction location is at about 70% of the FW semi-span, which was chosen as best location as shown by Wolkovitch in [31].

Basic aeroelastic investigations have been introduced early in the design process due to the non-negligible flexibility of the wing and the elastic-body natural frequencies quite close to the typical flight rigid-body frequencies of the vehicle.

HAPD is characterized by a Max Take-Off Weight of 184.4 kg with the center of gravity located at 81.3% of the FW mean chord. The expected limit vertical load factor is $n_{z\lim} = 3.8$, the stalling speed is 14.07 m/s, the design maneuvering speed is 28.94 m/s, the design cruising speed is 33.30 m/s while the dive speed is 39.00 m/s.

V_S, m/s	V_A, m/s	V_C, m/s	V_D, m/s
14.07	24.32	33.30	39.00

Table 1: HAPD Design Speeds

The HAPD primary structures are shown in the following figure.

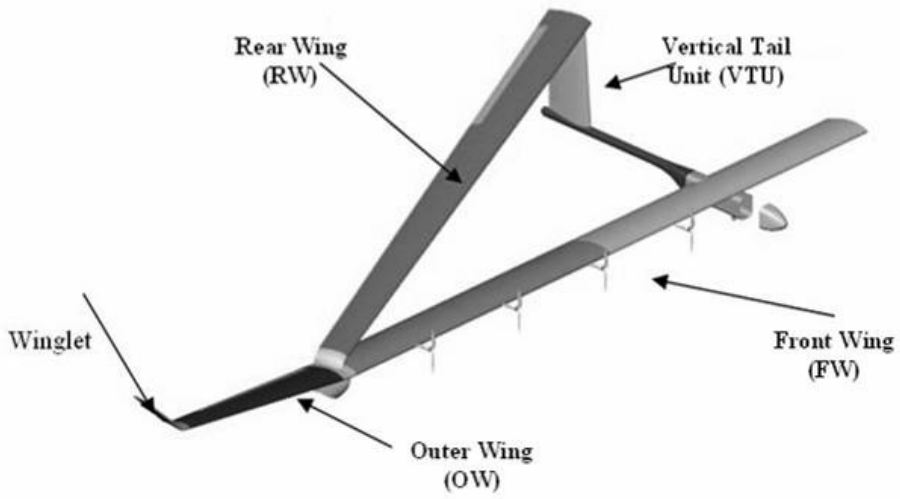

Fig. 8: HAPD Primary Structures

The innovative wing box conceived for the Inner Front Wing (IFW) and the RW consists of a main tubular spar running through the quarter-chord; a rear non-structural spar running through the 3/4 local chord; very lightweight and rigid ribs connecting the two spars and a non-structural, very thin and transparent plastic film wing covering. A high strength carbon/epoxy composite material is used for spar design. The main tubular spar is a cylindrical tube to be manufactured by means of a filament winding technique with two bonded caps for flexural stiffness. The LE is made of a plastic material whereas the TE is made with foam.

A single-spar wing box for the Outer Wing (OW) and a two-spar wing box for the fin, both entirely made with a carbon/epoxy composite material are adopted.

The fuselage main structure is composed of frames, stringers, and a structural floor plate in the ventral zone, all made of a high strength Aluminum Alloy (AA); the nose is made of a plastic material whereas the aft body is of a carbon/epoxy composite material.

The RW is joined to the apex of the Vertical Tail Unit (VTU). The VTU and FW are joined to the fuselage in two different sections.

Three numerical models of the airplane have to be developed in order to evaluate the Aerodynamic Derivatives. A dynamic model for the symmetrical normal modes calculation; an aerodynamic model; and a so-called “Interface Model” (IM) that represents the link between the first two models. The IM is made up of a set of grids on which aerodynamic loads, inertia loads and modal displacements are transferred.

Geometric structural nonlinearities can be considered negligible since the deformations experienced during balanced maneuver analyses at maximum vertical load factor are quite close to the values typically attained during a balanced maneuver of a large conventional aircraft (about 10% of the semi-span). The following figure shows the maximum displacements at each station along the FW semi-span of HAPD.

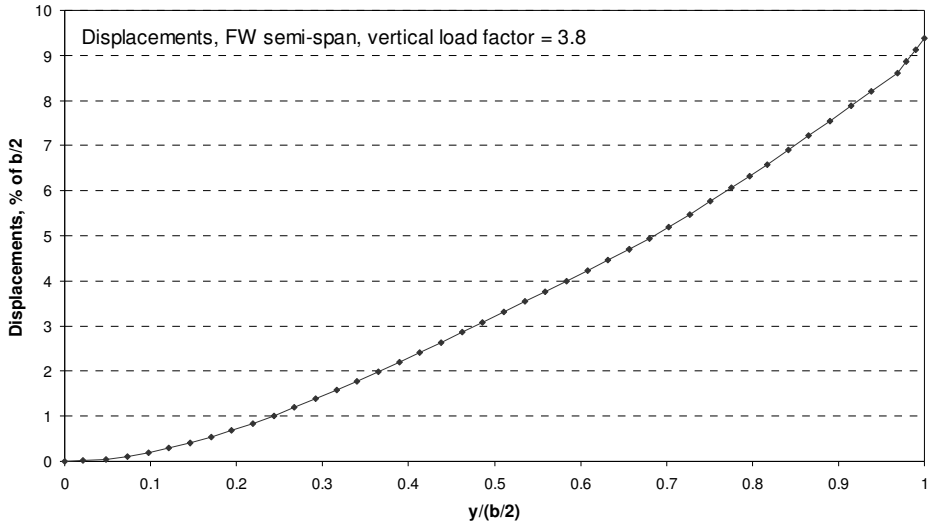

Fig. 9: HAPD Front Wing Semi-span displacements

2.3.1. Dynamic Model

A dynamic model for the semi-airplane has been developed with the aid of MSC.Nastran software. Suitable constraint sets are introduced in the plane of symmetry xz in order to reproduce symmetrical flight conditions.

By means of a semi-automatic mesh generation a reasonably accurate structural model of the wings has been generated with a relatively little effort. The fuselage model, as well as the wing junctions and the fin model, resulting from a rather detailed structural design process, are integrated into the global model.

The inner FW and RW cylindrical spar models are made of beam elements (PBEAM and PBEAML property entries), whereas plate elements are adopted to simulate the LE and the TE structures (PSHELL entries). The outer wing model together with the winglet and the fin models, are made of beam elements for the spar caps, plate elements for the structural wing covering (PCOMP entries) and for LE and TE structures (PSHELL entries). Concentrated masses (CONM2 entry) are used in order to reproduce the wing inertia distribution. The inertia behavior of control surfaces is simulated by means of DMIG mass matrices, for which a two nodes scheme is adopted.

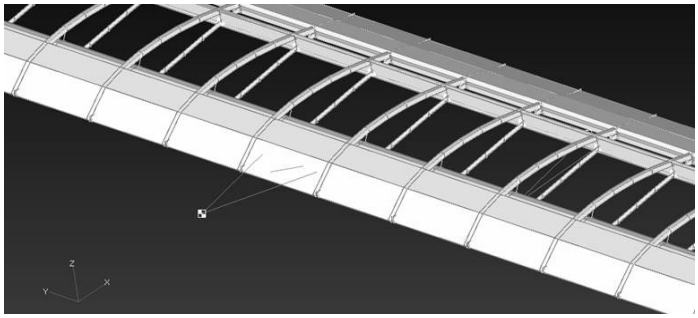

Fig. 10: Inner FW and RW FE model.

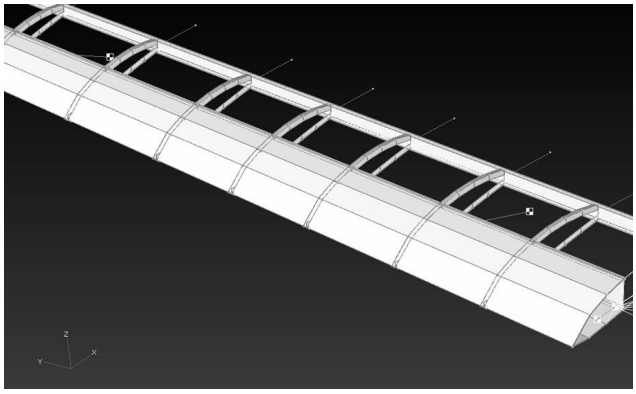

Fig. 11: Outer FW FE model.

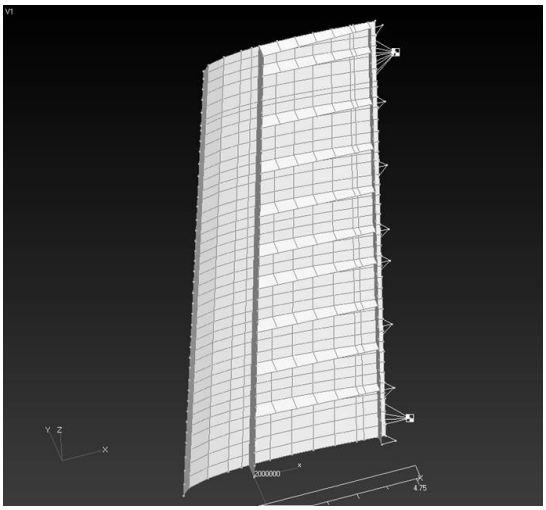

Fig. 12: Fin FE model

Fuselage frames and stringers are modeled with bar elements (PBAR entries) whereas the ventral floor-plate is modeled with plate elements (PSHELL entries). The aft body structure together with the nose are simulated using plate elements (PSHELL and PCOMP entries). The inertia distribution along the x-axis is reproduced by means of four groups of concentrated masses (CONM2 elements).

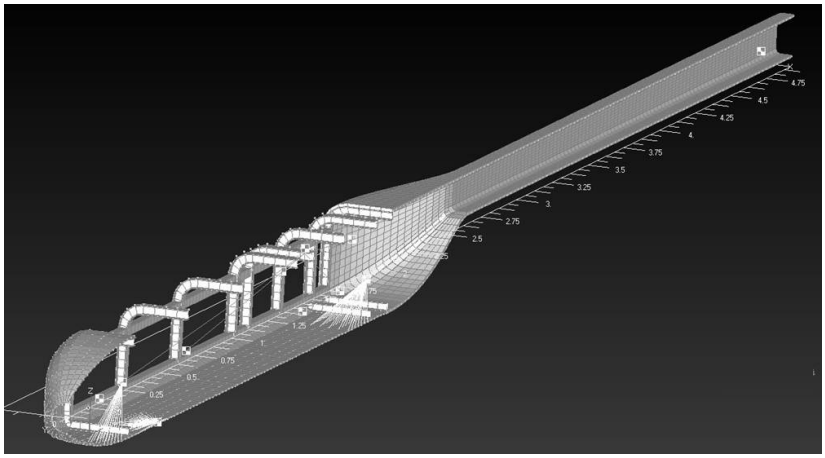

Fig. 13: Fuselage FE model

The wing junction is made up of two elements: a lower part having a barrel shape, connecting the inner and the outer FW, and an upper part having a typical wing box type structure connecting FW and RW. The whole structure is designed using a high strength carbon/epoxy composite material. The dynamic model of the wing junction makes use of plate elements (PCOMP entries) and CONM2 elements for the non-structural masses.

The rear junction connects RW to the fin, it is made up of a machined frame in AA. The rear junction is replaced in the global dynamic model by two equivalent DMIG matrices simulating its structural and inertia behavior.

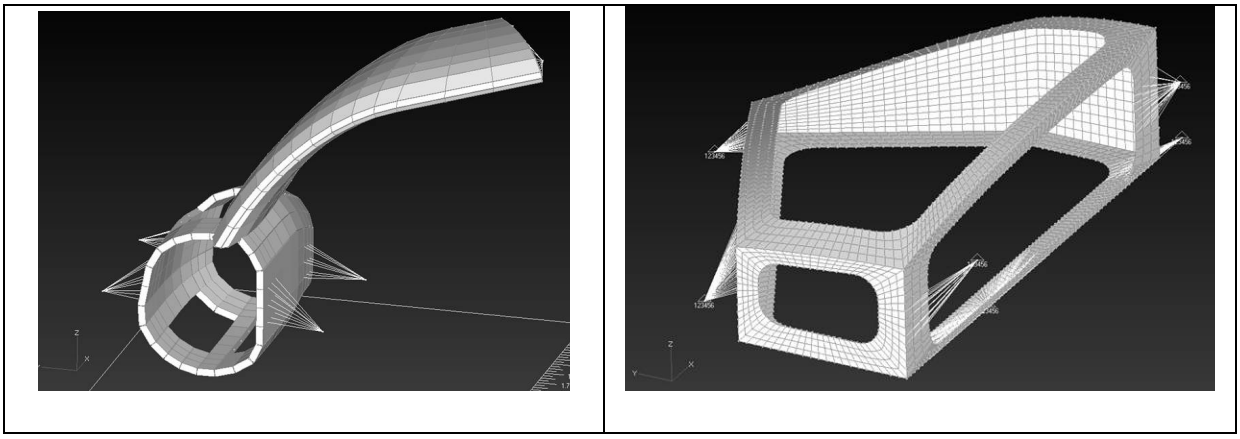

Fig. 14: Front and Rear Junction models

An isometric views of the dynamic model are depicted in the following figure.

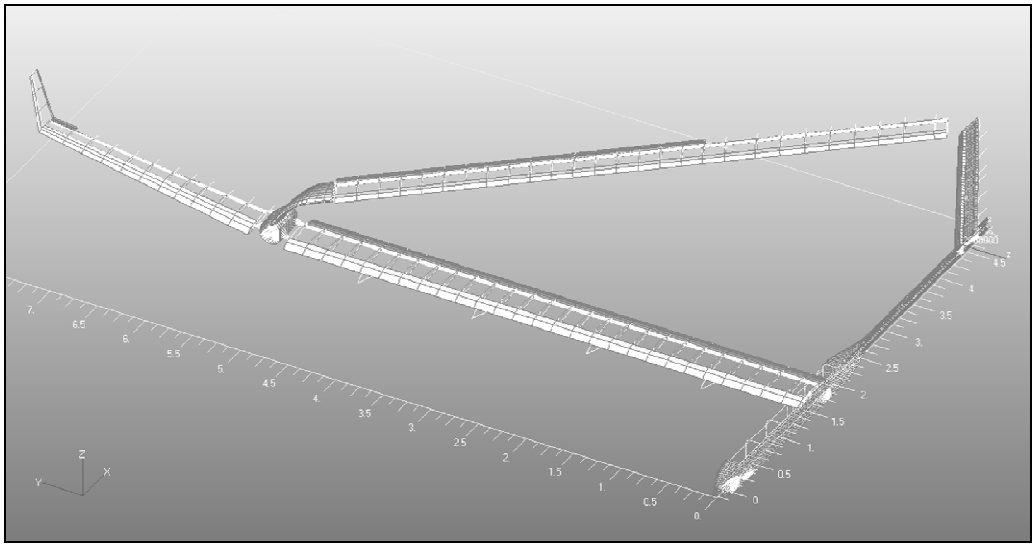

Fig. 15: Isometric view of the Dynamic Model.

2.3.2. Aerodynamic Model

The Aerodynamic Analyses are carried out by using a linear panel method, the Doublet Lattice Method (DLM), based on the pulsating doublet theory.

DLM was developed by E. Albano and W. P. Rodden in 1969 [41], it is based on the linearized theory of the aerodynamic potential. The free stream is considered uniform but it can be steady or harmonically variable. DLM can be used as an aerodynamic load evaluator for aeroelastic purposes in a fast, reliable and relatively simple way, especially if compared with more modern unsteady aerodynamic solvers, such as those based on the direct integration of Navier-Stokes equations.

The aerodynamic model is made up of 940 aerodynamic boxes. Fig. 16 shows how the aerodynamic mesh is more refined on flight control surfaces and in their neighborhood, in order to perform more accurate calculations. The aerodynamics of the fuselage has not been accounted for because of its very slight influence on the symmetric aerodynamic behavior of the entire airplane resulting from CFD calculations.

All aerodynamic analyses are executed by taking into account airfoil cambers and aerodynamic corrections due to viscous effects since the aerodynamic model has been calibrated at zero angle of attack by means of comparison with CFD calculations. Such a correction has been performed by imposing $C_{n'}$ and $C_{m'}$ distributions obtained through

integration of the aerodynamic pressures coming from CFD. The equivalent pressures on the aerodynamic boxes are adopted as aerodynamic "Zero Effect".

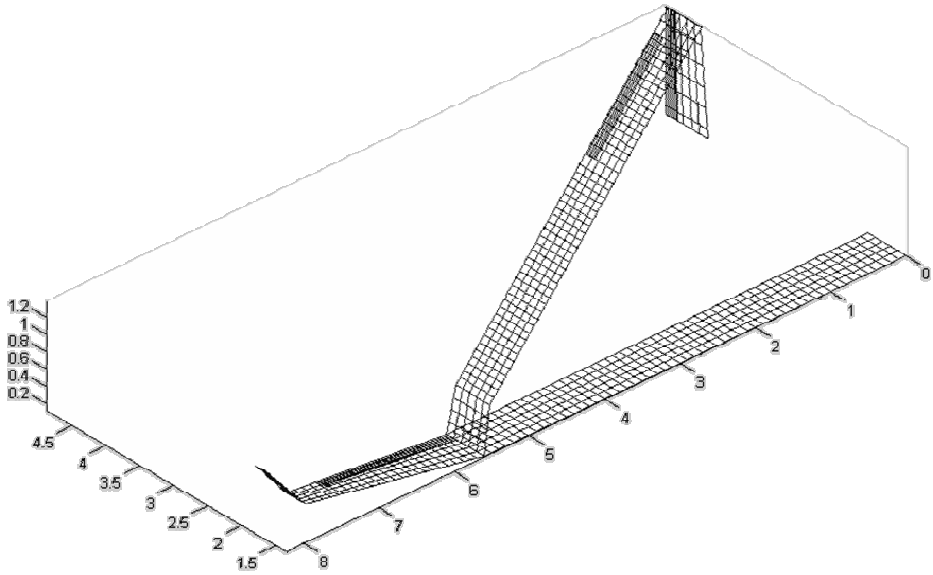

Fig. 16: DLM Aerodynamic Model.

2.3.3. Inteface Model

In order to transfer the data between dynamic and aerodynamic models, a link between a set of master grids belonging to the dynamic model (Interchange Data Grids, IDGs) and all aerodynamic boxes is created. This link is guaranteed by using spline type and bilinear type interpolation operators [42].

All six degrees of freedom of IDGs are constrained to the dynamic model through RBE2 elements (for each RBE2 element, the master grid coincides with the associated IDG).

Fig. 17 shows the geometric superposition of aerodynamic model and IDGs.

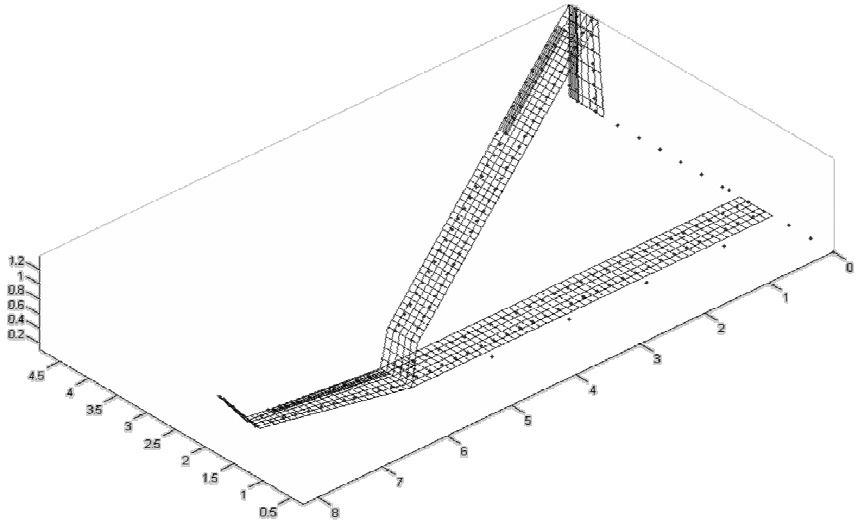

Fig. 17: Geometric Superposition of Aerodynamic and Interface Model.

2.3.4. Aerodynamic Derivatives

The evaluation of the Aerodynamic Derivatives is carried-out by using a Modal Approach, typical of the Dynamic Aeroelasticity domain.

Normal Modes are used extensively in the dynamic analyses of airplane responses, including investigations into aeroelastic instabilities such as flutter. Extensive calculations (NASTRAN) have to be carried-out in order to estimate the normal modes and their associated natural frequencies of a generic unrestrained airplane. With the respect to a conventional approach, the principal advantage is that it is possible to solve a generic structural static problem without fixing suitable constraints in order to make the problem isostatic: the airplane can be considered unrestrained. Furthermore, since the normal modes are available, there is benefit to be gained from using them for static problems as well as for dynamic problems and so unifying the approaches to static and dynamic aeroelasticity. This is an important aspect if a Load Alleviation is implemented when considering unsteady maneuvers.

The general equation of the Dynamic Aeroelasticity in a modal approach in the frequency domain, for a symmetric maneuver is:

$$\left\{(j\omega)^2\begin{bmatrix}\underline{\underline{m}}_{RR} & 0\\ 0 & \underline{\underline{m}}_{EE}\end{bmatrix}+(j\omega)\begin{bmatrix}0 & 0\\ 0 & \underline{\underline{\sigma}}_{EE}\end{bmatrix}+\begin{bmatrix}0 & 0\\ 0 & \underline{\underline{K}}_{EE}\end{bmatrix}\right\}\begin{bmatrix}\underline{q}_R(j\omega)\\ \underline{q}_E(j\omega)\end{bmatrix}=$$
$$=\frac{1}{2}\rho V^2\begin{bmatrix}\underline{\underline{Q}}_{RR} & \underline{\underline{Q}}_{RE}\\ \underline{\underline{Q}}_{ER} & \underline{\underline{Q}}_{EE}\end{bmatrix}\begin{bmatrix}\underline{q}_R(j\omega)\\ \underline{q}_E(j\omega)\end{bmatrix}+\frac{1}{2}\rho V^2\begin{bmatrix}\underline{q}_{R\delta}\\ \underline{q}_{E\delta}\end{bmatrix}\delta(j\omega) \tag{6}$$

where single and double underlines denote respectively vectors and tensors. Eq. (6) is written by distinguishing the rigid modes from the elastic ones through subscripts R and S, the components of $\underline{q}_R$ are the degrees of freedom of the rigid airplane: the plunge and the pitch mode.

$$\underline{q}_R=\begin{pmatrix}h\\ \theta\end{pmatrix}=\begin{cases}Plunge\\ Pitch\end{cases} \tag{7}$$

The quasi-steady aerodynamic pressures are determined by adopting a quadratic approximation of the unsteady pressures obtained from DLM calculations.

$$\underline{\underline{\tilde{P}}}(jk)=\underline{\underline{P}}_0+jk\,\underline{\underline{P}}_1+(jk)^2\underline{\underline{P}}_2 \tag{8}$$

Since quasi-steady aerodynamic pressures are interpolated on the IM, for each normal mode shape, the quasi-steady Generalized Aerodynamic Forces $\underline{\underline{Q}}$ are evaluated as follows.

$$\frac{1}{2}\rho V^2\underline{\underline{Q}}\,\underline{q}=\frac{1}{2}\rho V^2\,\underline{\underline{\Phi}}^T\cdot\underline{\underline{\Delta S}}\cdot\underline{\underline{\tilde{P}}}(jk)\cdot\underline{q}=\frac{1}{2}\rho V^2\,\underline{\underline{\Phi}}^T\cdot\underline{\underline{\Delta S}}\cdot\left[\underline{\underline{P}}_0+jk\,\underline{\underline{P}}_1+(jk)^2\underline{\underline{P}}_2\right]\cdot\underline{q}, \tag{9}$$

$$\frac{1}{2}\rho V^2\underline{\underline{Q}}\,\underline{q}=\frac{1}{2}\rho V^2\,\underline{\underline{G}}_0\cdot\underline{q}(t)+\frac{1}{2}\rho V c_r\,\underline{\underline{G}}_1\cdot\dot{\underline{q}}(t)+\frac{1}{2}\rho c_r^2\,\underline{\underline{G}}_2\cdot\ddot{\underline{q}}(t), \tag{10}$$

where:

$$\begin{cases}\underline{\underline{G}}_0=\underline{\underline{\Phi}}^T\cdot\underline{\underline{\Delta S}}\cdot\underline{\underline{P}}_0\\ \underline{\underline{G}}_1=\underline{\underline{\Phi}}^T\cdot\underline{\underline{\Delta S}}\cdot\underline{\underline{P}}_1\\ \underline{\underline{G}}_2=\underline{\underline{\Phi}}^T\cdot\underline{\underline{\Delta S}}\cdot\underline{\underline{P}}_2\\ j\omega\underline{q}=\dot{\underline{q}}(t);(j\omega)^2\underline{q}=\ddot{\underline{q}}(t)\end{cases}, \tag{11}$$

and

$$k = \frac{\omega c_r}{V} \tag{12}$$

is the Reduced Frequency.

The quasi-steady aerodynamic pressures are evaluated for the following two values of the reduced frequency

$$\begin{aligned} k &= 0 \\ k &= \varepsilon \end{aligned} \tag{13}$$

with ε very close to zero. By substituting eq. (13) in eq. (8) one gets

$$\begin{aligned} \underline{\underline{\tilde{P}}}(0) &= \underline{\underline{P}}_0 \\ \underline{\underline{\tilde{P}}}(j\varepsilon) &= \underline{\underline{P}}_r + j\underline{\underline{P}}_i = \underline{\underline{P}}_0 + j\varepsilon\underline{\underline{P}}_1 + (j\varepsilon)^2\underline{\underline{P}}_2 \end{aligned} \tag{14}$$

where the subscripts r and i mean real and imaginary part of the aerodynamic pressures at the reduced frequency equal to ε.

From eq. (14) it follows:

$$\begin{aligned} \underline{\underline{P}}_0 &= \underline{\underline{\tilde{P}}}(0) \\ \underline{\underline{P}}_1 &= 1/\varepsilon\,\underline{\underline{P}}_i(\varepsilon) \\ \underline{\underline{P}}_2 &= \left(\frac{1}{\varepsilon^2}\right)\left(\underline{\underline{\tilde{P}}}(0) - \underline{\underline{P}}_r(\varepsilon)\right) \end{aligned} \tag{15}$$

from which $\underline{\underline{\tilde{P}}}(jk)$ and $\underline{\underline{Q}}$ are determined.

Under the hypothesis of quasi-steady conditions, for $\varepsilon << 1$, eq. (10) becomes

$$\frac{1}{2}\rho V^2 \underline{\underline{Q}}\,\underline{q} = \frac{1}{2}\rho V^2\left[\underline{\underline{G}}_0 + jk\underline{\underline{G}}_1\right]\underline{q} = \eta_0\underline{\underline{G}}_0\underline{q} + \eta_1\underline{\underline{G}}_1\dot{\underline{q}} \tag{16}$$

with $\eta_0 = \frac{1}{2}\rho V^2$; $\eta_1 = \frac{1}{2}\rho Vc$.

Eq. (6), written in the time domain, becomes:

$$\begin{bmatrix} \underline{\underline{m}}_{RR} & 0 \\ 0 & \underline{\underline{m}}_{EE} \end{bmatrix} \begin{pmatrix} \ddot{\underline{q}}_R \\ \ddot{\underline{q}}_E \end{pmatrix} + \begin{bmatrix} 0 & 0 \\ 0 & \underline{\underline{\sigma}}_{EE} \end{bmatrix} \begin{pmatrix} \dot{\underline{q}}_R \\ \dot{\underline{q}}_E \end{pmatrix} + \begin{bmatrix} 0 & 0 \\ 0 & \underline{\underline{K}}_{EE} \end{bmatrix} \begin{pmatrix} \underline{q}_R \\ \underline{q}_E \end{pmatrix} =$$
$$\begin{bmatrix} \eta_0 \underline{\underline{G}}_{0,RR} \underline{q}_R + \eta_1 \underline{\underline{G}}_{1,RR} \dot{\underline{q}}_R & \eta_0 \underline{\underline{G}}_{0,RE} \underline{q}_E + \eta_1 \underline{\underline{G}}_{1,RR} \dot{\underline{q}}_E \\ \eta_0 \underline{\underline{G}}_{0,ER} \underline{q}_R + \eta_1 \underline{\underline{G}}_{1,ER} \dot{\underline{q}}_R & \eta_0 \underline{\underline{G}}_{0,EE} \underline{q}_E + \eta_1 \underline{\underline{G}}_{1,EE} \dot{\underline{q}}_E \end{bmatrix} + \begin{bmatrix} \eta_0 \underline{G}_{0,R\delta} \delta + \eta_1 \underline{G}_{1,R\delta} \dot{\delta} \\ \eta_0 \underline{G}_{0,E\delta} \delta + \eta_1 \underline{G}_{1,E\delta} \dot{\delta} \end{bmatrix}. \quad (17)$$

With the assumption of negligibility of:

- elastic accelerations with the respect to rigid ones;
- elastic velocities with the respect to rigid ones;
- control speed with the respect to control deflection;

it is possible to simplify eq. (17) as follows:

$$\underline{\underline{m}}_{RR} \ddot{\underline{q}}_R = \eta_1 \underline{\underline{G}}_{1,RR} \dot{\underline{q}}_R + \eta_0 \underline{\underline{G}}_{0,RR} \dot{\underline{q}}_R + \eta_0 \underline{G}_{0,R\delta} \delta + \eta_0 \underline{\underline{G}}_{0,RE} \underline{q}_E + \eta_0 \underline{G}_{0,Rq} + \underline{F}_{Rext} \quad (18)$$

$$\left(\underline{\underline{K}}_{EE} - \eta_0 \underline{\underline{G}}_{0,EE} \right) \underline{q}_E = \eta_0 \underline{\underline{G}}_{0,ER} \underline{q}_R + \eta_1 \underline{\underline{G}}_{1,ER} \dot{\underline{q}}_R + \eta_0 \underline{G}_{0,E\delta} \delta + \eta_0 \underline{G}_{0,Eq} + \underline{F}_{Eext}. \quad (19)$$

In equations (18) and (19), the aerodynamic terms depending exclusively on the dynamic pressure ($\eta_0 \underline{G}_{0,Rq}$ and $\eta_0 \underline{G}_{0,Eq}$) and the terms representing possible external forces (i.e. engine trust) ($\underline{F}_{Rext}$ and $\underline{F}_{Eext}$) have been taken into account.

By defining the following equalities:

$$\begin{aligned} \underline{\underline{A}}_{1,RR} &= \eta_1 \underline{\underline{G}}_{1,RR} \\ \underline{\underline{A}}_{0,RR} &= \eta_0 \underline{\underline{G}}_{0,RR} \\ \underline{\underline{A}}_{0,RE} &= \eta_0 \underline{\underline{G}}_{0,RE} \\ \underline{F}_{0,RC} &= \eta_0 \underline{G}_{0,R\delta} \\ \underline{F}_{0,Rq} &= \eta_0 \underline{G}_{0,Rq} \end{aligned} \quad ; \quad \begin{aligned} \underline{\underline{\tilde{K}}} &= \left(\underline{\underline{K}}_{EE} - \eta_0 \underline{\underline{G}}_{0,EE} \right) \\ \underline{\underline{F}}_{0,ER} &= \eta_0 \underline{\underline{\tilde{K}}}^{-1} \underline{\underline{G}}_{0,ER} \\ \underline{\underline{F}}_{1,ER} &= \eta_1 \underline{\underline{\tilde{K}}}^{-1} \underline{\underline{G}}_{1,ER} \\ \underline{F}_{0,EC} &= \eta_0 \underline{\underline{\tilde{K}}}^{-1} \underline{G}_{0,E\delta} \\ \underline{F}_{0,Eq} &= \eta_0 \underline{\underline{\tilde{K}}}^{-1} \underline{G}_{0,Eq} \\ \underline{F}_{0Eext} &= \underline{\underline{\tilde{K}}}^{-1} \underline{F}_{Eext} \end{aligned} \quad (20)$$

Eq. (18) and (19) become:

$$\underline{\underline{m}}_{RR} \ddot{\underline{q}}_R = \underline{\underline{A}}_{0,RR} q_R + \underline{\underline{A}}_{1,RR} \dot{q}_R + \underline{\underline{A}}_{0,RE} q_E + \underline{F}_{0,RC} \delta + \underline{F}_{0,Rq} + \underline{F}_{\mathrm{Re}xt}. \quad (21)$$

$$\underline{q}_E = \underline{\underline{F}}_{0,ER}\underline{q}_R + \underline{\underline{F}}_{1,ER}\dot{\underline{q}}_R + \underline{F}_{0,EC}\delta + \underline{F}_{0,Eq} + \underline{F}_{0Eext}\,. \tag{22}$$

By substituting eq. (22) into eq. (21), a second order differential equation system is obtained.

$$\underline{\underline{m}}_{RR}\ddot{\underline{q}}_R + \hat{\underline{\underline{C}}}_{RR}\dot{\underline{q}}_R + \hat{\underline{\underline{K}}}_{RR}\underline{q}_R = \underline{F}_{extq} + \underline{F}_{ext0} + \underline{F}_C\delta(t)\,, \tag{23}$$

where:

$$\begin{cases} \hat{\underline{\underline{K}}}_{RR} = -(\underline{\underline{A}}_{0,RR} + \underline{\underline{A}}_{0,RE}\underline{\underline{F}}_{0,ER}) \\ \hat{\underline{\underline{C}}}_{RR} = -(\underline{\underline{A}}_{1,RR} + \underline{\underline{A}}_{1,RE}\underline{\underline{F}}_{1,ER}) \\ \underline{F}_{extq} = \underline{F}_{0,Rq} + \underline{\underline{A}}_{0,RE}\underline{F}_{0,Eq} \\ \underline{F}_C = \underline{F}_{0,RC} + \underline{\underline{A}}_{0,RE}\underline{F}_{0,EC} \\ \underline{F}_{ext0} = \underline{F}_{\mathrm{Re}xt} + \underline{\underline{A}}_{0,RE}\underline{F}_{0Eext} \end{cases} \tag{24}$$

With the previous assumptions, the general equation of the Dynamic Aeroelasticity, a system of N differential equations, becomes a system of 2 differential equations of motion (rigid degrees of freedom only) plus N-2 algebraic equations, uncoupled from the first ones. Eq. (23), together with eq. (22) are the main equations in the symmetric quasi-steady aeroelasticity, from which it is possible to determine the evolution of a symmetric maneuver during time or to evaluate the parameters of a balanced and steady symmetric maneuver.

The Aerodynamic Derivatives are calculated as follows.

Depending on the aeroelastic properties of the airplane in terms of modal characteristics and quasi-steady aerodynamics, the terms $\underline{\underline{F}}_{0,ER}$, $\underline{\underline{F}}_{1,ER}$, $\underline{F}_{0,EC}$, $\underline{F}_{0,Eq}$, $\underline{F}_{0Eext}$ are calculated as shown previously.

The elastic modal degrees of freedom $\underline{q}_E$ are determined for each unit aerodynamic condition (including unit control surface deflections) by putting in eq. (22) the different sets of $\underline{q}_R$, δ, etc, representative of each unit aerodynamic contribution.

The aerodynamic forces on each box are:

$$\underline{F}_{aero}(\hat{t}) = \frac{1}{2}\rho V^2\underline{\underline{\Delta S}}\;\underline{\underline{\tilde{P}}}(\hat{t})\underline{q}(\hat{t}) = \frac{1}{2}\rho V^2\underline{\underline{\Delta S}}\left(\underline{\underline{P}}_0\underline{q}(\hat{t}) + \underline{\underline{P}}_1\dot{\underline{q}}(\hat{t})\frac{c}{V}\right), \tag{25}$$

where $\underline{\underline{\Delta S}}$ is the diagonal matrix of the aerodynamic box areas.

By representing the aerodynamic pressures in their explicit form ("Zero effect", Control Surface deflection effect and the effect due to elastic and rigid modal degrees of freedom), eq. (25) becomes:

$$\underline{F}_{aero}(\hat{t}) = \frac{1}{2}\rho V^2 \underline{\underline{\Delta S}}\left(\underline{\underline{P}}_{0R}\underline{q}_R(\hat{t}) + \underline{\underline{P}}_{0E}\underline{q}_E(\hat{t}) + \underline{\underline{P}}_{1R}\dot{\underline{q}}_R(\hat{t})\frac{c}{V}\right) + \frac{1}{2}\rho V^2 \underline{\underline{\Delta S}}\left[\underline{P}_q + \underline{P}_\delta \delta(\hat{t})\right] \quad (26)$$

The resultant Lift and Pitching Moment, evaluated by integrating the aerodynamic forces of eq. (26) calculated for each aerodynamic contribution (and for all the flight conditions of interest in terms of Mach number, altitude and dynamic pressure) are just the aerodynamic Lift and Pitching Moment Derivatives.

Fig. 18 shows a schematic of the whole process.

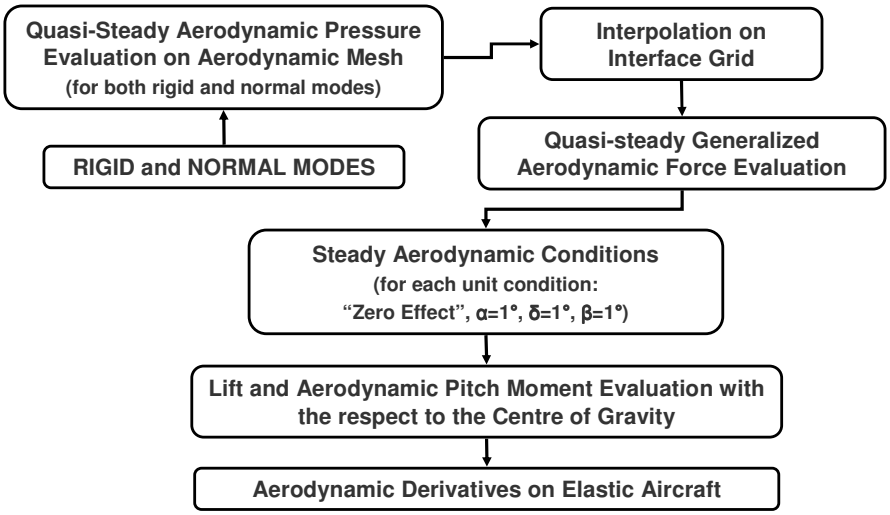

Fig. 18: Aerodynamic Derivatives Calculation taking into account aeroelastic effects

2.3.5. Load Derivatives

In the case of airplanes having a conventional configuration, the main structure of the wing can be considered statically determinate. The Load Derivatives (or Bending Moment Derivatives) have to be calculated through integration of the aerodynamic pressure due to each unit aerodynamic load contribution and of single forces and concentrated moments due to the unit inertia load condition.

In the case of airplanes having an unconventional configuration such as a Joined-Wing one, the main structure is redundant. Under this hypothesis it is not possible to calculate the internal load characteristics by means of a simple integration of the external load distribution because the internal stresses are strictly dependent on the stiffness behavior of the structure. Consequently, it is necessary to solve the static problem by applying the external loads and a suitable constraint set in order to make the problem isostatic. Then the internal load characteristics are evaluated through integration of the internal nodal forces, resulting from the finite element force balance (Grid Point Forces Balance, GPFORCE, [43]).

The static problem is solved with the aid of MSC.NASTRAN by loading the structural model with each unit aerodynamic and inertia load contribution. The unit bending moment distributions and thus the bending moment derivatives are evaluated by integrating the GPFORCE resulting from the post-processing performed with MSC.PATRAN. Fig. 19 summarizes the process.

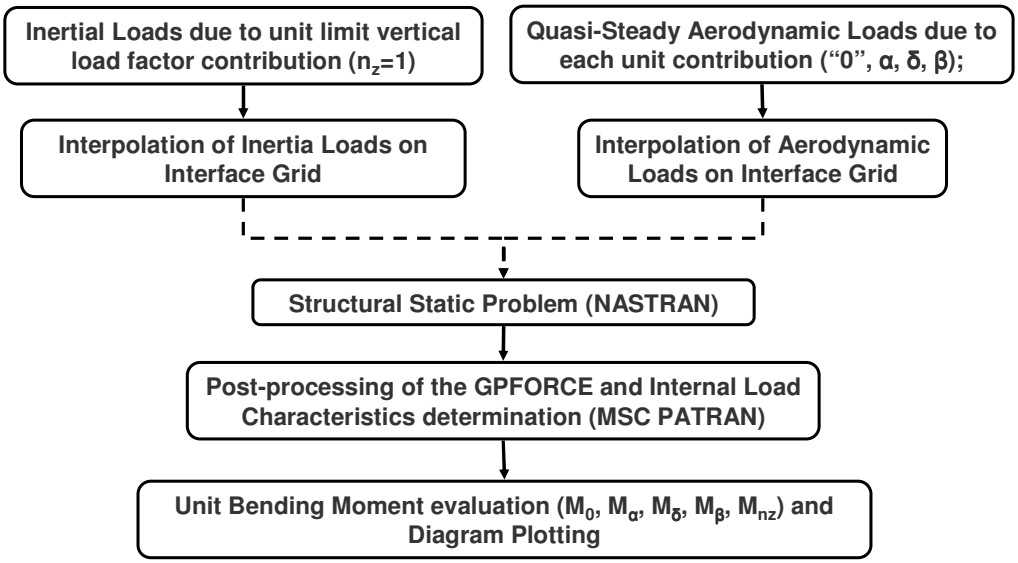

Fig. 19: Bending Moment Derivatives Calculation for an aircraft in a non-conventional configuration (Joined-Wing)

2.3.6. Input Data and Derivatives Calculation

Due to specific requirements related to Guidance, Navigation, and Control, HAPD has ten flight control surfaces: four ailerons, four elevators and two rudders.

The control surfaces used as Load Alleviators are the inner ailerons, and the Wing Control Section used for monitoring the principal bending moment in the front wing root station as illustrated in Fig. 20.

The calculations are carried out for different values of aircraft speed from the design maneuvering speed to the dive speed, at sea level, for a vertical load factor variable between 1.0 and 3.8. Due to the quite regular behavior of the test aircraft under load alleviation, in this paper only the calculations involving the design cruising speed are reported. All derivatives are evaluated taking into account the structural flexibility according to the above-illustrated method, at the dynamic pressures reported in the following table.

Input calculation data, Lift and Moment Aerodynamic Derivatives together with Bending Moment Derivatives are also reported in the following table.

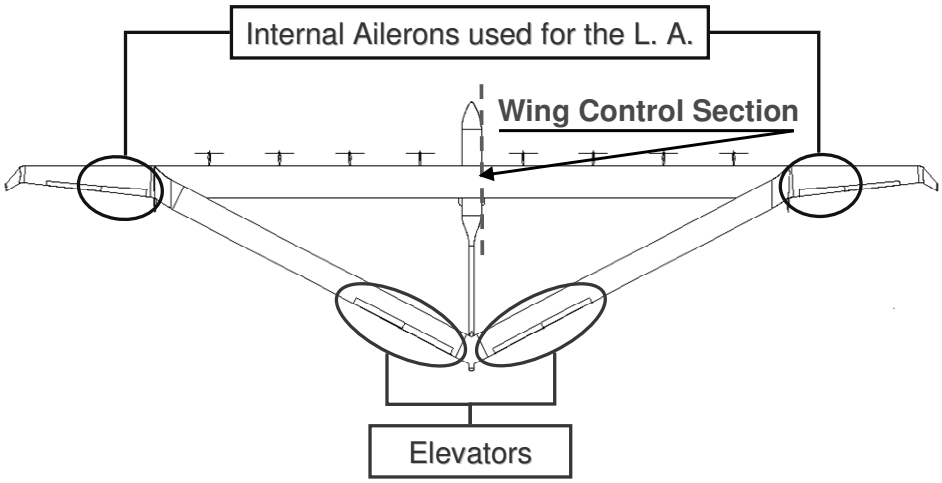

Fig. 20: HAPD Flight Control Surfaces and WCS.

V, m/s	**Mach**	**ρ, kg/m^3**	**q, Pa**	
33.30	0.00	1.23	679.20	
C_{z0}	**$C_{z\alpha}$, 1/deg**	**$C_{z\delta}$, 1/deg**	**$C_{z\beta}$, 1/deg**	
0.3458	0.0785	0.0071	0.0002	
C_{m0}	**$C_{m\alpha}$, 1/deg**	**$C_{m\delta}$, 1/deg**	**$C_{m\beta}$, 1/deg**	
0.1398	-0.06021	-0.0210	-0.00005	
M_0, Nm	**M_α, Nm/deg**	**M_δ, Nm/deg**	**M_β, Nm/deg**	**M_{nz}, Nm**
3389.38	660.71	28.3	17.49	-1589.26

Table 2: HAPD Calculation Data, Aerodynamic and Load Derivatives.

2.3.7. Results

Different levels of load alleviation are performed in order to establish a relationship between flight parameters such as α, β, δ, the vertical load factor nz, and the Alleviation Factor AF.

Flight parameters together with the control function G of eq. (5) are plotted both against the vertical load factor parameterized with AF and against AF parameterized with the vertical load factor (Fig. 21 and Fig. 22).

Fig. 21 and Fig. 22 show that if nz increases the load alleviator deflection β linearly decreases; furthermore the stronger the drop in β the higher the value of AF. Hence, the maximum attainable value of AF (and thus of the alleviation level) is bounded by the maximum deflection of the ailerons. AF=0.37 is chosen as maximum value because it produces, at the maximum vertical load factor, an inner aileron deflection of 25 degrees that is the largest allowable value of the load alleviator deflection.

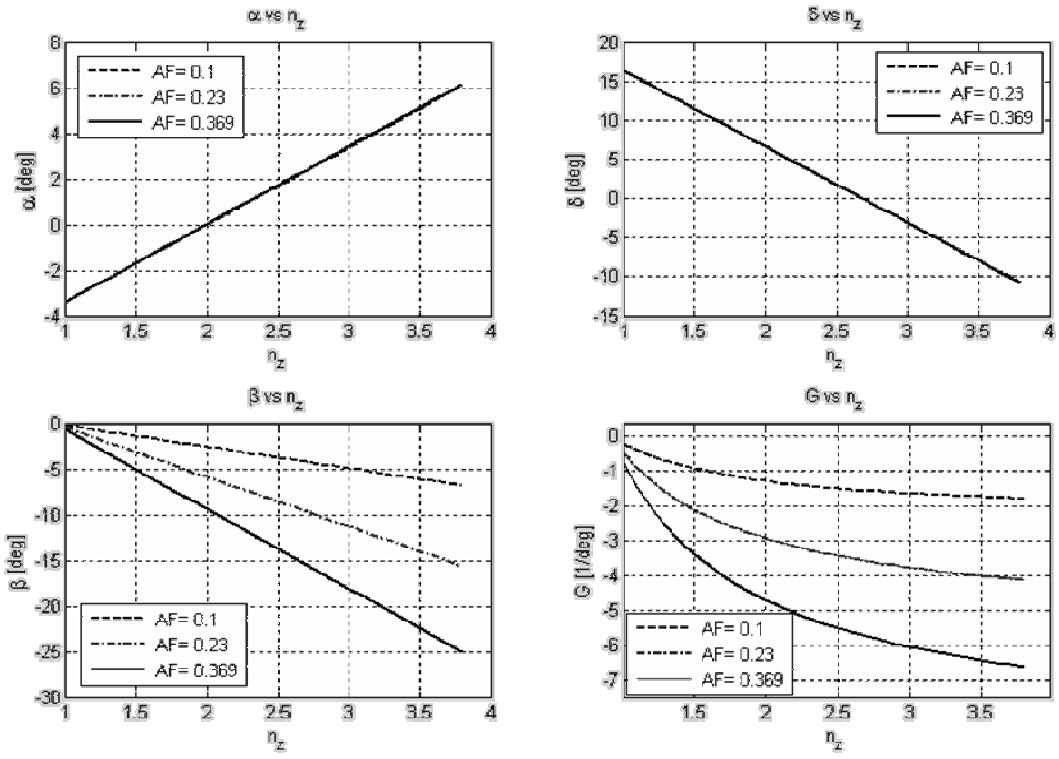

Fig. 21: Attitude, Elevator Deflection, Aileron Deflection, and Control Function vs Vertical Load Factor.

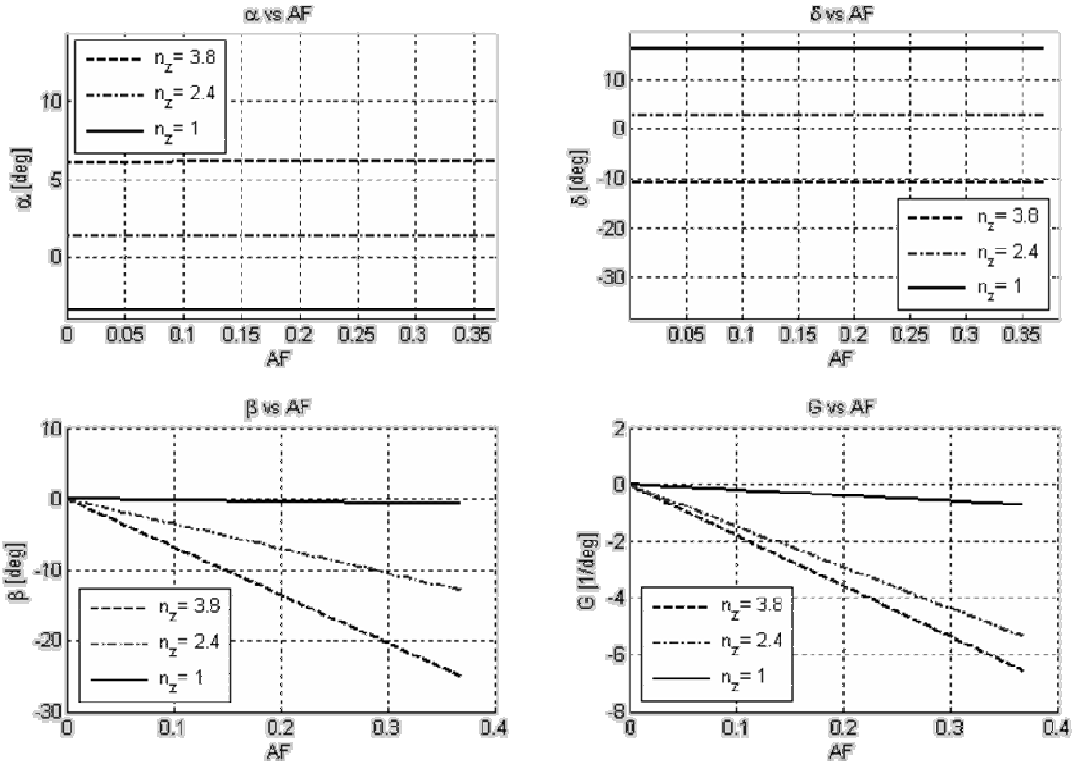

Fig. 22: Attitude, Elevator Deflection, Aileron Deflection, and Control Function vs AF.

Calculations performed at V_A, not reported for reasons of conciseness, result in an increase of the angle of attack α with the respect to n_z and AF. Also in this case the higher the rise of α with the respect of nz the higher is the value of AF. This behavior leads to an important conclusion: the adoption of a load alleviator that induces a positive aerodynamic pitch derivative ($C_{m\beta}$=0.00143), typical of the airplanes having a negative sweep angle wing, makes this method not applicable in high lift conditions, such as at the point V_A of the Maneuver Diagram. In such a situation, with the aircraft at its maximum attitude, the activation of the load alleviation system may lead to aircraft stall.

Instead, when the load alleviator induces a negative or zero aerodynamic pitch derivative, typical of the airplanes having a positive sweep angle wing, a negative and symmetric actuation of the control surfaces does not produce an increase in the angle of attack. Such a situation can also occur because of aeroelastic effects, as well as in the results presented herein (Fig. 21 and Fig. 22), for which the elastic deformation of the wing modifies the aerodynamic behavior induced by the control surfaces as load alleviators, leading to a $C_{m\beta}$ practically equal to zero. In this case the elevator deflection does not vary with the respect to AF.

Nevertheless, if at the point V_A of the Maneuver Diagram the load alleviator is such that $C_{m\beta}<0$, then the illustrated load alleviation method can be applied also at high lift conditions.

Calculations performed using this method give a set of diagrams of the Control Function G with the respect to n_z, AF, Mach number and dynamic pressure. Such an abacus can be viewed as an indication for the preliminary design of a control system aimed at controlling the load alleviation in real time, i.e. by adopting the values of G as a first estimation of the controller gain. Otherwise, starting from the values of the airplane derivatives with the respect to the dynamic pressure and the Mach number actually measured in flight, a computer system calculating in real time the function G can be designed and engineered as an inboard system.

Starting from the unit Bending Moment and Shear distributions for each unit aerodynamic and inertial contribution, and combining them together with the flight parameters shown above, the Bending Moment distribution on the entire wing system of the aircraft can be plotted for different values of n_z and AF. For sake of clarity, the Bending Moment distributions on Front Wing (Fig. 23) and Rear Wing (Fig. 24) are normalized with the respect to the value of the Bending Moment at the FW root @ n_z=1.0 and AF=0.0. Again, evaluating the unit Shear distributions for each unit aerodynamic and inertial contribution, and combining them together with the previous flight parameters, the principal Shear distribution on the front and rear wings of the aircraft can be plotted for different values of n_z and AF.

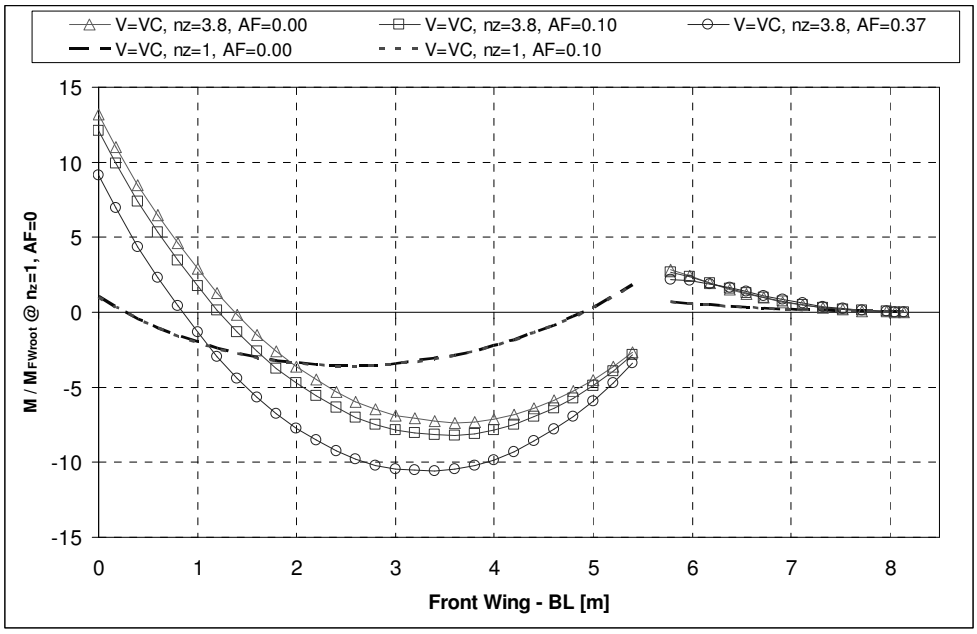

Fig. 23: Bending Moment distribution on the FW normalized with the respect to the Principal Bending Moment at FW root @ n_z=1 and AF=0. (AF=[0.00, 0.10, 0.37], n_z=[1.0, 3.8], sea level)

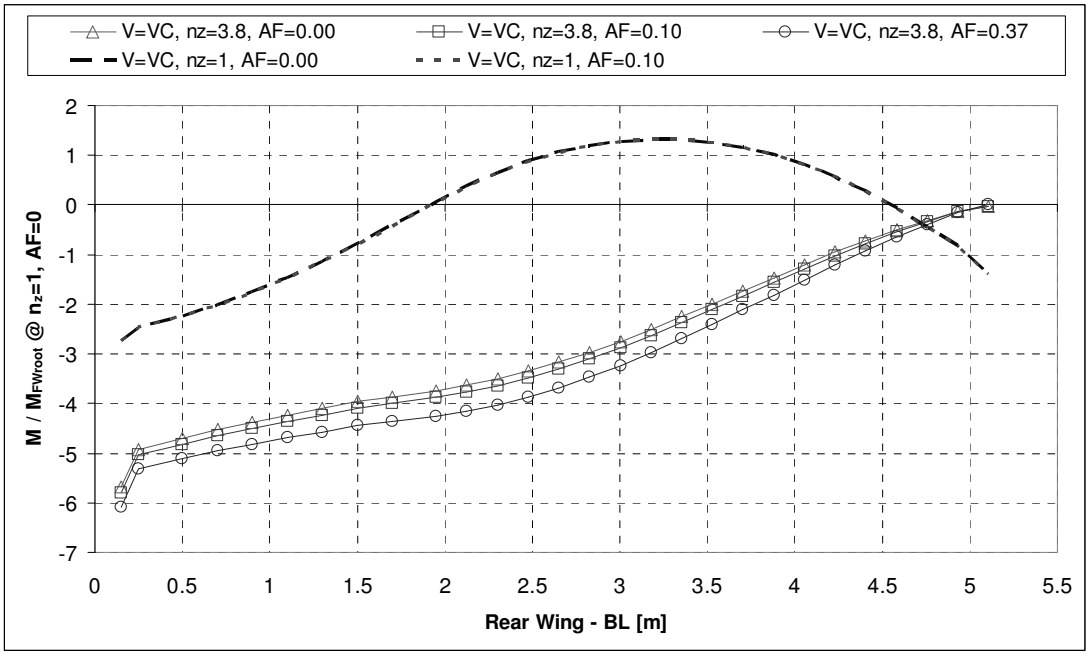

Fig. 24: Bending Moment distribution on the RW normalized with the respect to the Principal Bending Moment at FW root @ n_z=1 and AF=0. (AF=[0.00, 0.10, 0.37], n_z=[1.0, 3.8], sea level)

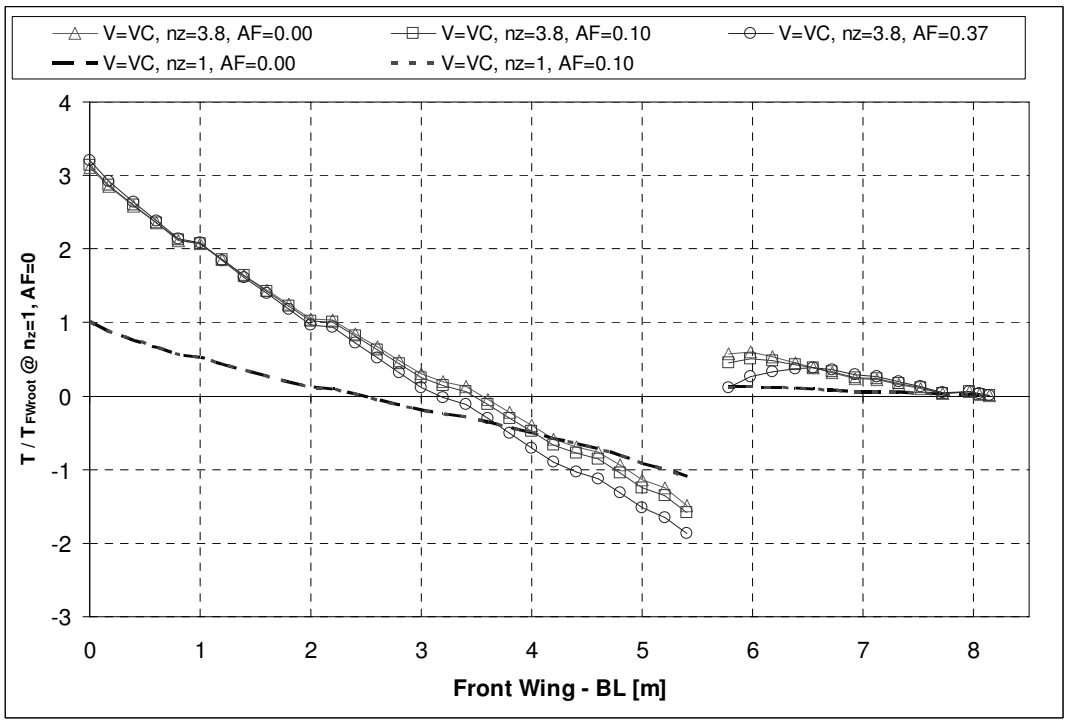

Fig. 25: Shear distribution on the FW normalized with the respect to the Principal Shear at FW root @ n_z=1 and AF=0. (AF=[0.00, 0.10, 0.37], n_z=[1.0, 3.8], sea level)

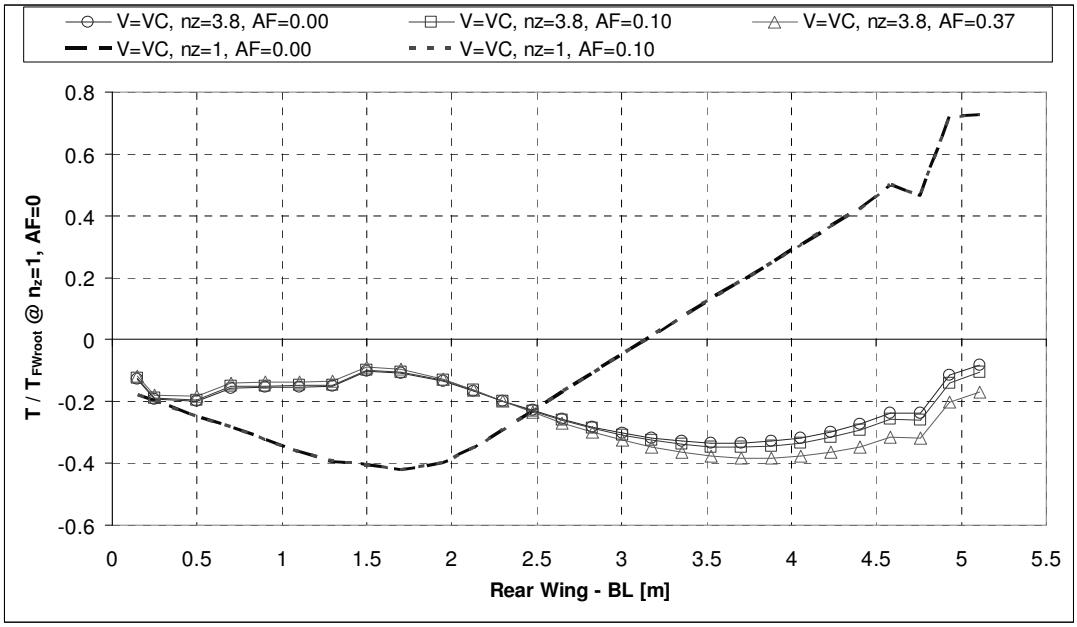

Fig. 26: Shear distribution on the RW normalized with the respect to the Principal Shear at FW root @ n_z=1 and AF=0. (AF=[0.00, 0.10, 0.37], n_z=[1.0, 3.8], sea level)

Fig. 23 shows that for both n_z=1 and n_z=3.8, an important decrease of the Bending Moment on WCS is obtained. For AF=0.37 and n_z=3.8 a decrease of the bending moment at center wing section (BL=0) equal to 30% (normalized with the respect to the Bending Moment evaluated on the FW root @ n_z=1.0 without any load alleviation system (AF=0.0)), is also experienced.

For the Rear Wing (Fig. 24), for both n_z=1 and n_z=3.8, even having different bending moment distribution shapes, there is a decrease of principal bending moment at the wing root. Nevertheless, in this case, there is no benefit to be gained from this trend since the bending moment increases in absolute value.

Furthermore both Fig. 23 and Fig. 24 show a generalized drop of bending moment throughout the whole wing system, from the inner aileron location up to the wing root. It should be noted that the overall decrease in Bending Moment could result in a local increase (in absolute value) far from WCS, close to the inner FW half span. Moreover the higher the imposed alleviation factor the stronger the bending moment increasing far from WCS, thus resulting in a significant limitation to the alleviation. As a result, during the design phase, the absence of local structural failures has to be assured.

Fig. 25 shows that there is a slight shear increasing with respect to the Bending Moment reduction on WCS. Instead, Fig. 26 shows that at the RW root there is a reduction of principal

Shear (an increase in absolute value). This behavior is peculiar to an unconventional configuration such as the Joined-Wing one. Conversely, for a cantilever wing configuration, even if the load alleviator is activated, the principal Shear on the wing root must be constant (the load factor is kept constant). For an aircraft having a Joined Wing configuration, the increase in angle of attack, as a consequence of the load alleviator deflection, produces a rearranging of the aerodynamic load with a subsequent redistribution of internal load characteristics. Since the Front Wing is stiffer, the load augmentation on the FW is higher than on the RW.

2.4. Conclusion Remarks

A formulation for a Symmetric and Balanced Maneuvering Load Alleviation taking into account the aircraft flexibility has been derived. Starting from the linear system (4), it has been illustrated how it is possible to obtain a desired value of the bending moment alleviation in a generic fixed wing station close to the wing root. In order to solve the system (4) in a specific flight condition (depending on vertical load factor, dynamic pressure, and Mach number), the aerodynamic and load derivatives of the airplane must be calculated. A method to determine such derivatives of an aircraft in an unconventional configuration such as a Joined-Wing one, using a modal approach and taking into account aeroelastic effects, has been presented.

The hypothesis of linear aerodynamics leads to a decomposition of the aerodynamic forces making possible the evaluation of the aerodynamic derivatives. The hypotheses of linear structure and unvarying tensor of inertia are supported both by the literature [30] and by the structural behavior of the airplane leading to small structural displacements under limit loads. Moreover the load derivatives are calculated by adopting a method conceived for Joined Wing configurations and mainly based on the structural linearity.

The application to the Joined Wing Unmanned aircraft HAPD has been carried-out.

Having once evaluated the unit Shear and Bending Moment distributions for each unit aerodynamic and inertial contribution, and combining them together with the flight parameters resulting from the solution of the Load Alleviation system (4), the load characteristic distributions can be plotted for different values of nz and AF. Fig. 23 and Fig. 24 show that an important reduction of the bending can be gained, especially in the case of high aspect-ratio

and non-negligible structural flexibility. For the test-case aircraft, an increase of the maximum attainable value of AF with the respect to the dynamic pressure has been observed although the load distribution over the FW and the RW varies because of rising aeroelastic effects (AF varies from 0.19 at V_A to 0.37 at V_C at sea level).

A limitation of the method is its inapplicability in high lift conditions, such as those falling between the points V_S and V_A of the Maneuver Diagram, at the vertical limit load factor, in the case of a positive value of $C_{m\beta}$. In such a situation, with the aircraft at its maximum attitude, the activation of the load alleviation system may produce the aircraft stall. Another limitation consists in the uncontrollability of the internal load far from WCS, for which extensive calculations are to be performed in order to prevent sudden load increase with consequent unexpected structural failures.

Furthermore, Fig. 21 and Fig. 22 are examples of how is possible to obtain, for each value of dynamic pressure and Mach number, a Control Function abacus yielding the change of G with the respect to n_z and AF. Such an abacus can be viewed as an indication for the preliminary design of a control system aimed at controlling the load alleviation in real time, during an unsteady longitudinal maneuver; G is a first estimation of the gain to be used in a SISO (Single Input, Single Output) system in order to link the vertical load factor (output) to the load alleviator deflection (input).

As a further experimental implication, knowing the airplane derivatives for the dynamic pressure and the Mach number measured in flight, a computer system can be designed and engineered as an inboard system aimed at calculating the function G in real time (for a desired value of AF) hence the associated load alleviator deflection for the correct reduction wing bending.

For all the aspects explained above, benefits can be gained from integrating such a system on HAPD: expected fatigue life extension (reflecting on the reusability) and structural weight reduction resulting in greater pay-loads (scientific test devices) for more accurate flight tests and/or better ground observation missions.

3. Longitudinal unsteady maneuvers (open loop): a method to predict the Control Surface Effectiveness when used as Load Alleviator

The activity object of this part of the thesis has been presented at the 4th IC-SCCE, the Fourth International Conference from Scientific Computing to Computational Engineering, held in Athens (Greece) in July of 2010 [44].

The main purpose is again a drop in structural wing bending for improved performances and fatigue life and/or decreased structural weight. The alleviation is performed by means of a symmetric actuation of dedicated control surfaces during an unsteady longitudinal maneuver. The effectiveness of the involved control surfaces, named load alleviators, is evaluated in terms of required deflection angle for a desired bending moment reduction in the wing.

When high maneuver performance is important, internal structural loads reduction becomes significant if the alleviated maneuver can be performed with the vertical load factor kept unvarying. Consequently evaluations on the load alleviator effectiveness in the early design process are appropriate to find the best set of controls.

Performing a LA by means of a symmetrical actuation of ailerons, flaps or other dedicated control surfaces in order to rearrange the aerodynamic loads and thus to shift the aerodynamic center inboard is an old way of working, indeed it has currently become a “must” in the aeronautic scientific community. Consequently evaluations on the load alleviator effectiveness in the early design process are necessary to find the best set of controls to be adopted.

The following methodology offers a practical approach to predict the control surface effectiveness when they are used as load alleviators during a longitudinal unsteady maneuver. The load alleviator deflection time history is evaluated a priori, simply depending upon elevators time history, system characteristics and flight condition. The whole process is based on open loop calculations only (without feed-back calculations) and involves methods that take into account the aircraft flexibility together with plunge and pitch rigid-body motions by applying a modal approach.

An application to a business aircraft has been performed for two kinds of symmetric maneuvers taking into account the structural flexibility. By adopting the outboard ailerons as

load alleviators, the maximum bending reduction at the wing root is about 37 percent, with a maximum aileron deflection less than 12 degrees.

3.1.Methodology

The hypotheses of this study are:

- the airplane is in level flight with the longitudinal balance assured by a symmetric deflection of the elevators;
- the aircraft performs a symmetric maneuver by deflecting the elevators according to a chosen time history starting from their trim position;
- there is complete linearity of structure and aerodynamics;
- the tensor of inertia is kept constant;

The driving idea of the survey is to calculate the alleviated maneuver and to asses the control surfaces (load alleviator) effectiveness by means of open loop calculations, that is the load alleviator moves without feedback inputs, but its time history is calculated from the elevator deflection time history and the flight condition only. If the aircraft flexibility is accounted for, the load alleviator deflection depends on the aircraft structure too.

The load alleviator deflection time history is assigned as having the same shape and frequency content of the elevator one, but having a time delay depending on the flight condition (Mach number, dynamic pressure, altitude) and on the aircraft structure (stiffness and inertia distributions): it is calculated as shown in section 3.2.

The alleviated maneuver is completely determined when the Alleviation Factor (AF) is established. It specifies the percentage of the maneuver incremental load reduction in a specific control section. Since the load characteristic to be alleviated is the bending moment (Mx), AF is calculated as follows:

$$AF = \frac{\Delta M_x - \Delta M_{xALL}}{\Delta M_x} \cdot 100 \qquad (27)$$

where the subscript ALL specifies that the bending moment refers to the alleviated maneuver.

Then the deflection time histories of elevators and load alleviators are re-modulated in order to get the desired load reduction (according to AF) and keeping the maximum vertical load factor attained during the unalleviated maneuver. The maximum attainable value of AF is bounded by the maximum deflection and/or deflection velocity of the load alleviator, depending on the flight condition or on mechanical limit stops.

The maximum AF value, in a generic flight condition, measures the load alleviator effectiveness.

Calculations are carried-out by using a Modal Approach, typical of the Dynamic Aeroelasticity domain. With the respect to a conventional approach, the principal advantage is that, it is possible to solve a generic structural static problem without fixing a suitable number of constraints: the airplane can be considered unrestrained. By using such an approach the structural deformation of the airplane is approximated by a set of N symmetrical normal modes (free-free): 2 rigid modes (plunge and pitch modes) plus N-2 elastic modes.

$$\begin{cases} u(x,y) = \sum_{i=1}^{N} q_i \, \phi_i^x(x,y) \\ v(x,y) = \sum_{i=1}^{N} q_i \, \phi_i^y(x,y) \\ w(x,y) = \sum_{i=1}^{N} q_i \, \phi_i^z(x,y) \end{cases} \tag{28}$$

The theoretical aeroelastic model is the same as that presented in the section 2.3.4: starting form the general equation of Dynamic Aeroelasticity (Eq. (6)), being the quasi-steady aerodynamic pressures evaluated for small values of the reduced frequency, with the hypotheses of negligibility of:

- elastic accelerations with the respect to rigid ones;
- elastic velocities with the respect to rigid ones;
- control speed with the respect to control deflection;

two uncoupled differential equations are obtained (Eqs. (22) and (23)), now rewritten for reasons of simplicity:

$$\underline{q}_E = \underline{\underline{F}}_{0,ER}\,\underline{q}_R + \underline{\underline{F}}_{1,ER}\,\dot{\underline{q}}_R + \underline{F}_{0,EC}\,\delta + \underline{F}_{0,Eq} + \underline{F}_{0Eext}\,. \tag{22}$$

$$\underline{\underline{m}}_{RR}\ddot{\underline{q}}_R + \hat{\underline{\underline{C}}}_{RR}\dot{\underline{q}}_R + \hat{\underline{\underline{K}}}_{RR}\underline{q}_R = \underline{F}_{extq} + \underline{F}_{ext0} + \underline{F}_C\delta(t)\,. \qquad (23)$$

Eq. (22), together with eq. (23) are the main equations in the symmetric quasi-steady aeroelasticity, from which the evolution of a symmetric maneuver during time can be evaluated. The equations above are written for a single control surface (i.e. the elevator for an unalleviated maneuver), but it is possible to write the same equations by involving two or more controls (i.e. the elevator and the load alleviator for an alleviated maneuver), by simply changing some formal notations.

3.2. Load Alleviator Delay and Alleviated Maneuver Calculation

Once developed a quasi-steady maneuver due to any control surface deflection, it is possible to evaluate the Bending Moment time-history at each wing control station.

In order to reduce the bending moment at the wing root, a symmetrical actuation of the ailerons is applied with their deflection having the same shape and frequency content of the elevator deflection time-history. Ailerons are chosen to be used as load alleviators.

The following method provides a practical way (although not rigorous by a strict mathematical point of view) of estimating the delay of the Load Alleviator input signal and to "re-modulate" in amplitude the elevator and aileron signals in order to get an effective (desired) reduction of the wing root bending and thus of measuring the effectiveness of the load alleviators. It has to be emphasized that the alleviation is always performed by keeping the same maximum vertical load factor attained during the unalleviated maneuver. The load alleviator delay is evaluated according to the following steps:

- Choice of flight condition parameters such as Mach number, altitude, aircraft speed;
- Aeroelastic balanced maneuver calculation in order to compute initial maneuver conditions;
- Choice of the elevator time history signal;
- Symmetric quasi-steady maneuver calculation in order to evaluate the maximum bending in the control station and the maximum vertical load factor during the

unalleviated maneuver (imposed if the maneuver is of a "checked" type according to the EASA Airworthiness Requirements);

- Fast Fourier Transformation (FFT) of the elevator signal in order to compute its main frequency (an example is depicted in Fig. 27);
- Evaluation of the aeroelastic aircraft response to a Dirac-type elevator deflection signal in order to compute the response delay with the respect to the input frequency (see Fig. 28);
- Estimation of the aileron deflection signal delay as the phase delay corresponding to the main frequency of the elevator FFT signal (see Fig. 28).

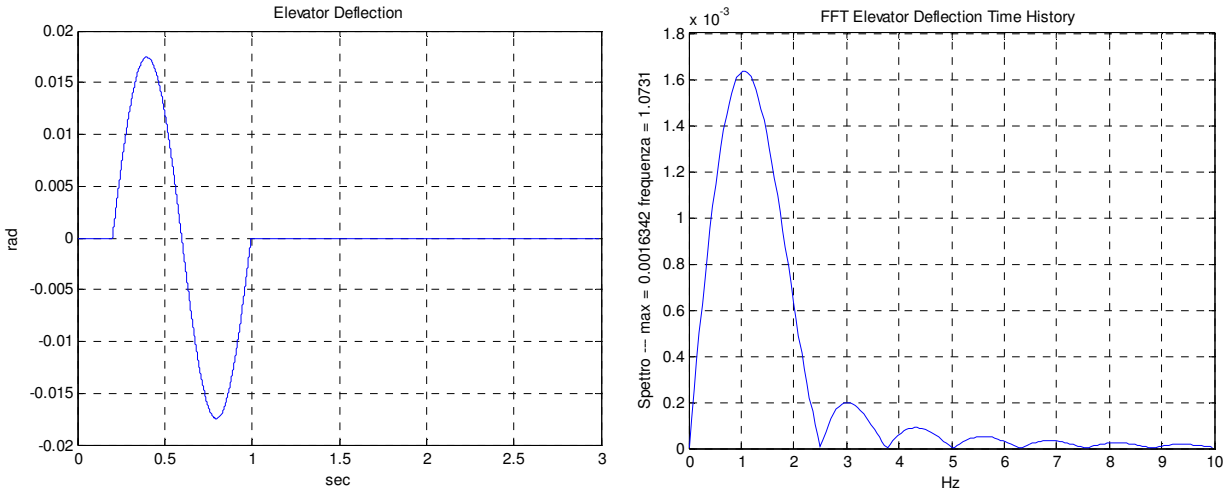

Fig. 27: Example of Elevator Deflection signal and its frequency content.

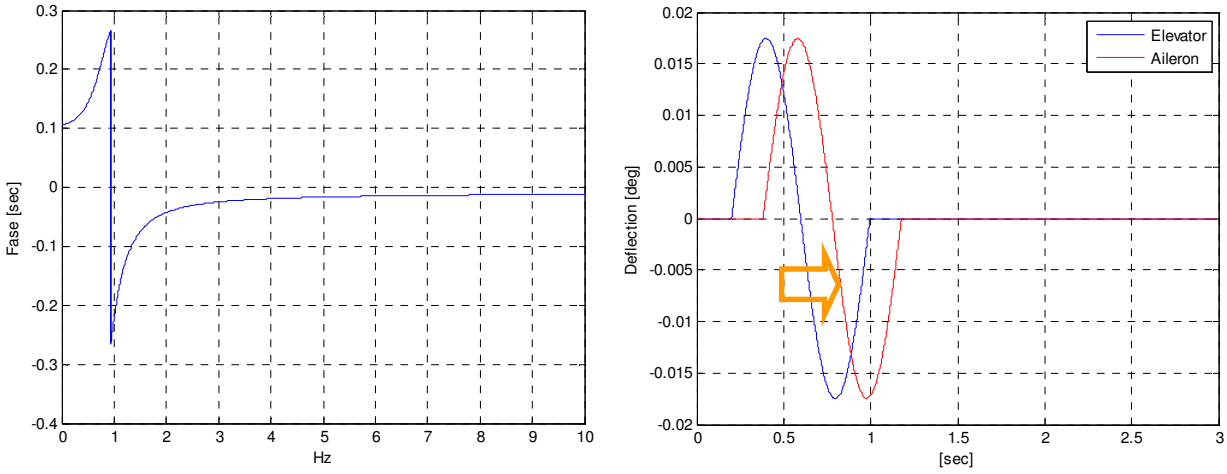

Fig. 28: Response delay with the respect to the input frequency; Unit elevator and aileron signals.

The flow diagram of Fig. 29 summarizes the whole process (blue: starting points; black: unalleviated maneuver; green: calculation steps for estimating the aileron delay; red: iterative process).

The iterative process of Fig. 30 consists in a series of symmetric and quasi-steady maneuver calculations with two input control surface signals. Figure 4 shows each logical step of the iterative process.

The Iterative process converges when the root bending is that one specified by fixing AF and the maximum vertical load factor is the same as that one attained during the unalleviated maneuver.

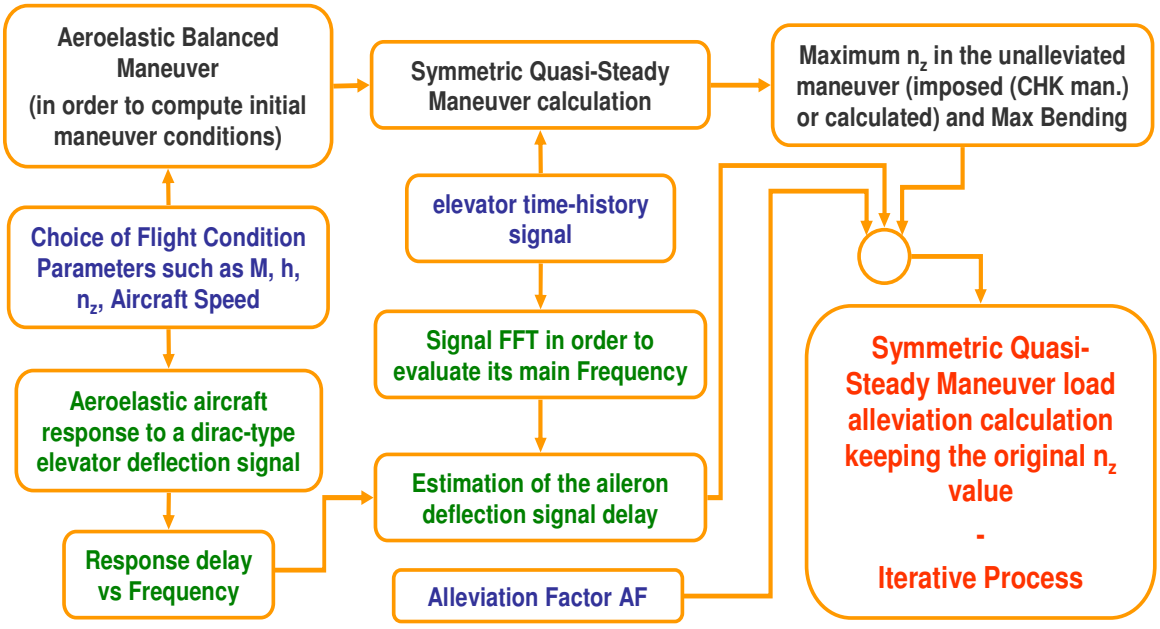

Fig. 29: Load Alleviator Delay Calculation, Flow Diagram.

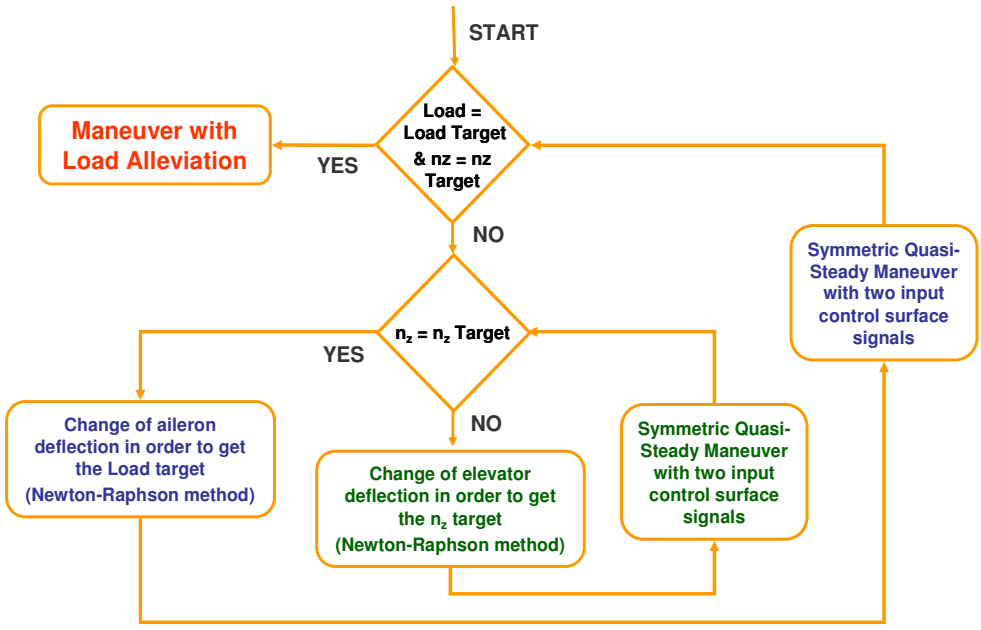

Fig. 30: The Iterative Process.

3.3. Application to a Business Aircraft

An application on an EASA CS-25 Business aircraft has been performed [45]. The aircraft platform together with the calculation parameters are presented in the following figure and tables. A single flight condition has been considered. The maximum vertical load factor is 2.6.

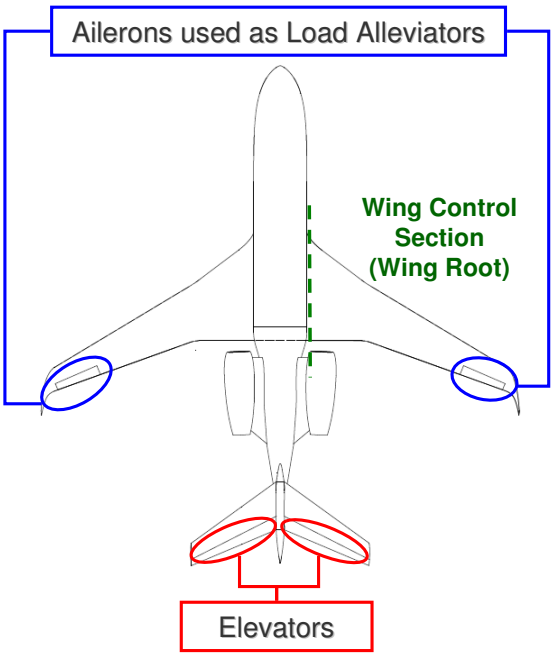

Fig. 31: Aircraft platform, elevators and ailerons used as load alleviators.

Altitude [ft]	Altitude [m]	KCAS [knot]	TAS [m/s]
8000.0	2438.40	330.00	189.62

Table 3: Calculation parameters: altitude and aircraft speed.

M	Density [kg/m^3]	Dyn Press [Pa]
0.573	0.9629	17309.6

Table 4: Calculation parameters: Mach number, air density and dynamic pressure.

Mass	Description	Mass [kg]	XcG %MAC
OEWMF	OEW + Max Fuel	---	21.25

Table 5: Mass properties (Operative Empty Weight + Max Fuel).

The aeroelastic model is made up of an aerodynamic model for DLM calculations, a dynamic model and a matching model. The dynamic model is of stick-beam type for wing, fuselage and tail-planes while the junctions are modeled by means of DMIG matrices [43]. Winglets and nacelles are considered rigid. The inertia is modeled by a set of concentrated masses with their own moments of inertia. The matching model – link between aerodynamics and structure – is made up of a set of grids (Interface Grids) for load and displacement interpolations.

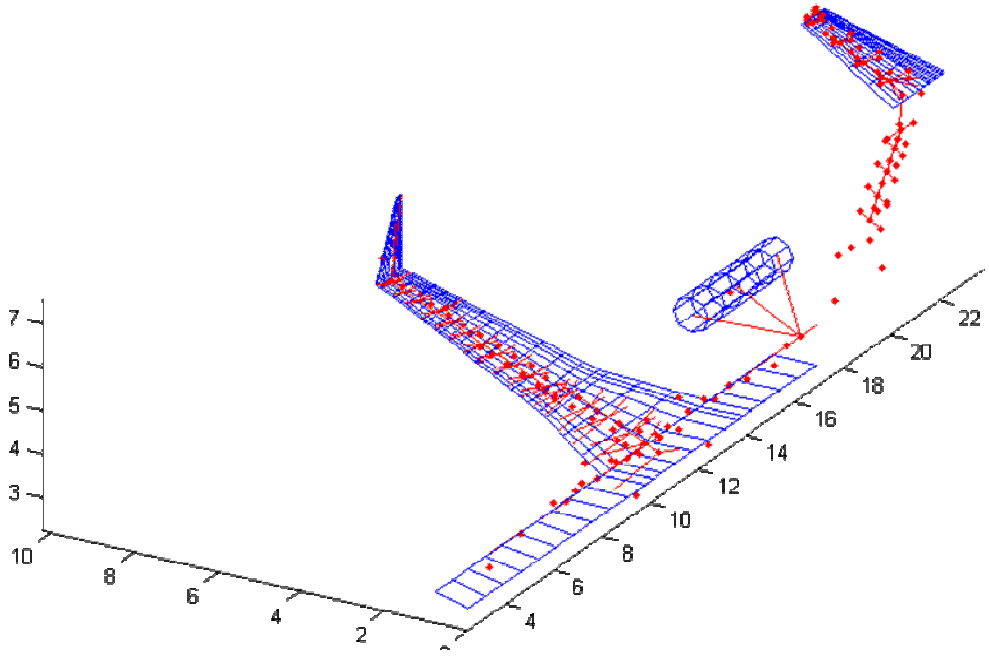

Fig. 32: Numerical Models (blue: aerodynamics, red: structural and inertia models).

The Load Integration Model contains all the information useful to calculate design loads (coming from the aerodynamic and the inertia distributed loads) in terms of load characteristics (bending, shear and torsion). It is made up of four different Load Coordinate Reference Systems (LCRS) each one with its own Load Reference Axis (LRA), functional to integrate external loads on wing, front fuselage, rear fuselage and horizontal tail.

The wing LCRS is obtained as follows:

- The Origin is the intersection between the extrapolation of the elastic axis of the outer wing box (from the kink to the wing tip) and the plane of symmetry;
- A generic point A belonging to that elastic axis belongs also to the y-axis;
- The point B=(x_A; y_A; z_A+Dz) belongs to the YZ-plane.

The y-axis of the LRCS represents the LRA. The wing LRCS and the LRA are depicted in the following figure.

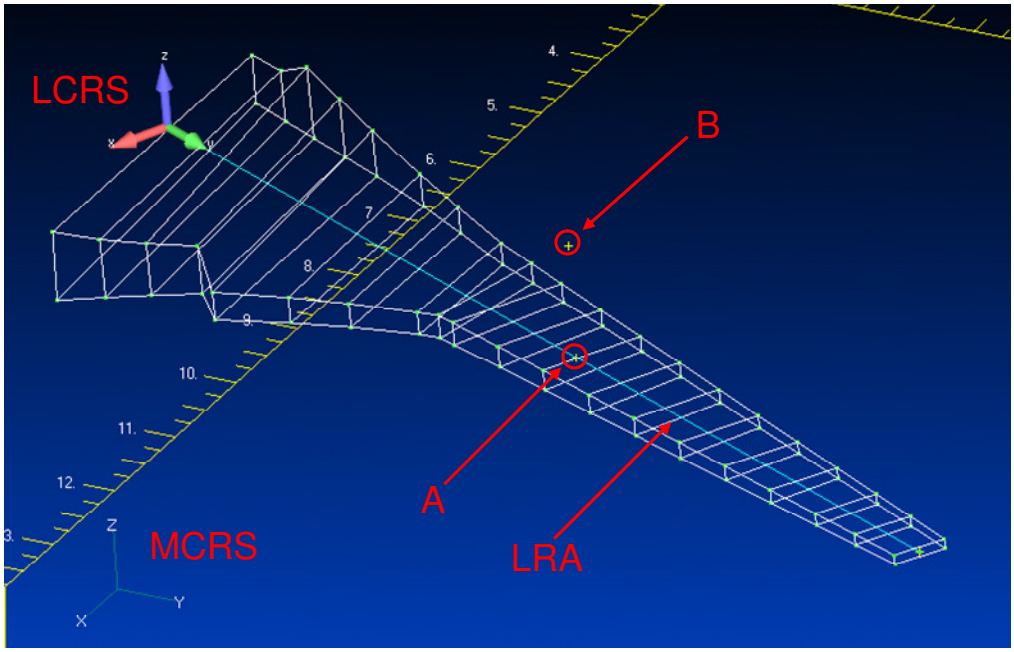

Fig. 33: Wing Load Coordinate Reference System and Load Reference Axis.

Fig. 34 shows LCRSs for the whole aircraft.

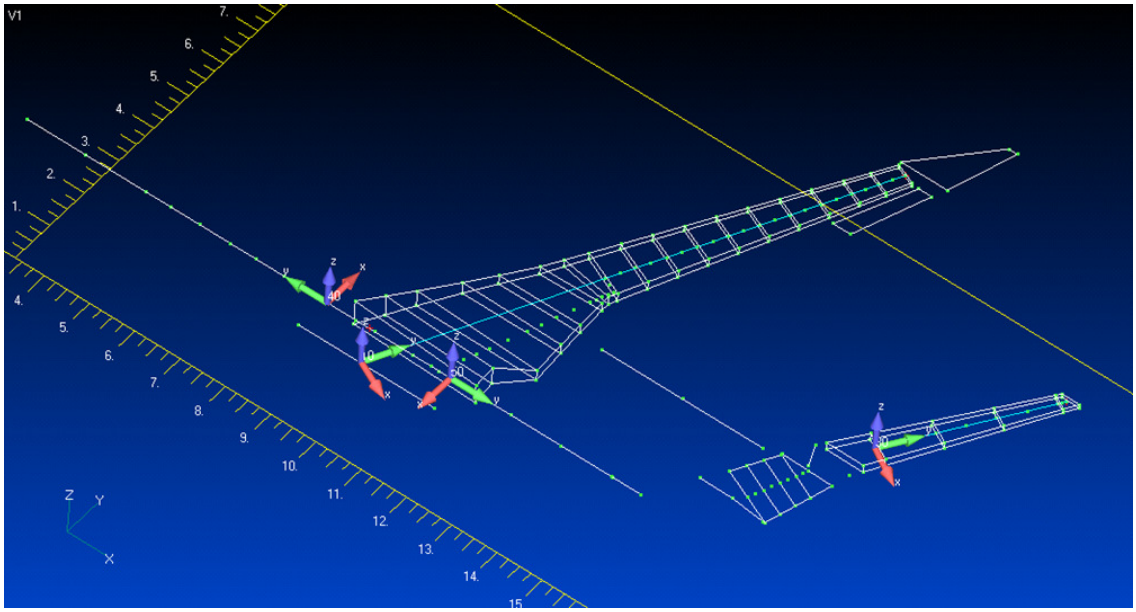

Fig. 34: Load Coordinate Reference Systems on the entire aircraft.

The numerical process has been tested for two kinds of longitudinal maneuvers: a checked maneuver according to Airworthiness Requirements and a generic climb start maneuver.

3.3.1. Checked Maneuver according to the EASA CS-25 Airworthiness Requirements

A checked maneuver has been performed according to EASA CS-25.331 (c) (2) [45]. The elevator deflection time history is that shown in Fig. 27, but re-modulated in order to get the limit vertical load factor. Several alleviated maneuvers have been developed corresponding to different values of AF. The following figure shows the vertical load factor at the center of gravity, elevator and aileron deflections, root bending and root shear versus time.

Notice that notwithstanding the incremental bending moment drops down, there is a shear reduction too. Furthermore when AF increases the maximum aileron deflection increases too and the maximum elevator deflection slightly decreases because of the positive sweep of the wing (the symmetrical actuation of the aileron helps to perform the maneuver).

No variation has been obtained as regards the maximum vertical load factor; the load alleviation so obtained causes only a shift in time (a delay) of the load factor time history.

The maximum attained values of the above mentioned quantities together with the maximum aileron deflection velocity are plotted in Fig. 36 against AF.

The aileron slope together with the aerodynamic hinge moment time history have to be monitored during time because their product results in the necessary actuator control power. This value represents a primary indication for an MLC feasibility. Such a concept will be discussed again in the next chapter.

The maximum AF (34 percent), measuring the aileron effectiveness when used as load alleviator, is bounded by the maximum allowed aileron deflection. This limit is less than the mechanical limit stop because it is necessary to provide margin for roll control command at high load factor. In fact, when aileron are used as load alleviators, an MLC system has to be in series with the roll control system until the mechanical control stops are reached.

The MLC series servo authority limits are established as 15 degrees both trailing-edge up and trailing-edge down.

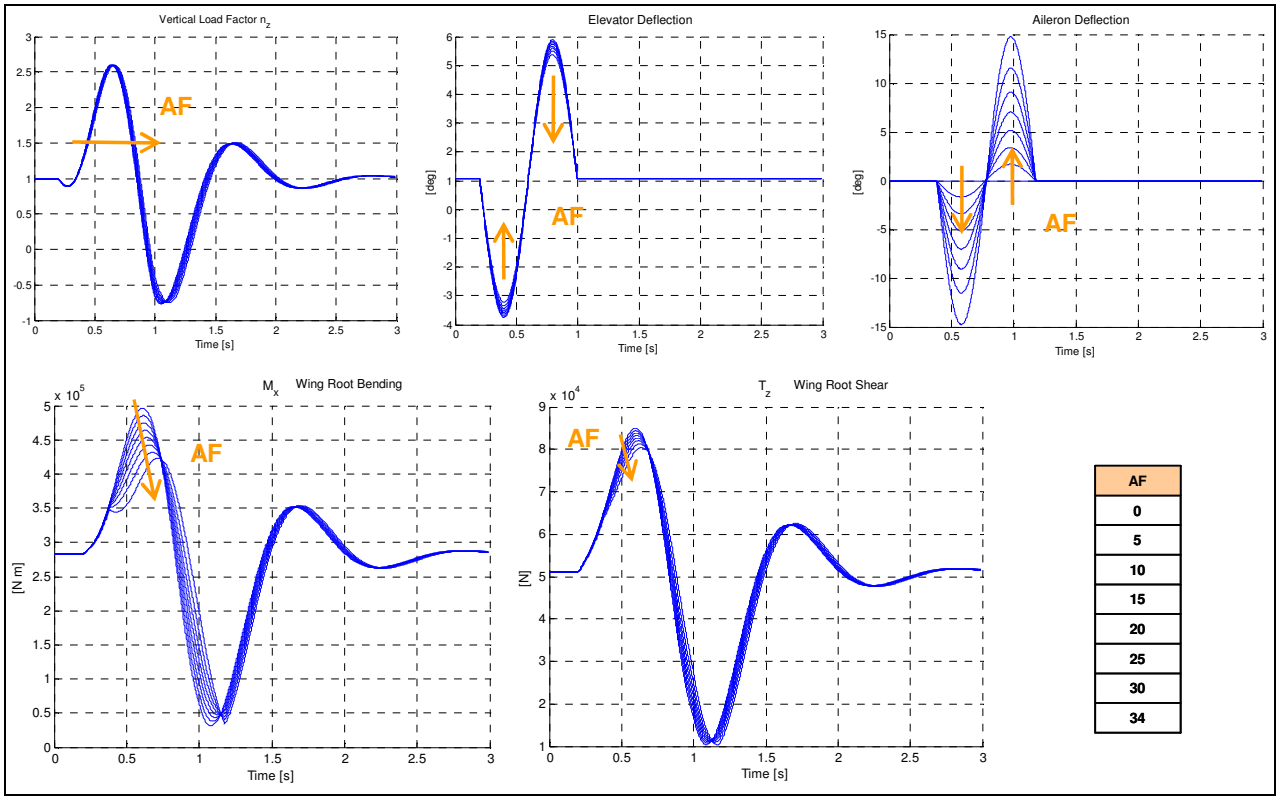

Fig. 35: Alleviated Checked Maneuver: load factor, control displacements, wing root loads.

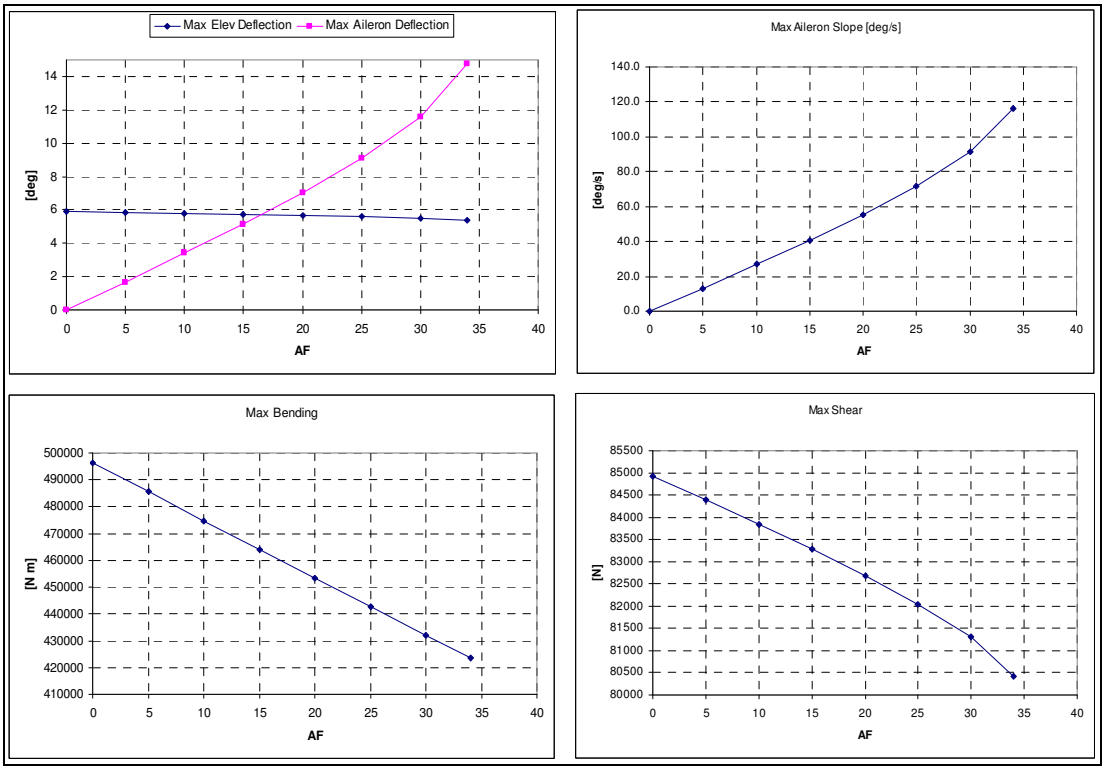

Fig. 36: Alleviated Checked Maneuver: maximum control deflections, wing root loads and aileron slopes.

3.3.2. Climb Start Maneuver

A symmetric maneuver similar to a generic climb start maneuver has been performed. Different alleviated maneuvers have been developed for a set of AF values. The following figure shows vertical load factor at the center of gravity, elevator and aileron deflections, root bending and root shear versus time.

Also in this case a reduction of the bending moment is followed by a (less pronounced) reduction of the shear. Moreover when AF increases the maximum aileron deflection increases (in absolute value) and the maximum incremental elevator deflection slightly decreases.

The maximum attained values of the above mentioned quantities together with the maximum aileron deflection velocity are plotted in Fig. 38 with the respect to AF.

The maximum possible value of AF is 37%. For this kind of maneuver, the limit is represented by the aircraft characteristics, even if a maneuver is performed with a maximum aileron deflection smaller than -12 degrees, AF does not increase. Moreover, if an AF greater than 37% is imposed in the iterative process, it does not converge.

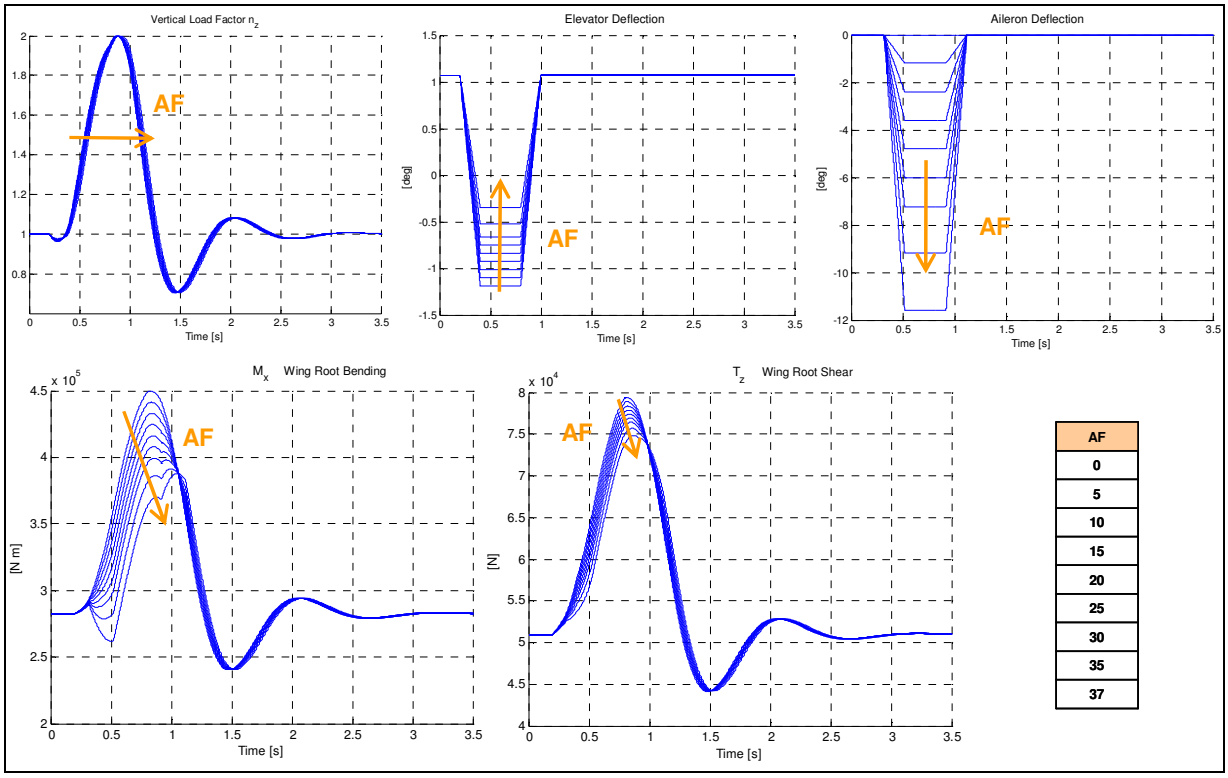

Fig. 37: Climb Start Maneuver: load factor, control displacements, wing root loads.

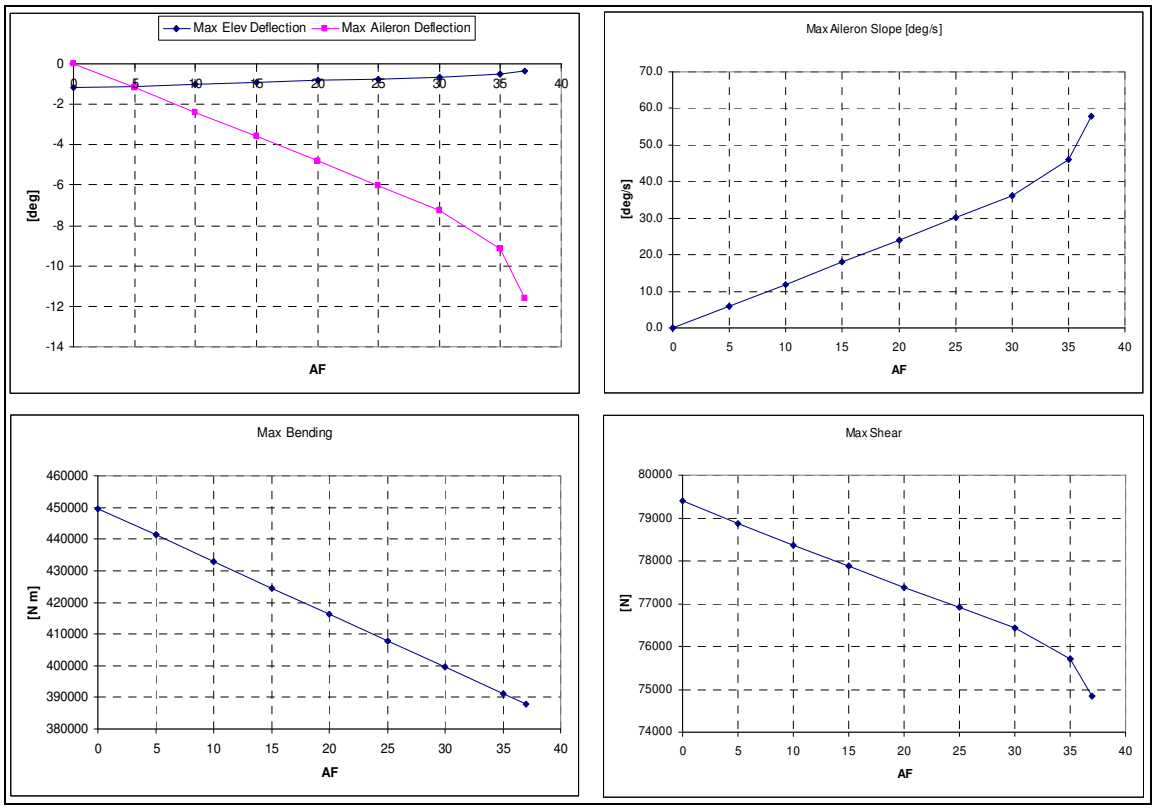

Fig. 38: Climb Start Maneuver: maximum control deflections, wing root loads and aileron slopes.

3.4. Conclusion Remarks

An approach to predict the Control Surface Effectiveness when used as Load Alleviator during a longitudinal unsteady maneuver has been shown. An application on an EASA CS-25 Business Aircraft has been performed for two kinds of maneuver.

The method provides a way of calculating the delay of the Load Alleviator input signal (deflection time history) and to "re-modulate" in amplitude the elevator and aileron signals in order to reduce the wing root bending moment. The alleviation is always performed by keeping the same maximum vertical load factor attained during the unalleviated maneuver.

The maximum attainable value of AF measures the load alleviator effectiveness. It is bounded by the maximum achievable aileron deflection during flight (aeroelastic or mechanical authority limits) or, in some cases (as that presented in section 3.3.2), by the inherent nature of the airplane. By adopting the ailerons as load alleviators, for a generic climb start maneuver, the maximum bending reduction at the wing root is about 37 percent, with a maximum aileron deflection less than 12 degrees.

The whole process is based on open loop calculations only and involves methods that permits to take into account the aircraft flexibility together with plunge and pitch rigid-body motions by applying a modal approach. No systems aimed at automatically reducing the root bending during maneuver are developed. Such a MLC system will be the focus of the next chapter.

Although for this application the ailerons are used as load alleviators, it is highly recommended – for providing margin for roll control command at high load factors - to have dedicated control surfaces for this purpose. For this reason the quite effortless method presented so far can be a helpful means during the conceptual design phase.

4. Longitudinal Unsteady Maneuvers (closed loop): Conceptual Design and Analysis of a MLC system

In this chapter, a conceptual design of an active control system for load alleviation due to longitudinal maneuvers is presented. This system has been conceived for the specific purpose of providing reduced incremental wing bending moments due to maneuvers for improved pay-loads/gross weight capabilities and/or extended structural fatigue life.

An application to a business aircraft responding to the EASA Certification Specifications, Part 25, has been performed. The aircraft used for the numerical application is considered only as a test case-study. Most of design and analysis considerations are applicable also to other aircraft, such as unmanned or military ones, although some design requirements can be clearly different.

All numerical analyses aimed at simulating the aircraft behavior during maneuver with MLC-on or MLC-off are performed both by taking into account and by neglecting the flexibility of the aircraft. Indeed the whole study is addressed to show how much is important to consider the effect of aeroelasticity early during the conceptual design of such a MLC system, hence by providing also much more reliable indications about the quality of flight mechanics and the design of other systems such as servos or control surfaces.

To better understand the entire work, Feedback Control Systems (FCS) have to be introduced. A much more detailed discussion than that presented herein can be found in [46] and [47].

Typically, three goals are associated with the analysis of a FCS:

- System stability evaluation;
- Transient response behavior determination (to some kinds of inputs);
- Steady state performance determination (to some kinds of inputs).

These objectives are accomplished by means of three analysis steps: determination of the transfer functions of all system components; system architecture construction concerning the flow of input, feedback and output signals; evaluation of system characteristics in terms of stability and performance.

Indeed, in case of **design** of a FCS, the following objectives have to be pursued:

- **Compliance with performance specifications**. These performance specifications serve as physical and/or mathematical constraints on the system and its components. In various military and civilian regulations, the following performance characteristics are usually specified:
  - Speed of response;
  - Relative stability;
  - System accuracy (allowable error).
- **Robustness and Simplicity.** A system can be considered robust if its closed loop performance characteristics do not vary greatly with changes in its parameters. Robustness involves not only changes in parameters depending on flight conditions but also errors and/or uncertainties related to engineering estimations and/or measurements. Moreover a system should be as simple as possible because of possible problems related to feasibility, unreliability, maintainability and/or reparability.

4.1.Feedback Control Systems installed on modern aircraft

Several Feedback Control Systems are currently installed on civilian and military aircraft. Some of them are aimed at increasing the airplane stability and others at controlling flight parameters (such as autopilot systems).

A stability augmentation system has the purpose of increasing static and/or open-loop dynamic stability of the aircraft. Examples of this kind of systems are the pitch and yaw dampers, necessary for high performance aircraft that tends to deteriorate their short period and dutch roll damping at high altitude and/or low speed (i.e. at low dynamic pressure).

Several military aircraft (fighters) are commonly designed by following the purpose of poor static longitudinal and directional stability for enhanced maneuverability. Even in the case of longitudinal stability many fighters are designed by having inherent negative static margins (unstable airplane). Thus some form of stability augmentation is required to make such airplanes appear to the pilot as normally responding airplanes.

Another interesting form of stability augmentation is found in the so-called control-wheel-steering system (or, in the case of a fighter, control-stick-steering system). With the aid of such a system it is possible to control an airplane with the control wheel (or control stick) by adding a force o position transducer to the control column and to consider the output of that transducer to be a pitch rate command signal.

Most of long range commercial transport are equipped with autopilot systems in order to reduce the pilot workload. Autopilots allow some form of automatic control or navigation: in the first case they are utilized for keeping constant pitch attitude, angle of attack, altitude, bank and heading angle; in the second case typical navigation modes are glide slope intercept and hold, localizer intercept and hold or automatic landing modes.

In either case, the automatic FCS uses always aerodynamic controls, commonly aerodynamic control surfaces. Several airplanes still have reversible flight control systems. Integration of automatic feedback loops for this kind of flight controls leads to feedback of control system motions to the cockpit controls. Notwithstanding this can be desirable for autopilots, it becomes outcome when the system is in a stability control mode. The most used way to solve this problem is the use of separate control surface systems.

4.2. An automatic LAS/MLC system for high performance aircraft

The most used types of FCSs to alleviate inherent stability problems or to control flight parameters are:

- Angle of Attack Feedback to the longitudinal controls (elevators or canards);
- Load factor feedback to the longitudinal controls (elevators or canards);
- Angle of sideslip feedback to the directional controls (rudders).

The LAS object of this work is aimed at obtaining wing bending reduction (near the wing root) but by attaining always the same design vertical load factor. In order to pursue this aim, the LAS incorporates a Load Factor Feedback (LFF) to the elevators in order to perform a longitudinal maneuver by automatically following a desired load factor time history as a reference signal.

The MLC is accomplished by observing the bending on the root wing station and acting on the load alleviators (specific control surfaces as ailerons and/or flaps) in order to shift the wing center of pressure inboard.

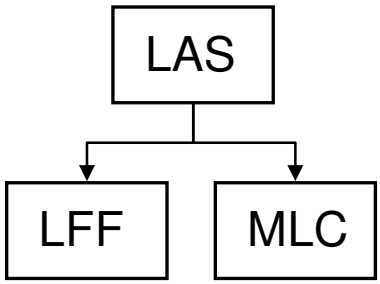

Fig. 39: LAS Macro-Systems.

The structural load reduction can be carried-out in two ways:

1. By activating the MLC when the bending reaches a specified absolute value (less than the limit design value with MLC-off);

2. By using a reference signal identically zero for the incremental bending so that the MLC immediately acts when the acting load exceeds the reference 1-g bending. Such reference is not a unique value, it is represented by a range of values, to be calculated for a combination of different flight conditions (Mach number versus altitude for each mass condition).

The main practical issue is related to the bending moment observation. This can be accomplished by means of strain gages measurements, as illustrated in literature [48]-[50]. Ground calibrations are needed in order to correlate all strain gage signals to the bending moment acting on the wing control station. The experimental procedure is not the topic of this work, thus the reader is referred to [51]-[54].

The load factor is kept compliant with the desired reference signal whether or not the MLC is switched on or off since the load factor perturbation is controlled and minimized by the action of the LFF. On the other hand the LFF acts on the longitudinal control by deflecting elevators and thus by varying angle of attack and other flight parameters that affect the wing root bending.

Several practical activity are involved in the conceptual design of such a composed system. One of them is the servo-actuator necessary power monitoring, coming from the

product of the load alleviator aerodynamic hinge moment and its deflection velocity. The resultant value, in a conceptual design stage, drives the choice of servo-line and actuators. If the system has to be installed on an existing airplane, the calculated value must always be less than the maximum available actuation power.

4.3.Application to a business aircraft

The aircraft used for the numerical application is a business jet responding to the EASA Certification Specifications Part 25. Generic information about the airplane are given in section 3.3, together with a brief description of the aeroelastic model (aerodynamic, dynamic and interface model). The WCS is the wing root.

Table 6 shows the combinations of speed and altitude chosen as flight conditions to be analyzed. The first four (#1, #2, #3, #4) are at the same CAS but with different altitude from sea level to about 30 kft. The other ones are chosen to carry-out sensitivities versus the Mach number (label "SM") and the dynamic pressure (label "Sq").

ID	Altitude [ft]	Altitude [m]	KEAS [knot]	EAS [m/s]	KTAS [knot]	TAS [m/s]	M	Density [kg/m3]	Dyn Press [Pa]
Altitude from sea level to 29275 ft with constant KCAS=330									
#1	0.0	0.0	330.0	169.8	330.0	169.8	0.499	1.225	17652.6
#2	8000.0	2438.4	326.8	168.1	368.6	189.6	0.573	0.963	17309.6
#3	20000.0	6096.0	319.7	164.5	437.9	225.3	0.713	0.653	16565.4
#4	29275.1	8923.0	311.5	160.2	502.5	258.5	0.850	0.471	15728.4
Sensitivity versus the Mach Number									
#2SM0	555.1	169.2	326.8	168.1	329.4	169.5	0.499	1.205	17309.6
#2	*8000.0*	*2438.4*	*326.8*	*168.1*	*368.6*	*189.6*	*0.573*	*0.963*	*17309.6*
#2SM1	18953.4	5777.0	326.8	168.1	439.8	226.3	0.713	0.676	17309.6
#2SM2	27136.2	8271.1	326.8	168.1	507.1	260.9	0.850	0.509	17309.6
Sensitivity versus the Dynamic Pressure									
#2Sq0	5466.4	1666.1	342.7	176.3	371.8	191.3	0.573	1.041	19040.6
#2	*8000.0*	*2438.4*	*326.8*	*168.1*	*368.6*	*189.6*	*0.573*	*0.963*	*17309.6*
#2Sq1	10709.9	3264.4	310.0	159.5	364.8	187.7	0.573	0.885	15578.7
#2Sq2	13695.7	4174.4	292.3	150.4	360.7	185.6	0.573	0.804	13847.7

Table 6: Calculation Data, Flight cases.

All of these flight conditions are analyzed for three different mass configurations, i.e. for empty fuel tank (MZFW), full fuel tank (MTOW) and an intermediate condition (50% fuel). Table 7 reports center of gravity positions normalized to the MAC.

ID	Mass	Description	Mass [kg]	XcG %MAC
M1	MTOW	OEW + Max Pay-Load + Fuel to get the MTOW	---	22.55
M2	---	OEW + Max Pay-Load + 1/2 Fuel to get the MTOW	---	25.74
M3	MZFW	OEW + Max Pay-Load	---	30.55

Table 7: Calculation Data, Mass Conditions.

All calculations have been performed for rigid and elastic aircraft.

4.3.1. State-Space Model for Longitudinal Maneuvers

The airplane, in level flight, is modeled by means of a state-space system aimed at simulating unsteady longitudinal maneuvers.

Being the aircraft flexibility accounted for, the theoretical model is based on the general equation of the dynamic Aeroelasticity (Eq. (6), a system of N+2 differential equations of motion, where N is the number of elastic modes). With the hypotheses of negligibility of

- elastic accelerations with the respect to rigid ones;
- elastic velocities with the respect to rigid ones;
- control speed with the respect to control deflection;

it becomes a system of two differential equations of motion in the two degrees of freedom of plunge and pitch rigid body motions (for a more detailed presentation see section 2.3.4).

$$\underline{\underline{m}}_{RR}\,\underline{\ddot{q}}_R + \underline{\underline{\hat{C}}}_{RR}\,\underline{\dot{q}}_R + \underline{\underline{\hat{K}}}_{RR}\,\underline{q}_R = \underline{F}_{extq} + \underline{F}_{ext\,0} + \underline{F}_C\,\delta(t) + \underline{F}_{CC}\,\beta(t)\,, \qquad (29)$$

$$\underline{q}_R = \begin{pmatrix} h \\ \theta \end{pmatrix} = \begin{cases} Plunge \\ Pitch \end{cases} \qquad (7)$$

In the Eq. (29), $\underline{F}_C$ and $\underline{F}_{CC}$ contain respectively the force coefficients for elevator and aileron controls. By choosing the state as

$$\underline{x} = \begin{bmatrix} \underline{q}_R \\ \underline{\dot{q}}_R \end{bmatrix}, \qquad (30)$$

and the input as

$$\underline{u} = \begin{bmatrix} \delta \\ \beta \end{bmatrix}, \tag{31}$$

Eq. (29) can be written in the controllable canonical form

$$\dot{\underline{x}} = \underline{\underline{A}}\,\underline{x} + \underline{\underline{B}}\,\underline{u}\,, \tag{32}$$

with

$$\underline{\underline{A}} = \begin{bmatrix} 0 & \underline{\underline{I}} \\ -\underline{\underline{m}}_{RR}^{-1}\underline{\underline{\hat{K}}}_{RR} & -\underline{\underline{m}}_{RR}^{-1}\underline{\underline{\hat{C}}}_{RR} \end{bmatrix}, \tag{33}$$

and

$$\underline{\underline{B}} = \begin{bmatrix} 0 & 0 \\ -\underline{\underline{m}}_{RR}^{-1}\underline{F}_{C} & -\underline{\underline{m}}_{RR}^{-1}\underline{F}_{CC} \end{bmatrix}. \tag{34}$$

The output vector contains Shear, Bending and Torsion at the WCS (wing root), vertical load factor, pitch acceleration and aileron hinge moment (HM_{ail}).

$$\underline{y} = \begin{bmatrix} S \\ M \\ T \\ n_z \\ \ddot{\theta} \\ HM_{ail} \end{bmatrix}. \tag{35}$$

Load Derivatives of Shear, Bending moment and Torsion are calculated for each load case (different altitude, Mach number and mass condition) at the WCS by following the same procedure as that presented in section 2.2.

With the same symbol meanings

$$\begin{cases} S = S_0 + \begin{bmatrix} 0 & S_\alpha \end{bmatrix}\underline{q}_R + \begin{bmatrix} S_{\dot{h}} & S_{\dot{\alpha}} \end{bmatrix}\dot{\underline{q}}_R + \begin{bmatrix} S_{\ddot{h}} & S_{\ddot{\alpha}} \end{bmatrix}\ddot{\underline{q}}_R \\ M = M_0 + \begin{bmatrix} 0 & M_\alpha \end{bmatrix}\underline{q}_R + \begin{bmatrix} M_{\dot{h}} & M_{\dot{\alpha}} \end{bmatrix}\dot{\underline{q}}_R + \begin{bmatrix} M_{\ddot{h}} & M_{\ddot{\alpha}} \end{bmatrix}\ddot{\underline{q}}_R \\ T = T_0 + \begin{bmatrix} 0 & T_\alpha \end{bmatrix}\underline{q}_R + \begin{bmatrix} T_{\dot{h}} & T_{\dot{\alpha}} \end{bmatrix}\dot{\underline{q}}_R + \begin{bmatrix} T_{\ddot{h}} & T_{\ddot{\alpha}} \end{bmatrix}\ddot{\underline{q}}_R \end{cases}. \tag{36}$$

By taking the following positions:

$$\begin{array}{lll} \underline{LD}_{\dot{h}} = \begin{bmatrix} S_{\dot{h}} & M_{\dot{h}} & T_{\dot{h}} \end{bmatrix}^T & \underline{LD}_{\alpha} = \begin{bmatrix} S_{\alpha} & M_{\alpha} & T_{\alpha} \end{bmatrix}^T & \underline{LD}_{\delta} = \begin{bmatrix} S_{\delta} & M_{\delta} & T_{\delta} \end{bmatrix}^T \\ \underline{LD}_{\ddot{h}} = \begin{bmatrix} S_{\ddot{h}} & M_{\ddot{h}} & T_{\ddot{h}} \end{bmatrix}^T & \underline{LD}_{\dot{\alpha}} = \begin{bmatrix} S_{\dot{\alpha}} & M_{\dot{\alpha}} & T_{\dot{\alpha}} \end{bmatrix}^T & \underline{LD}_{\beta} = \begin{bmatrix} S_{\beta} & M_{\beta} & T_{\beta} \end{bmatrix}^T \\ & \underline{LD}_{\ddot{\alpha}} = \begin{bmatrix} S_{\alpha} & M_{\ddot{\alpha}} & T_{\ddot{\alpha}} \end{bmatrix}^T & \end{array}; \quad (37)$$

$$\begin{array}{c} \underline{\underline{K}}_1 = \begin{bmatrix} 0 & \underline{LD}_{\alpha} \end{bmatrix} \\ \underline{\underline{K}}_2 = \begin{bmatrix} \underline{LD}_{\dot{h}} & \underline{LD}_{\dot{\alpha}} \end{bmatrix}; \\ \underline{\underline{K}}_3 = \begin{bmatrix} \underline{LD}_{\ddot{h}} & \underline{LD}_{\ddot{\alpha}} \end{bmatrix} \end{array} \quad (38)$$

$$\begin{array}{c} \underline{\underline{K}}_{p1} = \underline{\underline{K}}_1 - \underline{\underline{K}}_3 \underline{\underline{m}}_{RR}^{-1} \hat{\underline{\underline{K}}}_{RR} \\ \underline{\underline{K}}_{p2} = \underline{\underline{K}}_2 - \underline{\underline{K}}_3 \underline{\underline{m}}_{RR}^{-1} \hat{\underline{\underline{K}}}_{RR} \\ \underline{C}_{p1} = \underline{LD}_{\delta} + \underline{\underline{K}}_3 \underline{\underline{m}}_{RR}^{-1} \underline{F}_C \\ \underline{C}_{p2} = \underline{LD}_{\beta} + \underline{\underline{K}}_3 \underline{\underline{m}}_{RR}^{-1} \underline{F}_{CC} \end{array}; \quad (39)$$

$$HM_{ail} = HM_0 + \begin{bmatrix} 0 & HM_{\alpha} \end{bmatrix} \underline{q}_R + \begin{bmatrix} HM_{\dot{h}} & HM_{\dot{\alpha}} \end{bmatrix} \dot{\underline{q}}_R . \quad (40)$$

the output equation is written as follows:

$$\underline{y} = \underline{\underline{C}}\,\underline{x} + \underline{\underline{D}}\,\underline{u} , \quad (41)$$

with

$$\underline{\underline{C}} = \begin{bmatrix} \underline{\underline{K}}_{p1} & \underline{\underline{K}}_{p2} \\ -\underline{\underline{m}}_{RR}^{-1} \hat{\underline{\underline{K}}}_{RR} & -\underline{\underline{m}}_{RR}^{-1} \hat{\underline{\underline{C}}}_{RR} \\ \begin{bmatrix} 0 & HM_{\alpha} \end{bmatrix} & \begin{bmatrix} HM_{\dot{h}} & HM_{\dot{\alpha}} \end{bmatrix} \end{bmatrix}, \quad (42)$$

and

$$\underline{\underline{D}} = \begin{bmatrix} \underline{C}_{p1} & \underline{C}_{p2} \\ \underline{\underline{m}}_{RR}^{-1} \underline{F}_C & \underline{\underline{m}}_{RR}^{-1} \underline{F}_{CC} \\ HM_{\delta} & HM_{\beta} \end{bmatrix}. \quad (43)$$

Eqs. (32)-(34) together with Eqs. (41)-(43) represent the Multi Input – Multi Output (MIMO) state-space system of the airplane in longitudinal flight.

It results

$$rank\left[\underline{\underline{B}} \quad \underline{\underline{A}}\,\underline{\underline{B}} \quad \underline{\underline{A}}^2\,\underline{\underline{B}} \quad \underline{\underline{A}}^3\,\underline{\underline{B}}\right] = 4, \tag{44}$$

and

$$rank\begin{bmatrix} \underline{\underline{C}} \\ \underline{\underline{C}}\,\underline{\underline{A}} \\ \underline{\underline{C}}\,\underline{\underline{A}}^2 \\ \underline{\underline{C}}\,\underline{\underline{A}}^3 \end{bmatrix} = 3, \tag{45}$$

that is the system has full state controllability whereas it is not completely observable (in its first state).

In case of flexible aircraft, for the evaluation of both Load derivatives and matrices $\underline{\underline{\hat{C}}}_{RR}$ and $\underline{\underline{\hat{K}}}_{RR}$, the airplane flexibility is taken into account by considering the first 37 symmetric normal modes.

4.3.2. FCS Architecture

The FCS architecture is shown by the following SIMULINK® schematic.

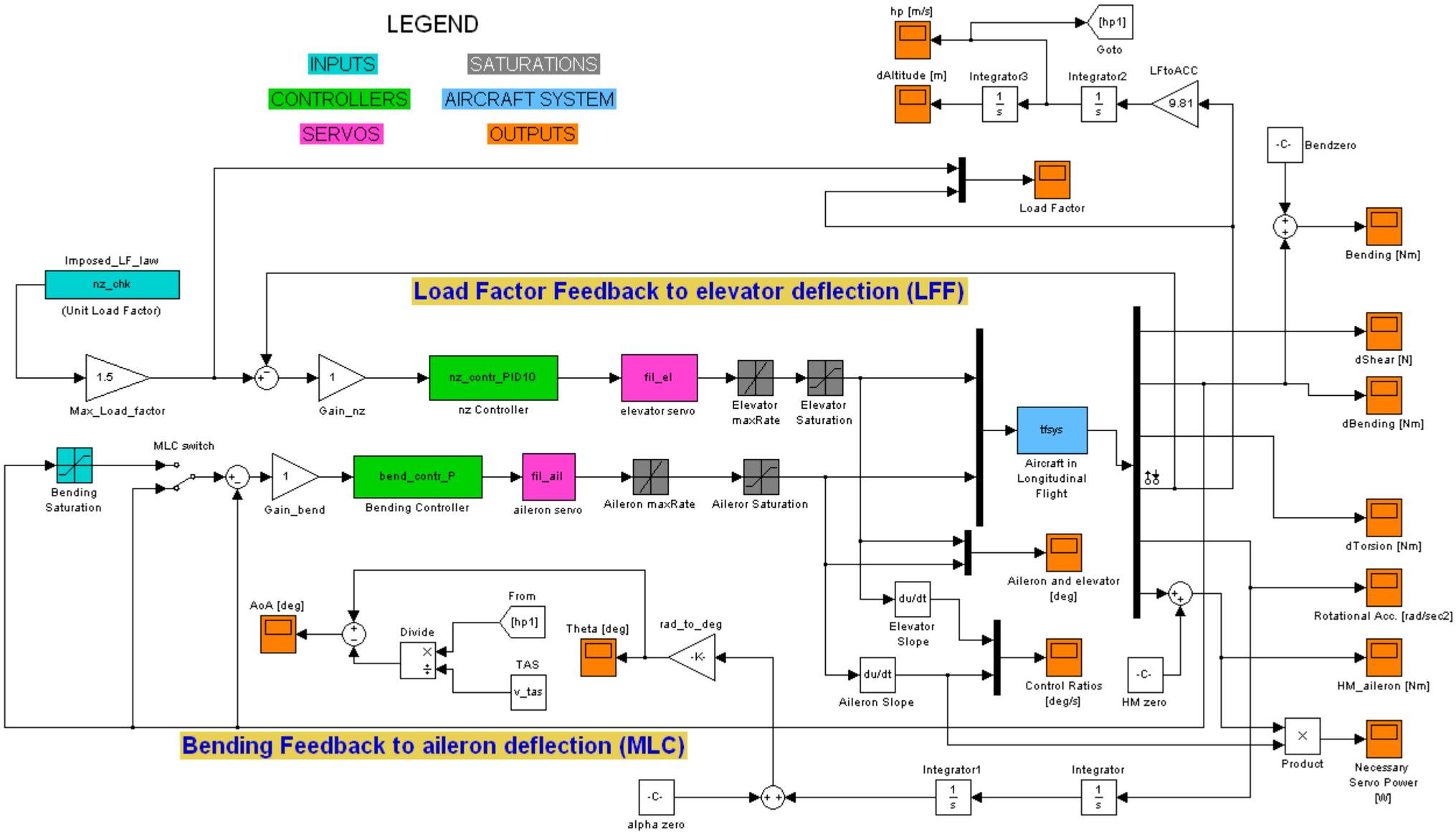

Fig. 40: Feedback Control System architecture.

The whole system is made up of two feedback SISO systems, simulating the Load Factor Feedback and the MLC system. The light blue block represents the aircraft dynamics in longitudinal flight (plant) and magenta blocks simulate the servo dynamics.

The transfer function adopted to model both servos is the following one:

$$\frac{7.994e004}{s^2 + 282.7\ s + 7.994e004}$$

which means a natural frequency of *45 Hz* and a damping ratio of *0.5*.

Cyan blocks are the inputs for the system. The "MLC switch" is used to activate the MLC system. Ones a load factor time history is established, only minimum and maximum WCS Bending moments have to be imposed. This is done by putting these values in the "*Bending Saturation*" block in order to give an allowable load range.

Grey blocks simulate saturations due to mechanical stops and maximum allowable deflection rates. Being the MLC using ailerons as load alleviators, it has to be in series with the roll control system in order to preserve lateral maneuverability, thus symmetric MLC deflections are additive to the anti-symmetric roll deflections until the mechanical control surface stops are reached. The MLC servo authority limits are established as 15 degrees trailing edge up and down. The maximum allowable deflection rate is chosen as ±30 degrees per second.

Orange blocks are the outputs of the system. Although the linear system is built with only six outputs (see Eq. (35)), other flight parameters are evaluated by external integrations, derivations and/or multiplications, as shown in Fig. 40.

The necessary aileron servo power is calculated according to Eq. (46) in order to provide preliminary indications about the feasibility of the hydraulic plant, type and numbers of aileron servo-actuators.

$$W_{AILservo} = HM_{Ail} \cdot \dot{\beta}. \tag{46}$$

4.3.3. LFF and MLC Controllers: Requirements and Synthesis

Three types of system performance specifications (requirements) have been considered:

- Frequency domain specifications;
- Time domain specifications;
- Error specifications.

As regards the **frequency domain specifications**, minimum gain and phase margins are fixed. The gain margin allows the designer to be sure that uncertainties related to the open loop system gain do not cause the instability of the closed loop system. As a general rule, the higher the gain margin, the better is the relative stability of the system. A de-facto gain margin of a factor of 2 is adequate not only to keep the stability but also to prevent great and undesired oscillatory overshoots. A factor 2 gain margin amounts to roughly 6 db on the Bode plot.

$$GM_{LFF} \geq 6\ db. \tag{47}$$

$$GM_{MLC} \geq 6\ db. \tag{48}$$

The phase margin of a system is defined as 180 degrees plus the phase angle of the open loop transfer function at unit gain. Again, as a general rule, the greater the phase margin, the better is the relative stability of the system. For aeronautical systems, a good rule is to accept only phase margins larger than 35 degrees. This choice is due to the presence of delays in the actual dynamics of the system, not considered in simulations with linear models, such as delays of computers and nonlinear delays (such as mechanical clearances) of servos and sensors usually installed on aircraft.

$$PM_{LFF} \geq 35°. \tag{49}$$

$$PM_{MLC} \geq 35°. \tag{50}$$

System **time domain specifications** are given in terms of the response of the system to a unit step input: Overshoot, Rise Time and Settling Time are the adopted time domain specifications (see the next figure for a graphical interpretation of these specifications).

The Overshoot is defined as the maximum difference between the transient response and the steady-state response of a system to a unit step input. It should be seen as a measure of the relative system stability. The allowable overshoot is 25% of the steady-state output.

$$Overshoot_{LFF}\ [\%] \leq 25.0\,. \tag{51}$$

No overshoot requirements are given to the response of the MLC system.

The Rise Time of a system is the time required for the response to rise from 10% to 90% of its steady-state value. The maximum Rise Time is 0.25 sec for the LFF system, and 0.10 sec. for the MLC system.

$$T_{r-LFF} \leq 0.25\,\text{sec.} \tag{52}$$

$$T_{r-MLC} \leq 0.10\,\text{sec.} \tag{53}$$

The Settling Time is defined as the time required for the response to reach and remain within a 2 percent of its final value (the steady-state value).

$$T_{s-LFF} \leq 1.0\,\text{sec.} \tag{54}$$

$$T_{s-MLC} \leq 1.0\,\text{sec.} \tag{55}$$

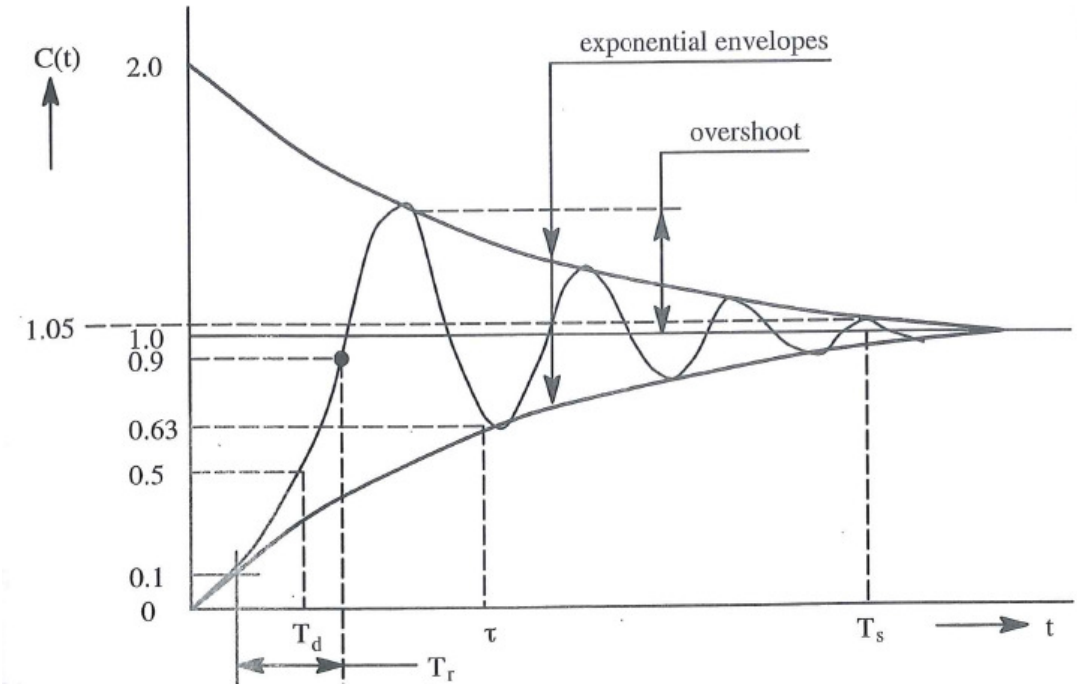

Fig. 41: Graphical interpretation of Time Domain Specifications (Figure from [47]).

The last specification regards the **Position Error** $\varepsilon(\infty)$ requirement. Consider a negative feedback system subject to a unit step input, the Position Error is the difference between the

unity and the steady-state response ($C(s)$ for $s \to \infty$). For the present application, the Position Error related to the LFF system has to be zero.

$$\varepsilon(\infty)\big|_{LFF} = 1 - C_{LFF}(\infty) = 0; \tag{56}$$

Since the MLC system does not have to follow an established bending moment value, but it is designed to keep the bending value in a small region i.e. it has to mitigate the incremental bending due to an automatic longitudinal maneuver, no position error requirements are given.

Another performance objective in the controller design is to keep the error between the controlled output and the set-point as small as possible, since each SISO closed-loop system (as well as LFF and MLC) can be (are) affected by external signals (the symmetric aileron deflection affects the load factor whereas the elevator deflection affects the bending moment at the WCS).

In order to assess the performance of controllers, we need to be able to quantify the relationship between the error mentioned so far to the Sensitivity function $S(s)$, that relates to disturbance rejection properties.

$$S(s) = \frac{1}{1 + G_C(s)G_P(s)}, \tag{57}$$

where:

- $G_C(s)$ is the transfer function of the Controller;
- $G_P(s)$ is the transfer function of the plant (the load factor transfer function to elevator deflections for the LFF and the bending moment transfer function to aileron deflections for the MLC).

In order to have errors between the controlled output and the set-point as small as possible in presence of external disturbances, the sensitivity function has to be as well as possible close to zero in the frequency range of interest.

However, most systems are “strictly proper”, in other words the denominator of the transfer function is of higher order than the numerator. This means that the sensitivity function

tends to the unity when the frequency increases. As a consequence, it is often difficult to keep the value of $S(s)$ low far from the steady-state range.

LFF Controller Synthesis. In order to fulfill all the requirements, the load factor is fed-back to the elevator deflection by using a negative feedback with a PID (Proportional Integral Derivative) controller (see Fig. 42, extracted from [56]).

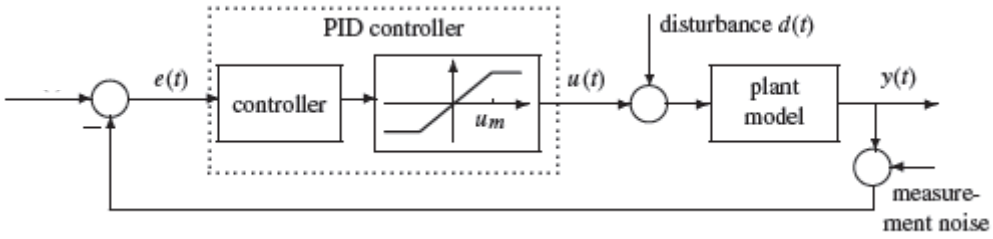

Fig. 42: Schematic of a negative feedback with a PID control.

The error signal *e(t)* is used to generate the proportional, integral, and derivative actions, with the resulting signals weighted and summed to form the control signal *u(t)* applied to the plant model.

PID control is one of the earlier control strategies. Its early implementation was in pneumatic devices, followed by vacuum and solid state analog electronics, before arriving at today's digital implementation of microprocessors. Since many control systems using PID control have proved satisfactory, it still has a wide range of applications in industrial control.

A PID controller is composed of three controllers in parallel: a simple proportional, an integral and a derivative controller. Notice that in practical applications the pure derivative action is never used due to the "derivative kick" produced in the control signal for a step input, and to the undesirable noise amplification. It is usually replaced by a first-order low pass filter. Thus, the Laplace transformation representation of the approximate PID controller can be written as:

$$G_{C-PID} = \frac{U(s)}{E(s)} = K_P + \frac{K_i}{s} + \frac{K_d\, s}{1+\frac{s}{N}} = K_P\left(1+\frac{1}{T_i s}+\frac{sT_d}{1+\frac{s}{N}}\right), \qquad (58)$$

where:

- K_p is the proportional constant. When K_p increases, the response speed of the system increases, the overshoot of the closed-loop system increases, and the steady-state error decreases. However when K_p is large enough, the closed-loop system becomes unstable;
- T_i is the integral time. When T_i increases, the overshoot tends to be smaller, but the speed of response tends to be slower. Moreover if T_i is enough smaller, the closed-loop system becomes unstable;
- T_d is the derivative time. When T_d increases the response has a smaller overshoot with a slightly slower rise time but similar settling time.
- N is the cut-off frequency of the first-order low pass filter.

The controller synthesis is done by applying the tuning method presented in [57], [58], and [59], and implemented in Matlab® through the SISOTOOL® graphic user interface [66]. A cut-off frequency of 10 Hz and a dominant time constant of 0.02 sec. are chosen in order to minimize the disturbance rejection, as following shown by Fig. 45.

The PID controller of the LFF system is designed for each flight case by taking into account the flexibility of the aircraft. The same controller is adopted also in the case of rigid aircraft by simply reducing the proportional constant K_p according to the stability requirements presented so far.

Just as an example, the closed-loop response to a unit step input is depicted in Fig. 43 for the flight case #2M3 and elastic aircraft. The white region is the allowable region according to the time domain specifications. Notice that the presence of the integral action automatically makes the specification on the position error fulfilled.

The Open Loop Bode Diagram is reported in Fig. 44. Gain and Phase margin requirements are specified together with the critical frequency.

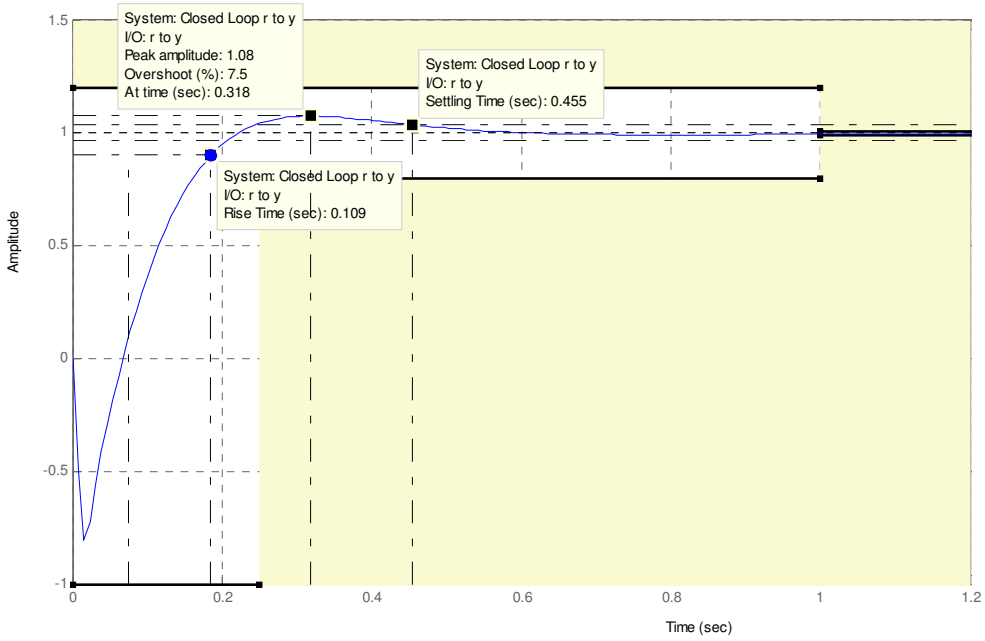

Fig. 43: Closed Loop Response of a unit step input, LFF System, Flight Case #2M3.

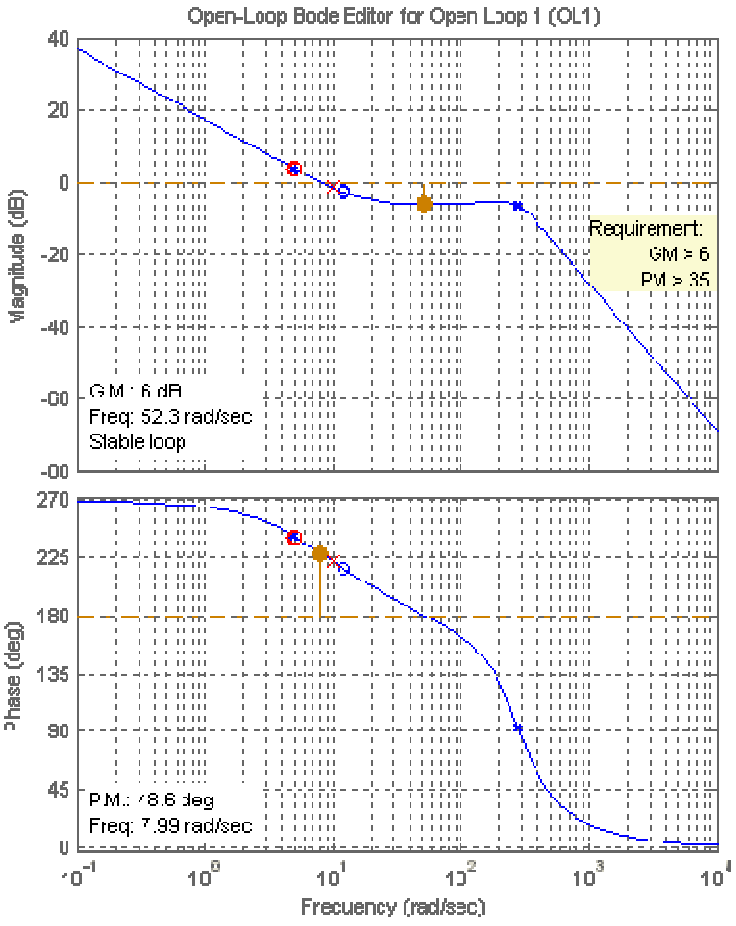

Fig. 44: Open Loop Bode Diagram, LFF System, Flight Case #2M3.

The next figure reports the Bode Diagram of the Sensitivity Function together with the controller and the aircraft dynamic model (load factor transfer function to the elevator) for the flight case #2M3. The magnitude is well less than the unity in the frequency band 10^{-1}-10^{0}, representing the typical bandwidth of longitudinal maneuvers of such a kind of aircraft. A mitigation of the external disturbance of aileron deflection due to the activation of the MLC system can be expected.

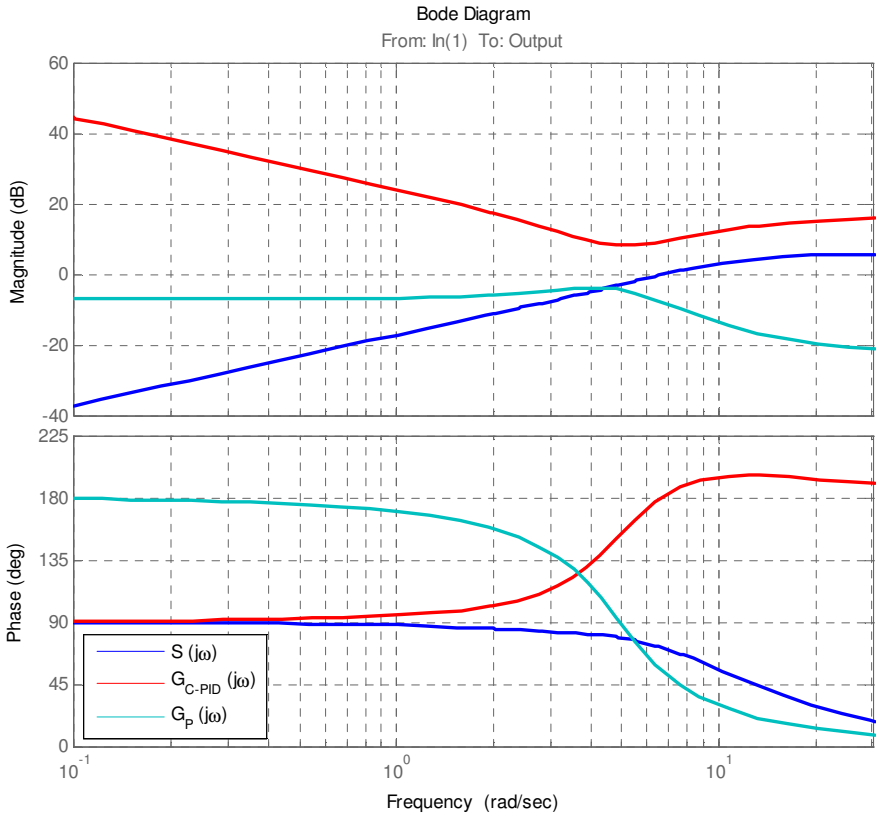

Fig. 45: Sensitivity Function Bode Diagram, LFF System, Flight Case #2M3.

Proportional, Integral and derivative constants of the PID controller transfer function have to be continuously varied in flight in order to keep the specifications fulfilled. This can be accomplished by an inboard computer interpolating the data presented in Table 8 and Table 9.

The dependency of PID parameters upon the dynamic pressure is shown in Fig. 46, Fig. 47, and Fig. 48, for mass condition M3 and M=0.573. The most evident result is the dependency of K_P for rigid aircraft upon the dynamic pressure much less marked if compared with K_P for elastic aircraft. The dependency upon the Mach number is shown by Fig. 49, Fig. 50, and Fig. 51. In this case the dependency of K_P upon the Mach number is analogous for both rigid and elastic aircraft. The trend of all parameters result quite quadratic.

	LFF control - PID DATA (N=10 Hz)			
ID	Kp elast	Kp rig	Ki	Kd
	Sensitivity versus the Mach Number			
#2SM0M3	-1.6297	-1.3722	-15.825	-0.5212
#2M3	-1.2643	-1.0304	-16.210	-0.5325
#2SM1M3	-0.9872	-0.8105	-15.050	-0.5283
#2SM2M3	-0.7601	-0.6042	-15.240	-0.4929
	Sensitivity versus the Dynamic Pressure			
#2Sq0M3	-1.2852	-1.0693	-16.080	-0.4776
#2M3	-1.2643	-1.0304	-16.210	-0.5325
#2Sq1M3	-1.2339	-1.0636	-16.380	-0.6004
#2Sq2M3	-1.1887	-1.0425	-16.570	-0.6864

Table 8: PID Data, dependency upon Mach Number and Dynamic Pressure

	LFF control - PID DATA (N=10 Hz)											
ID	Kp elast	Kp rig	Ki	Kd	Kp elast	Kp rig	Ki	Kd	Kp elast	Kp rig	Ki	Kd
#1	-1.636	-1.373	-15.78	-0.509	-1.531	-1.280	-20.40	-0.671	-1.448	-1.209	-24.67	-0.829
#2	-1.264	-1.030	-16.21	-0.532	-1.218	-1.015	-19.99	-0.696	-1.108	-0.914	-24.22	-0.856
#3	-0.982	-0.814	-15.04	-0.553	-0.795	-0.656	-19.74	-0.718	-0.627	-0.518	-24.13	-0.881
#4	-0.733	-0.596	-15.32	-0.544	-0.516	-0.419	-20.17	-0.705	-0.320	-0.259	-24.70	-0.863
	Mass Condition M3				Mass Condition M2				Mass Condition M1			

Table 9: PID Data, dependency upon Mass Conditions.

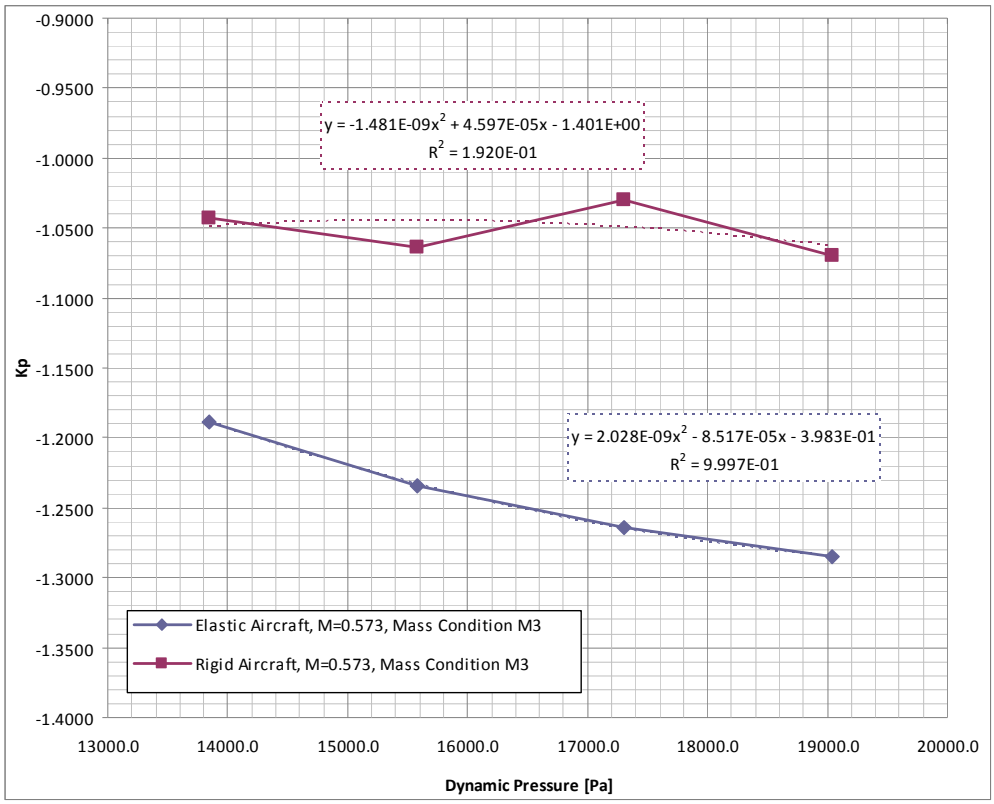

Fig. 46: K_P versus the Dynamic Pressure, M=0.573, Mass Condition M3.

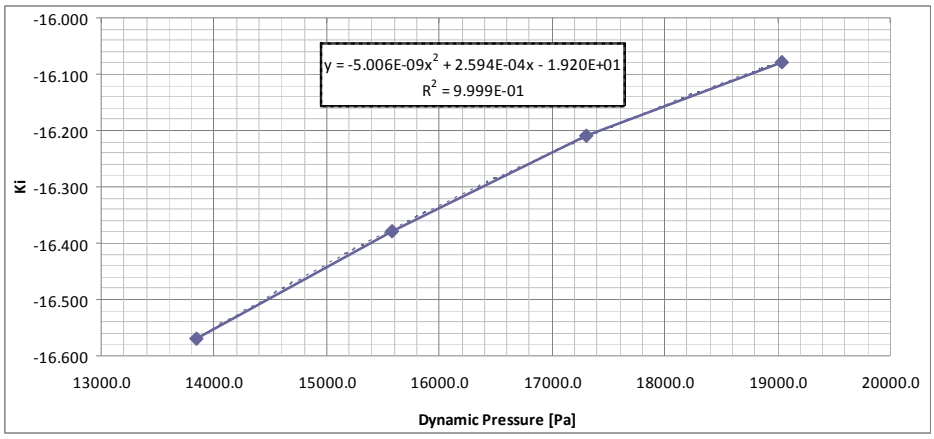

Fig. 47: K_i versus the Dynamic Pressure, M=0.573, Mass Condition M3.

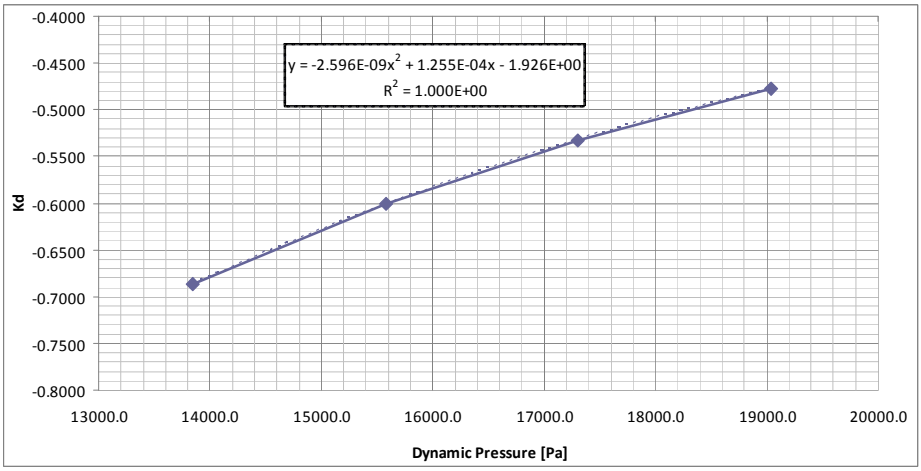

Fig. 48: K_d versus the Dynamic Pressure, M=0.573, Mass Condition M3.

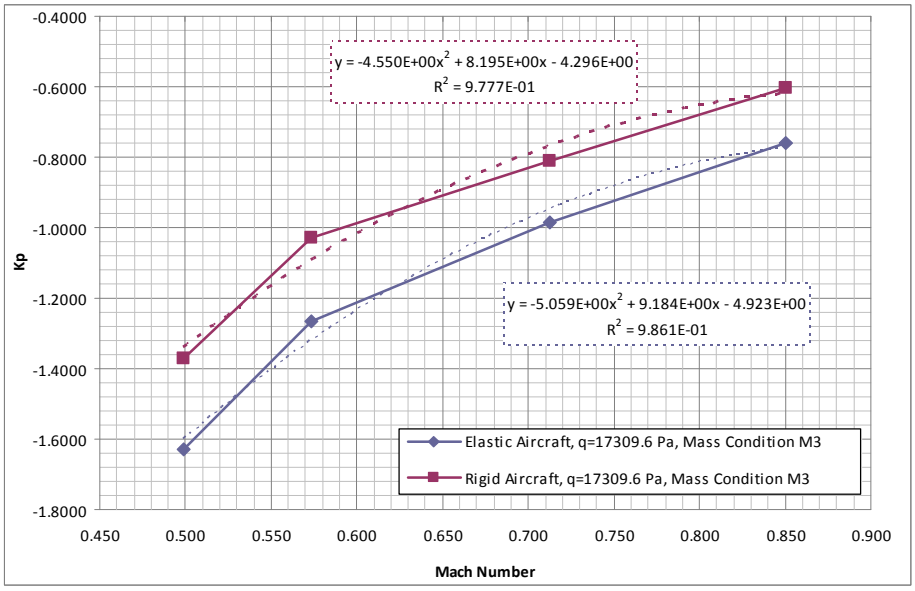

Fig. 49: K_P versus the Mach Number, q=17309.6 Pa, Mass Condition M3.

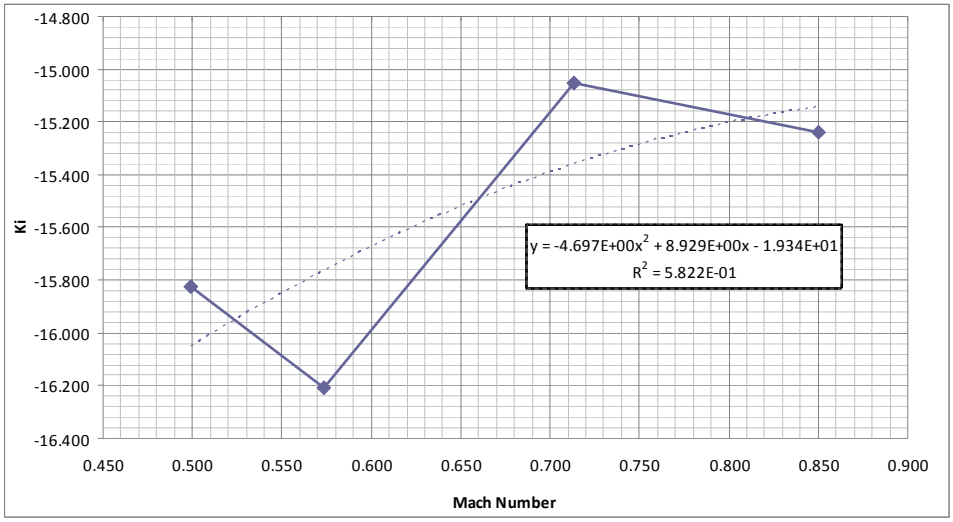

Fig. 50: K_i versus the Mach Number, q=17309.6 Pa, Mass Condition M3.

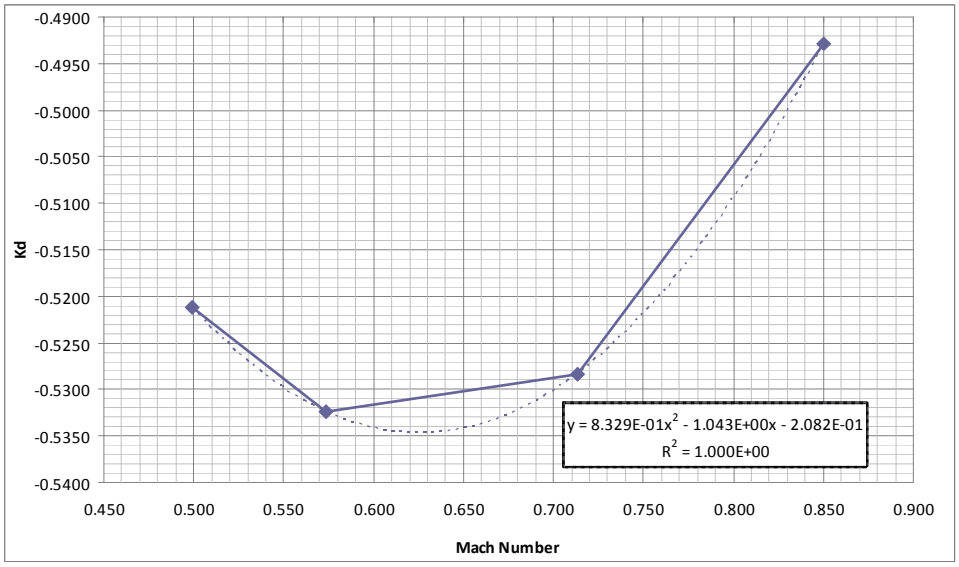

Fig. 51: K_d versus the Mach Number, q=17309.6 Pa, Mass Condition M3.

PID parameters of flight condition #2, for the three different mass conditions of Table 7, are depicted in Fig. 52, normalized with the respect to those obtained at the flight case #2M3 (MZFW, no fuel).

Notice that there are no appreciable differences in the dependence of K_P upon the mass condition on whether the aircraft is considered rigid or elastic. Calculated fitting curves show that the trend is quite linear.

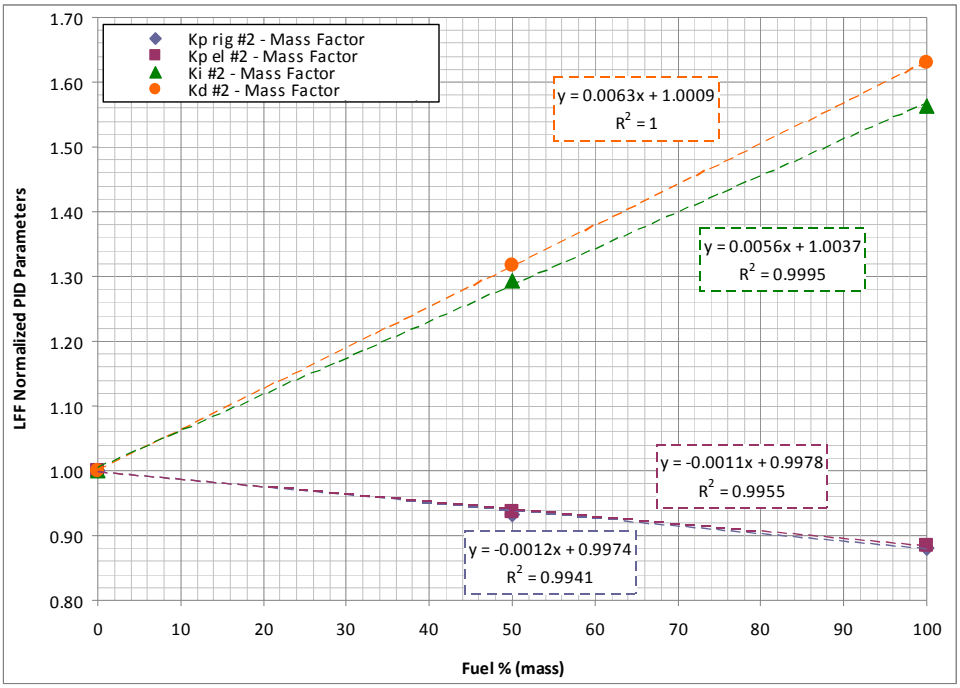

Fig. 52: Dependency of PID parameters upon mass conditions (fuel).

MLC Controller Synthesis. The Bending moment is fed-back to the aileron deflection by a negative feedback with a logical "if", a saturation block and a simple Proportional controller (see Fig. 53).

The P controller of the MLC system is designed for each flight case for both rigid and elastic aircraft by simply tuning the proportional constant K_p in order to fulfill all the specifications presented so far.

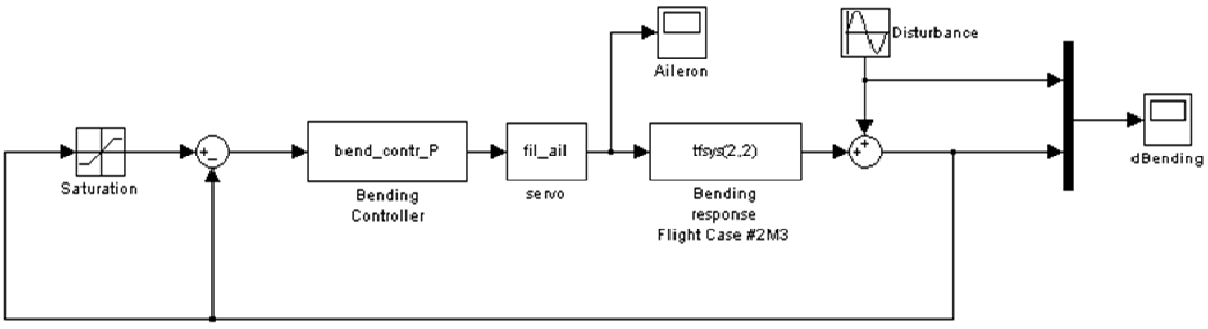

Fig. 53: Schematic of a negative feedback with a logical "if" and a saturation block.

Just as an example, the Open Loop Bode Plot for the flight case #2M3 is depicted in Fig. 54. Gain and Phase margin requirements are specified together with the critical frequency.

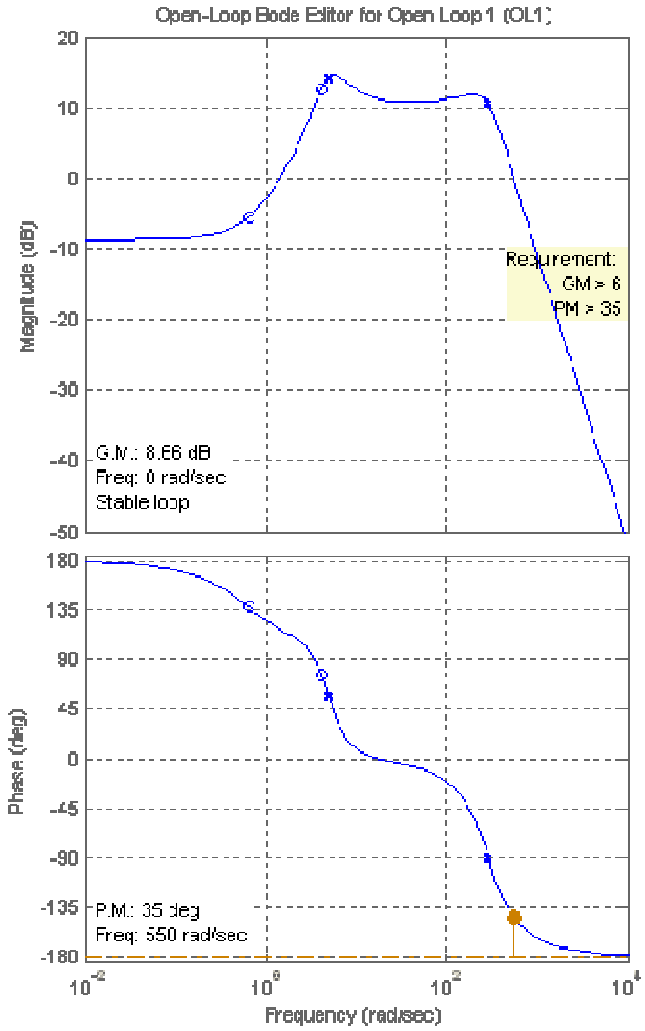

Fig. 54: Open Loop Bode Plot, MLC system, Flight Case #2M3.

The transient of the Closed Loop response to a unit step input is depicted in Fig. 55 whereas Fig. 56 shows the complete response of the system to a unit step input.

Notice that the non-zero constant error is very high and, as evident also from the Root Locus of Fig. 57, the transient due to non-dominant poles is very fast although the dominant dynamics makes the MLC system slow enough such that the change in the longitudinal balance (due to the swept wing so that the aileron deflection change the aircraft pitch moment) can be properly controlled by the LFF system which also operates by deleting this “adrift” bending behavior.

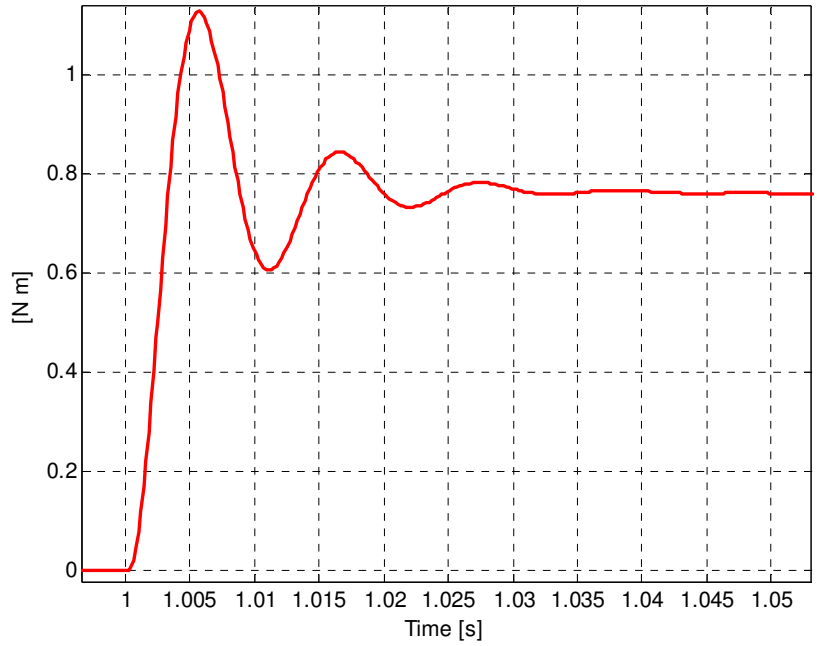

Fig. 55: Transient of the response to a unit step input, Flight Case #2M3.

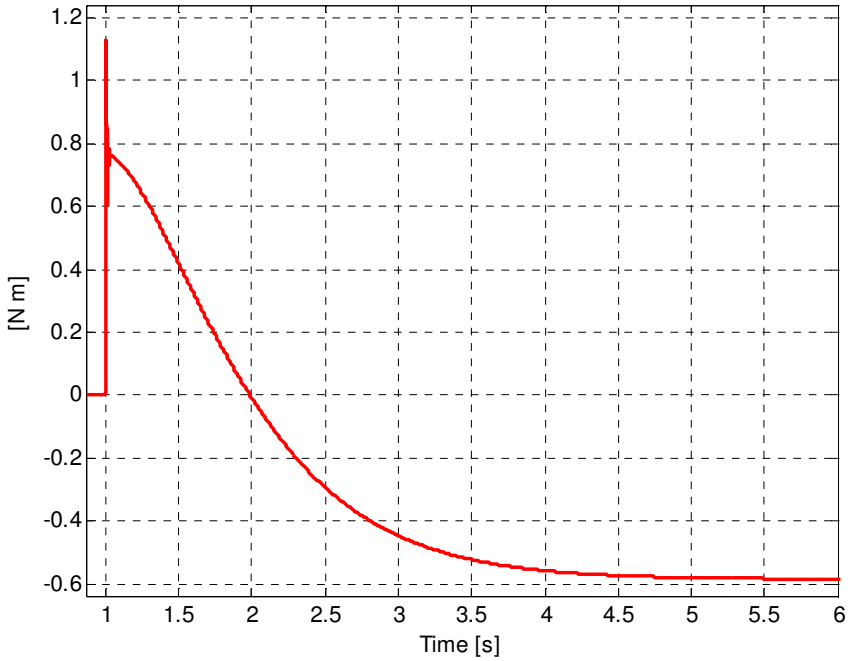

Fig. 56: Response to a unit step input, MLC system, Flight Case #2M3.

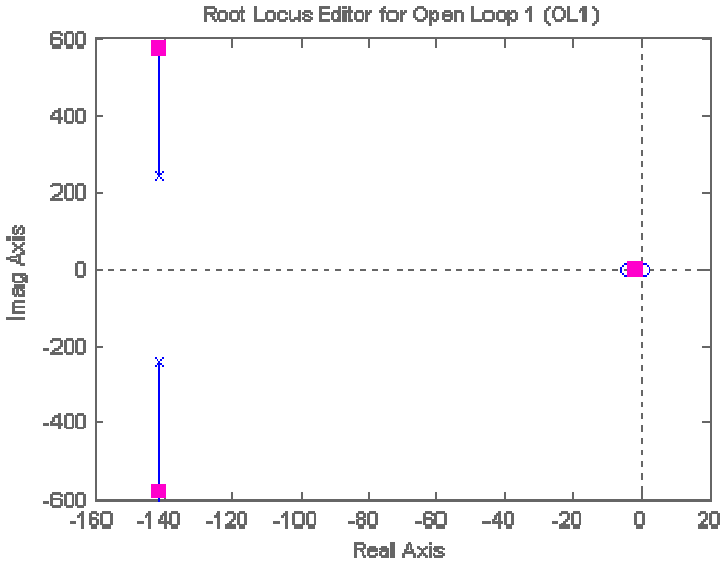

Fig. 57: Root Locus Diagram, MLC system, Flight Case #2M3.

On the other hand the very fast transient acts well to reduce the bending moment. Consequently the maximum Rise Time requirement together with the Settling Time requirements of the MLC system are fulfilled since their meaning is related to the non-dominant dynamics. Numerical simulations of the LAS, presented in the next section, demonstrate the effective behavior of the MLC system.

Fig. 58 and Fig. 59 depict the response of the MLC system (see Fig. 53) when it has to mitigate two different external bending disturbances. The first signal is a 0.5 Hz sine and the second is a 1.0 Hz sine.

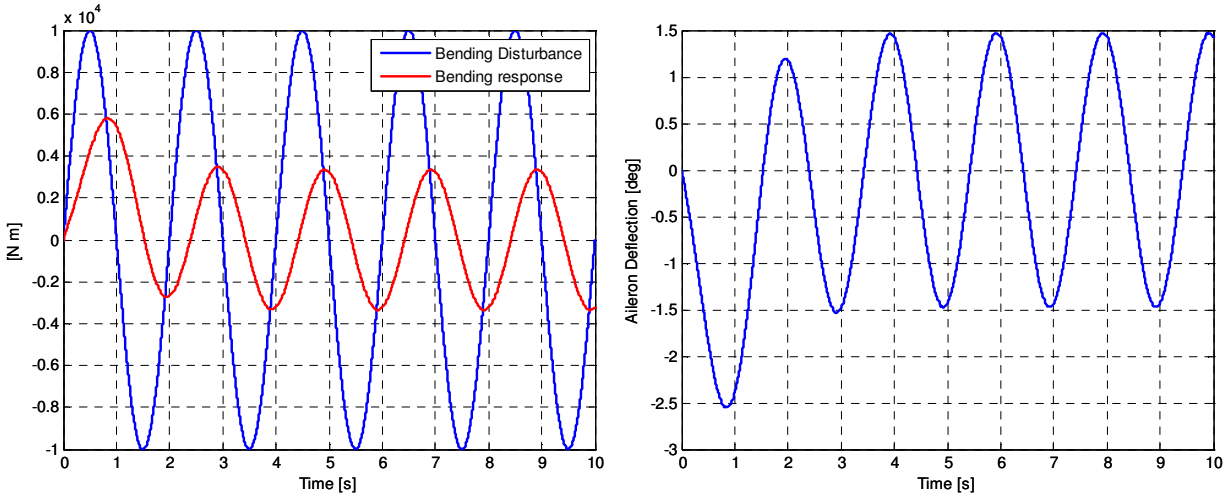

Fig. 58: Bending disturbance mitigation and aileron deflection, 0.5 Hertz, MLC system, Flight Case #2M3.

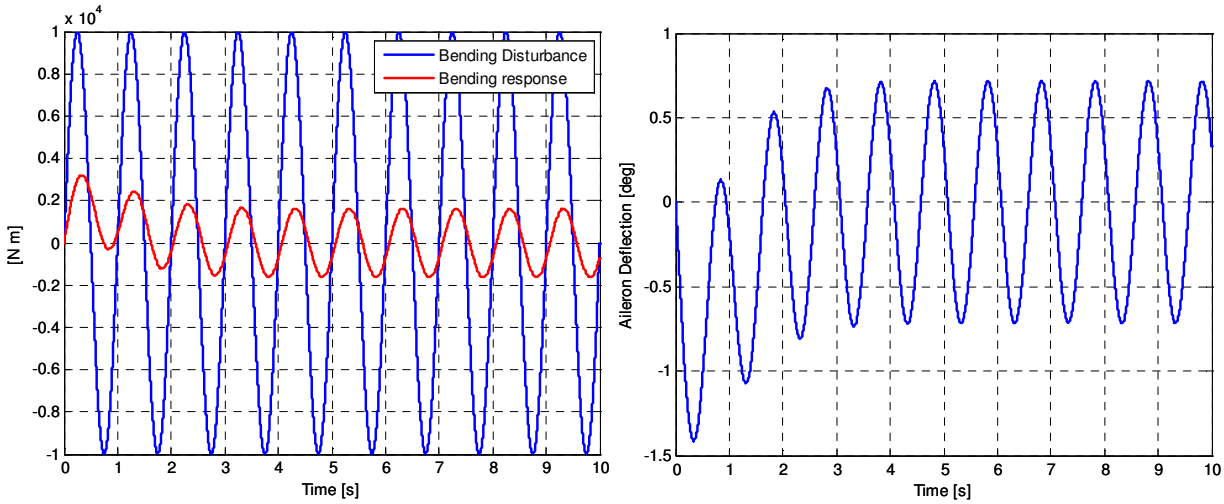

Fig. 59: Bending disturbance mitigation and aileron deflection, 1.0 Hertz, MLC system, Flight Case #2M3.

The ability of the MLC system to reject external disturbances increases with frequency until 1.12 Hz (7.05 rad/s) in which the magnitude of the Sensitivity Function attains its minimum value, as evident also from the Bode Plot of Fig. 60.

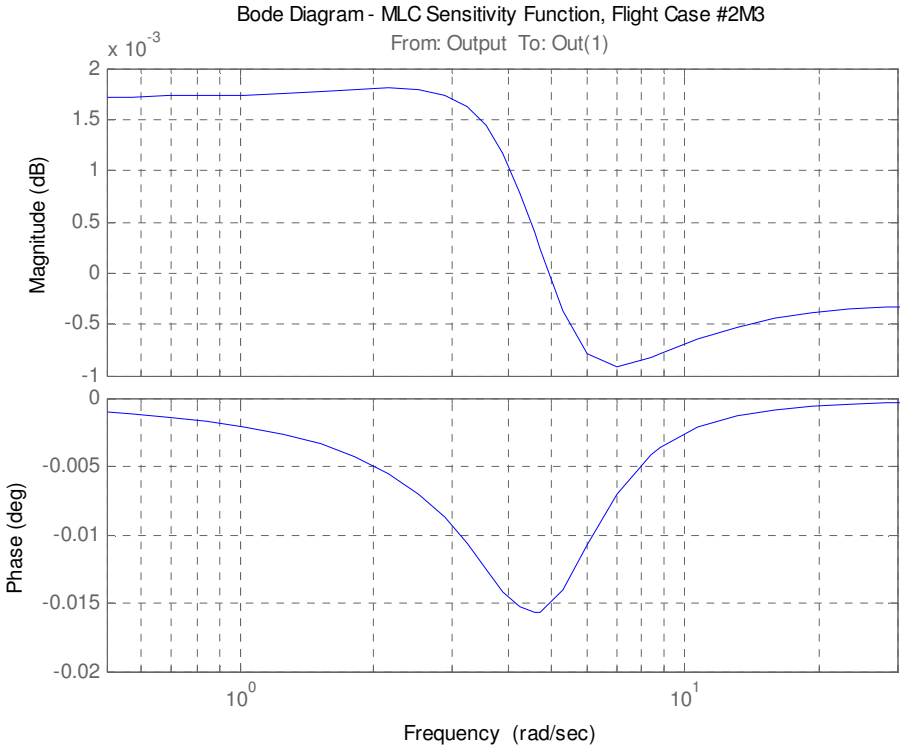

Fig. 60: Sensitivity Function Bode Plot, MLC system, Flight Case #2M3.

Concerning the other flight conditions, as done for the LFF controller, the gain of the MLC P controller has to be continuously varied in flight in order to keep the specifications fulfilled. Also in this case it could be done by an inboard computer interpolating the data reported in Table 10 and Table 11.

	MLC control - P DATA	
ID	**P elast**	**P rig**
	Sensitivity versus M	
#2SM0M3	0.000373	0.000205
#2M3	0.000440	0.000290
#2SM1M3	0.000209	0.000185
#2SM2M3	0.000155	0.000155
	Sensitivity versus q	
#2Sq0M3	0.000435	0.000175
#2M3	0.000440	0.000290
#2Sq1M3	0.000450	0.000221
#2Sq2M3	0.000467	0.000248

Table 10: MLC - P Data, dependency upon Mach Number and Dynamic Pressure.

	MLC control - P DATA					
ID	**P elast**	**P rig**	**P elast**	**P rig**	**P elast**	**P rig**
#1	0.0003574	0.0002011	0.0004250	0.0002006	0.0004250	0.0002015
#2	0.0004400	0.0002895	0.0004260	0.0001994	0.0004270	0.0002007
#3	0.0001284	0.0001284	0.0003524	0.0001931	0.0004310	0.0001931
#4	0.0001380	0.0001380	0.0002580	0.0001827	0.0003220	0.0001823
	Mass Condition M3		***Mass Condition M2***		***Mass Condition M1***	

Table 11: MLC - P Data, dependency upon Mass Conditions.

The dependency of MLC-P controller upon the dynamic pressure is shown in Fig. 61, for mass condition M3 and M=0.573. Notice that the dependency of P for rigid aircraft upon the dynamic pressure is slightly more marked if compared with P for elastic aircraft. This happens because, if the aircraft flexibility is accounted for, a stronger aileron aerodynamics due to increasing dynamic pressure is partially alleviated by a loss of aileron effectiveness. The dependency upon the Mach number is depicted in Fig. 62, where the difference between rigid and elastic aircraft outcomes more evident.

In either case, the most apparent result is the fact that data are not perfectly aligned. This behavior is due to the fact that in some cases the controller is constrained by the GM whereas in other cases the controller is designed at limit PM, with a GM larger than the limit defined so far. However the trend of all parameters turns out to be quite linear.

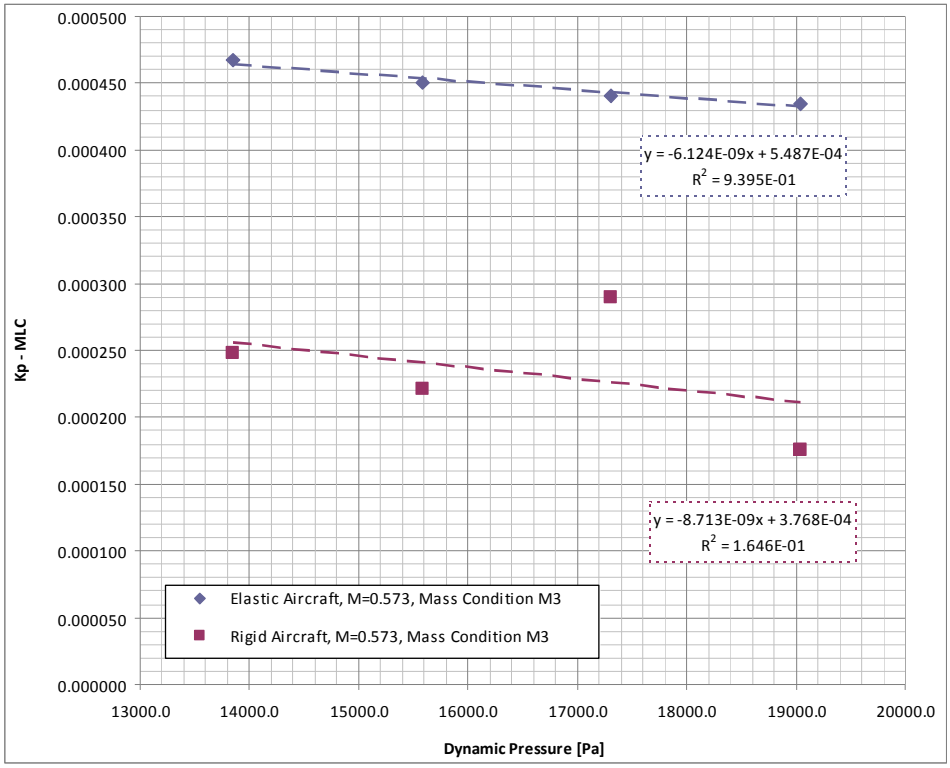

Fig. 61: MLC-P versus the Dynamic Pressure, M=0.573, Mass Condition M3.

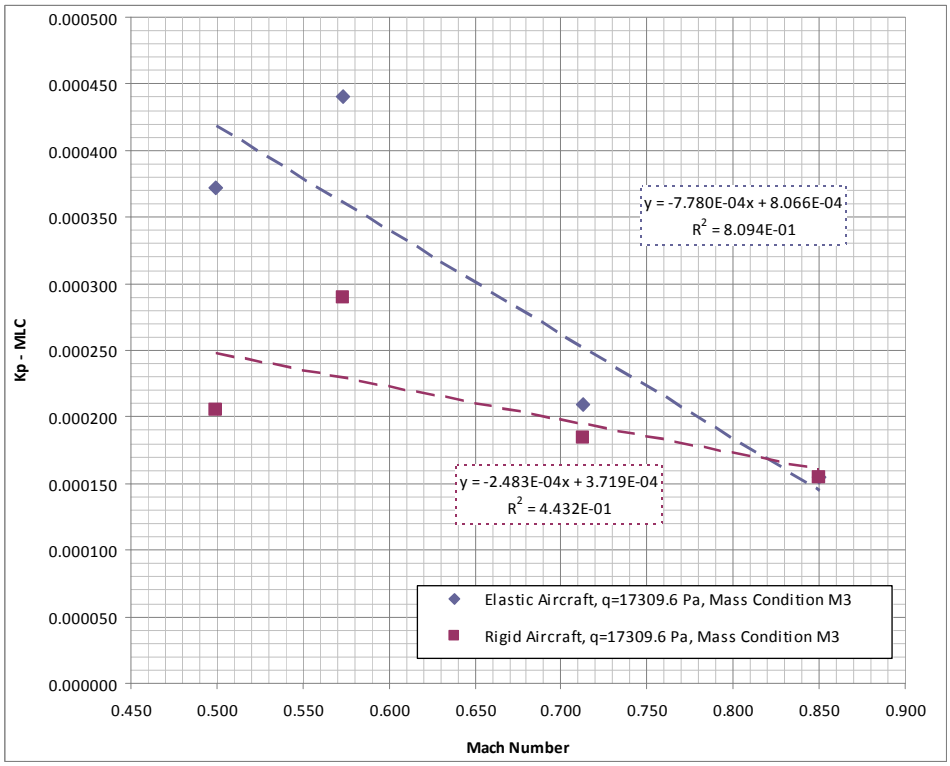

Fig. 62: MLC-P versus the Mach Number, q=17309.6 Pa, Mass Condition M3.

4.3.4. Performance of the LAS system – The Effect of Aeroelasticity

In this section an unsteady maneuver similar to a checked maneuver is presented for flight condition #2M3, for both rigid and elastic aircraft, each one with MLC-on and MLC-off. Results in terms of imposed and resulting vertical load factor, control surface deflections, loads at the wing root and horizontal tail root, aileron hinge moments and necessary aileron servo power are depicted in the following figures.

As shown in Fig. 63 and Fig. 72, respectively for elastic and rigid aircraft, the LFF system lets follow the desired load factor also when MLC is switched on, despite the symmetric aileron deflection helps the elevator in pitching up the airplane and thus in reaching the load factor peak in less time.

Fig. 64 and Fig. 73 show the control surface deflection time histories, respectively for elastic and rigid aircraft, for both MLC-on and off. Notice that the necessary load alleviator deflection in the case of flexible aircraft is greater than in the case of rigid aircraft. This is due to the loss of effectiveness of the outboard ailerons used as load alleviators. The same reason also drives the increase of the necessary servo power to actuate the load alleviators (see Fig. 81). The calculated necessary extra power when the structure flexibility is accounted for is more than 60% of that calculated for rigid aircraft. Despite the aileron hinge moment with rigid aircraft is mildly higher than that calculated for elastic aircraft (see Fig. 71 and Fig. 80), in this latter case the MLC actuation is much more fast, thus leading to a higher deflection angular velocity and a higher necessary servo power (see eq. 46).

Fig. 65 to Fig. 67 and Fig. 74 to Fig. 76 show the time histories of shear, bending and torsion at the WCS for respectively elastic and rigid aircraft. As expected the calculated bending reduction is much less significant when the aircraft flexibility is taken into account. This behavior suggests to consider the structure elasticity since the early stage of design of such systems in order to estimate their effectiveness in a more reliable way.

The time histories of shear, bending and torsion at the horizontal tail root are depicted in Fig. 68 to Fig. 70 and Fig. 77 to Fig. 79 for respectively elastic and rigid aircraft. Notice that a slight increase in shear and bending moment occurs when MLC is switched on for both rigid and elastic aircraft. This effect is very common for most load alleviation systems.

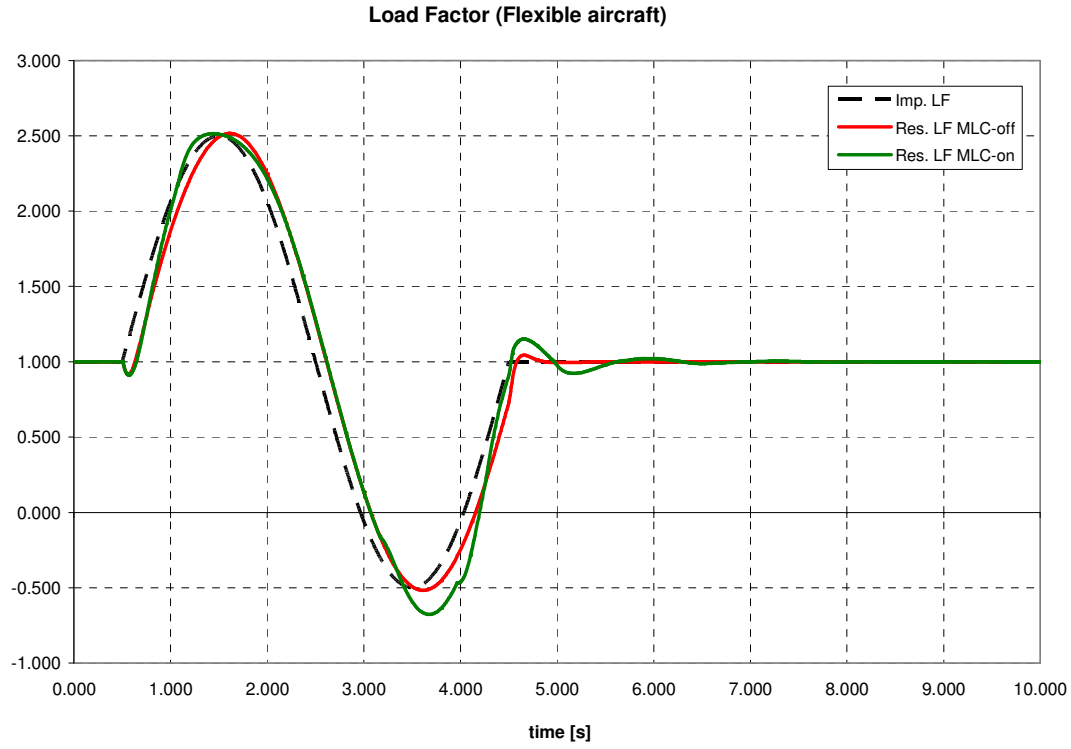

Fig. 63: Vertical Load Factor, Flight Case #2M3, Flexible aircraft.

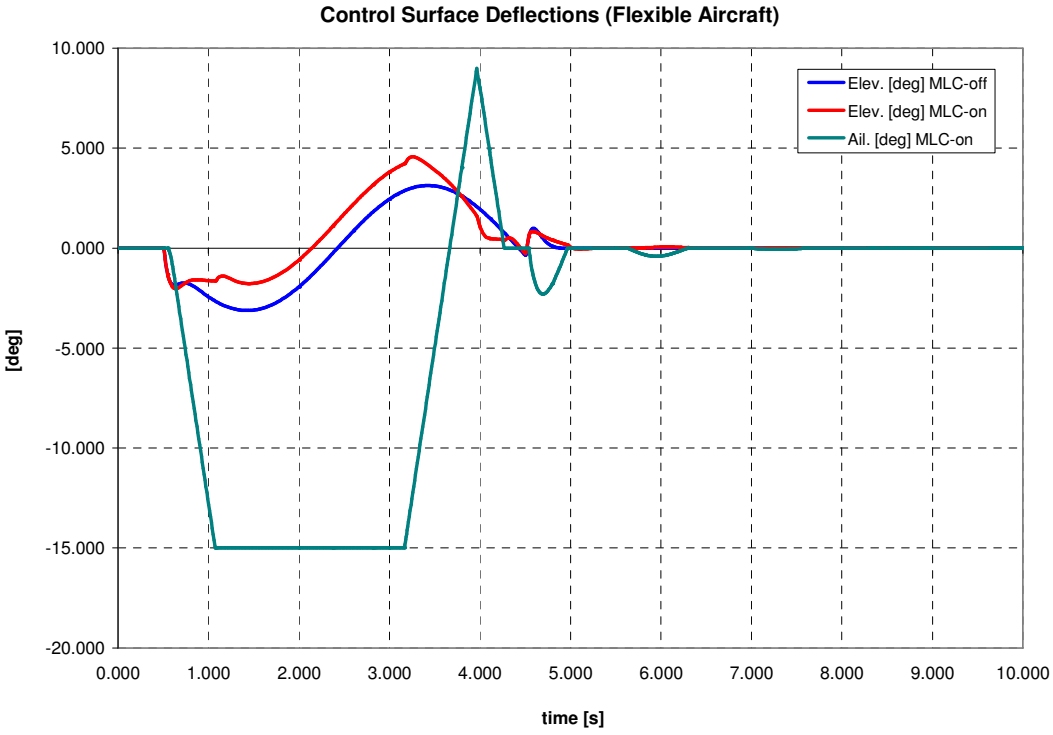

Fig. 64: Control Surface deflections, Flight Case #2M3, Flexible aircraft.

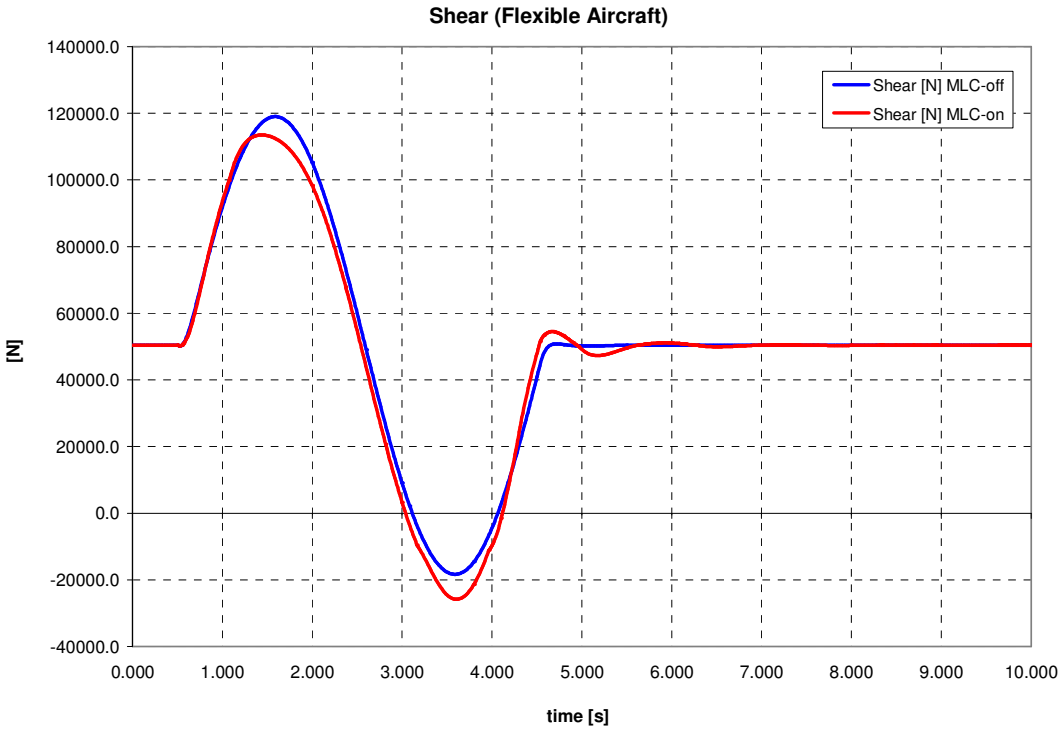

Fig. 65: Shear at the wing root (WCS), Flight Case #2M3, Flexible aircraft.

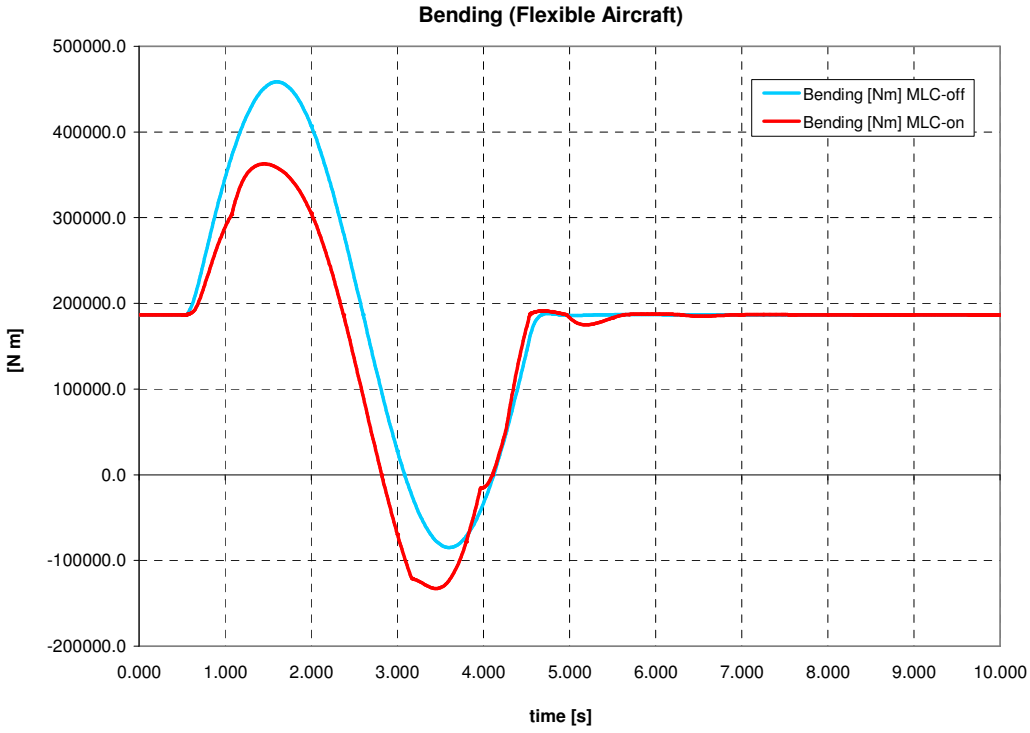

Fig. 66: Bending at the wing root (WCS), Flight Case #2M3, Flexible aircraft.

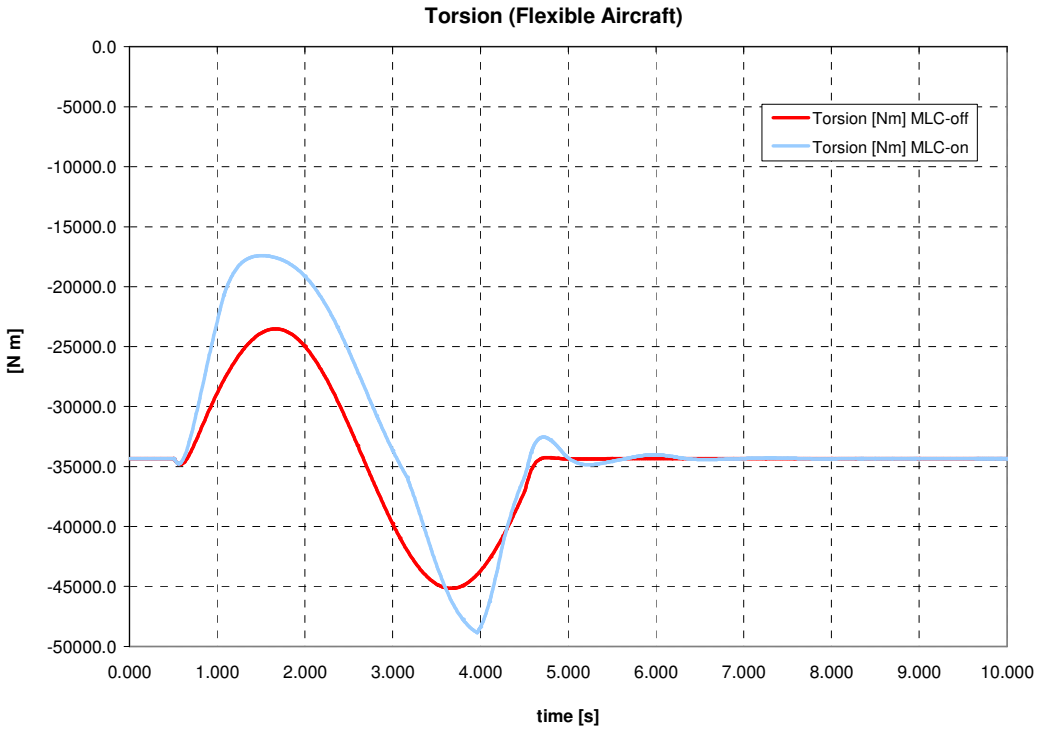

Fig. 67: Torsion at the wing root (WCS), Flight Case #2M3, Flexible aircraft.

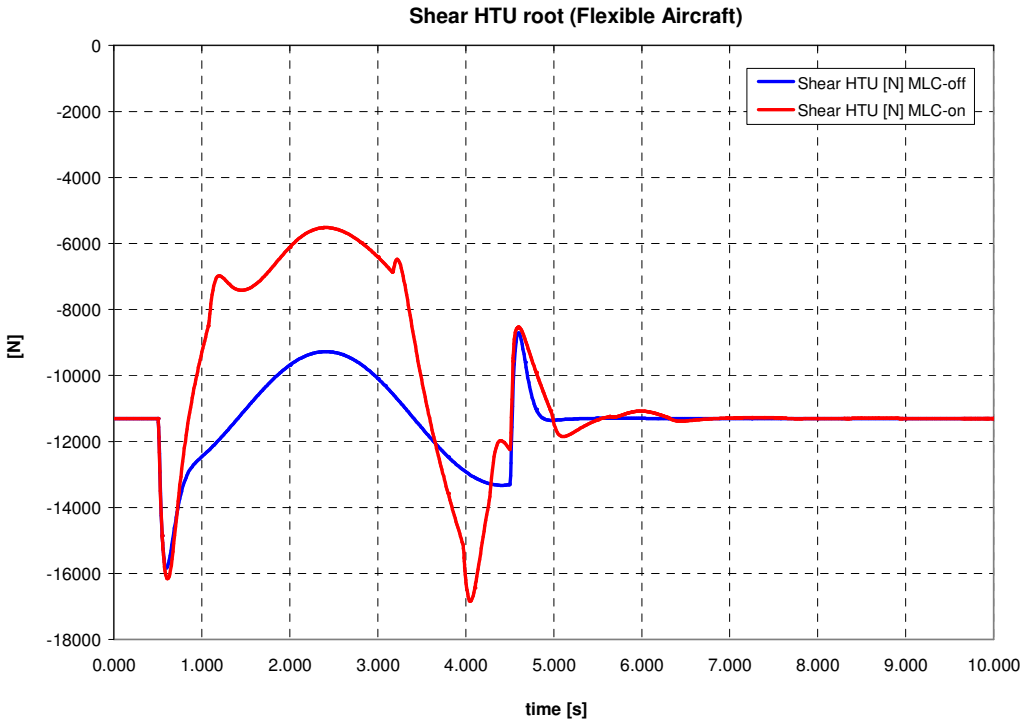

Fig. 68: Shear at the horizontal tail root, Flight Case #2M3, Flexible aircraft.

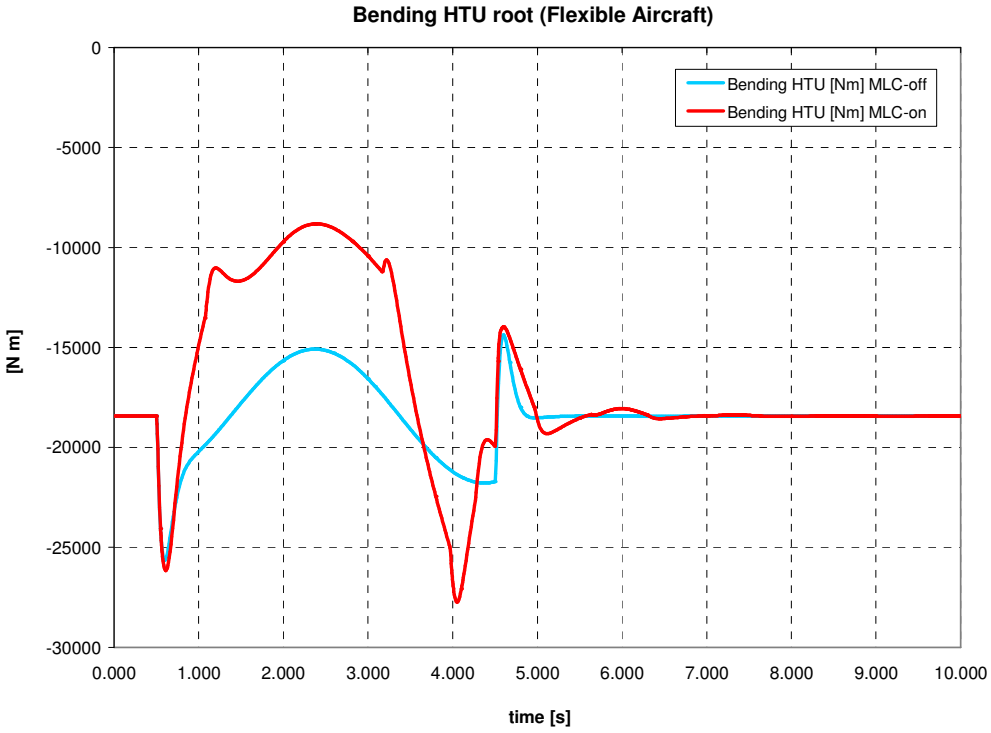

Fig. 69: Bending at the horizontal tail root, Flight Case #2M3, Flexible aircraft.

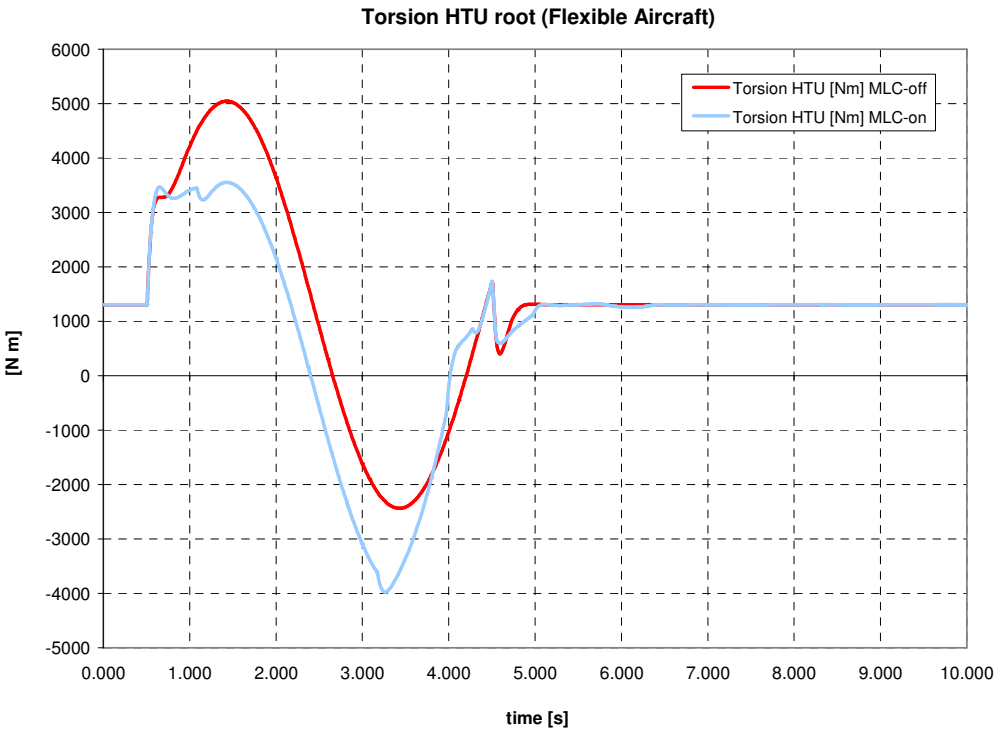

Fig. 70: Torsion at the horizontal tail root, Flight Case #2M3, Flexible aircraft.

Fig. 71: Aileron Hinge Moments, Flight Case #2M3, Flexible aircraft.

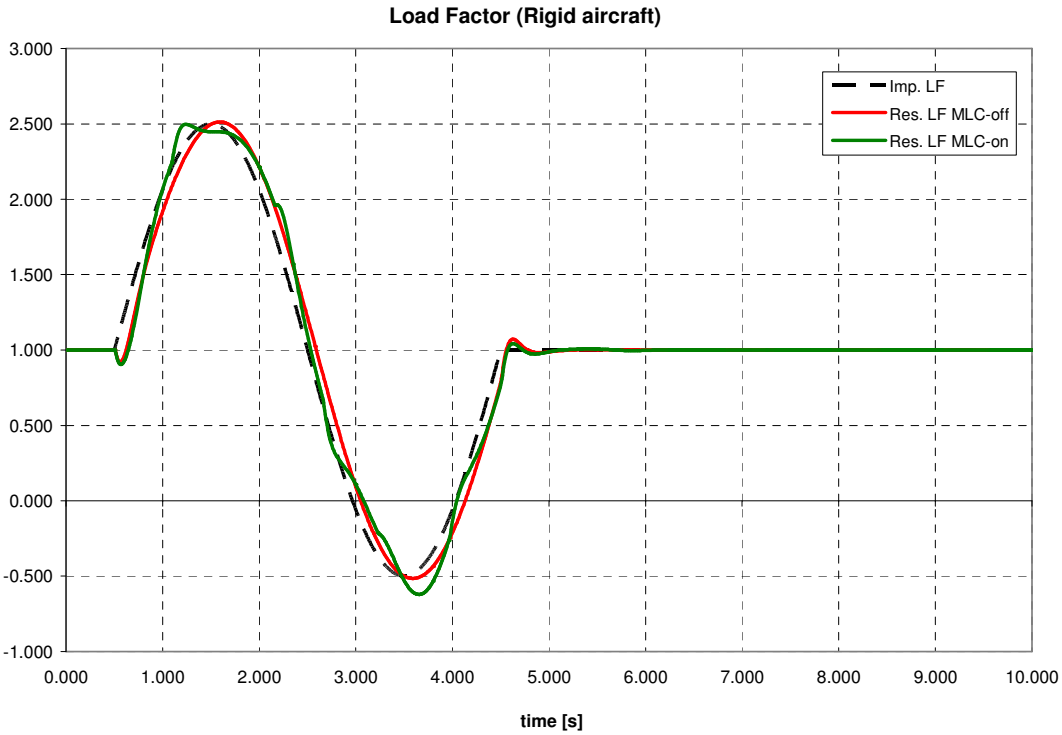

Fig. 72: Vertical Load Factor, Flight Case #2M3, Rigid aircraft.

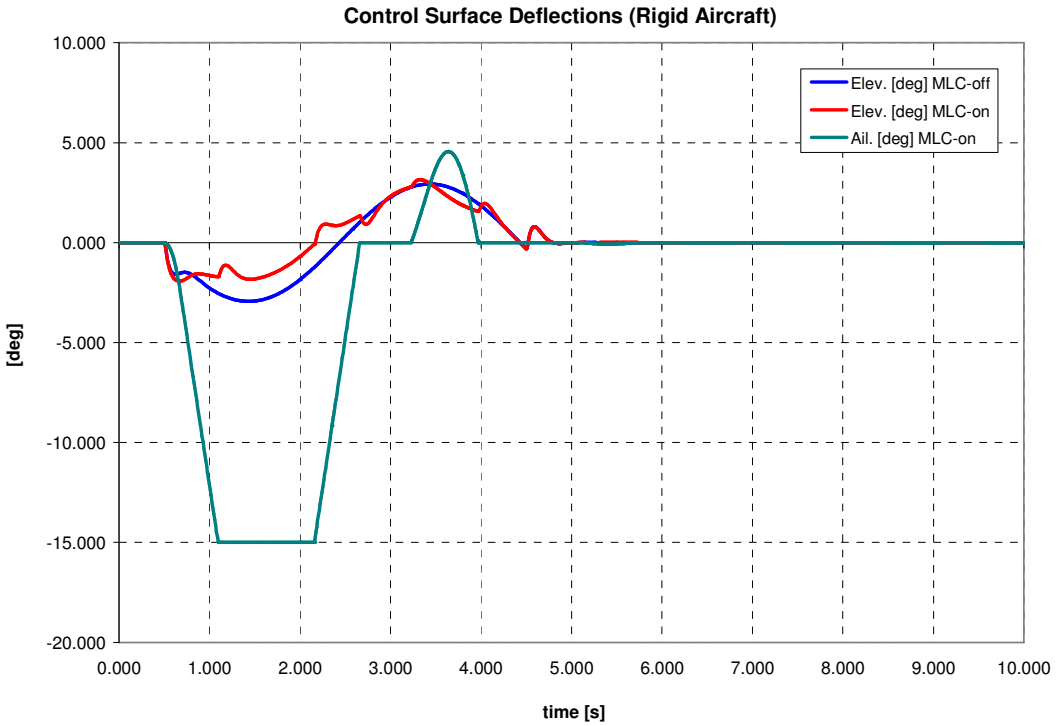

Fig. 73: Control Surface deflections, Flight Case #2M3, Rigid aircraft.

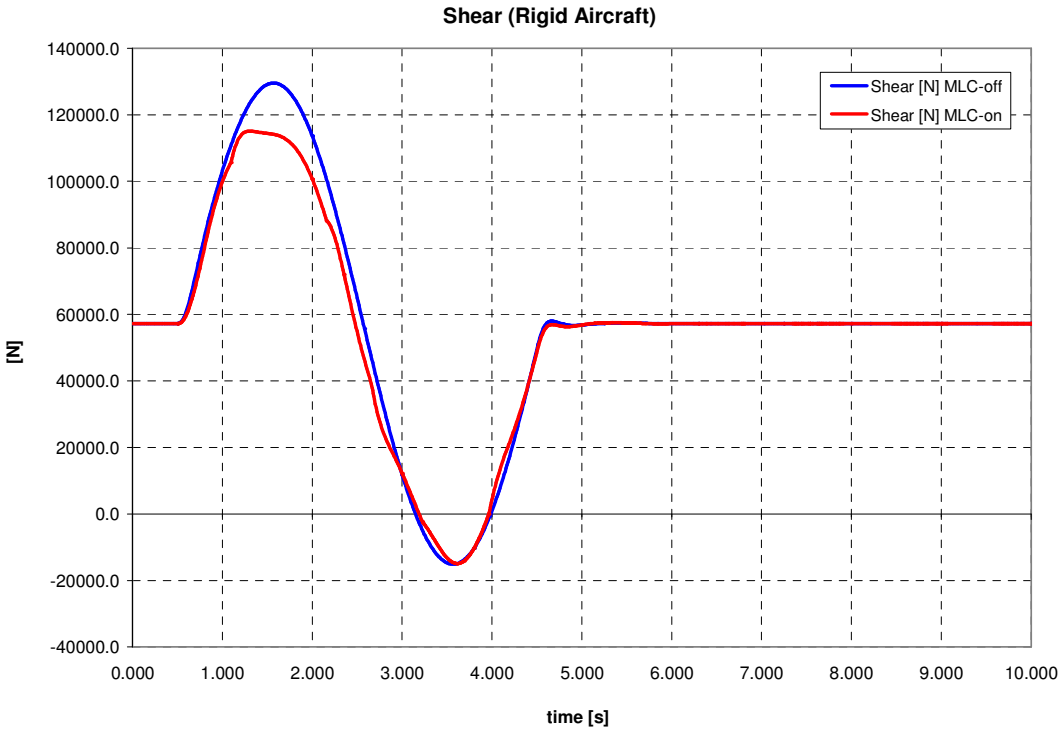

Fig. 74: Shear at the wing root (WCS), Flight Case #2M3, Rigid aircraft.

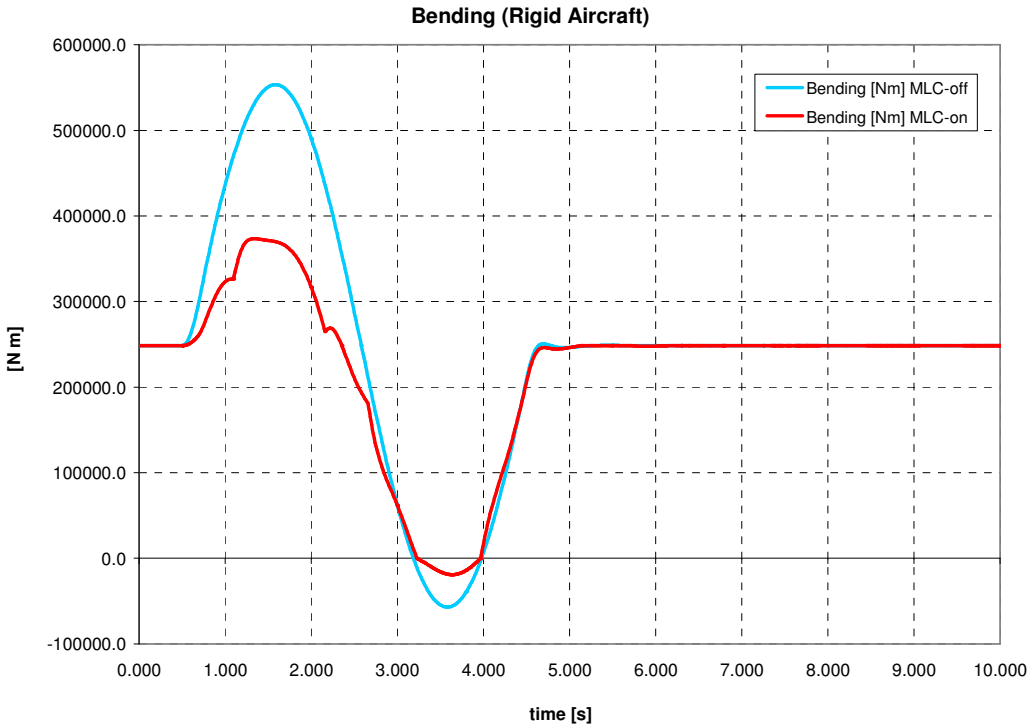

Fig. 75: Bending at the wing root (WCS), Flight Case #2M3, Rigid aircraft.

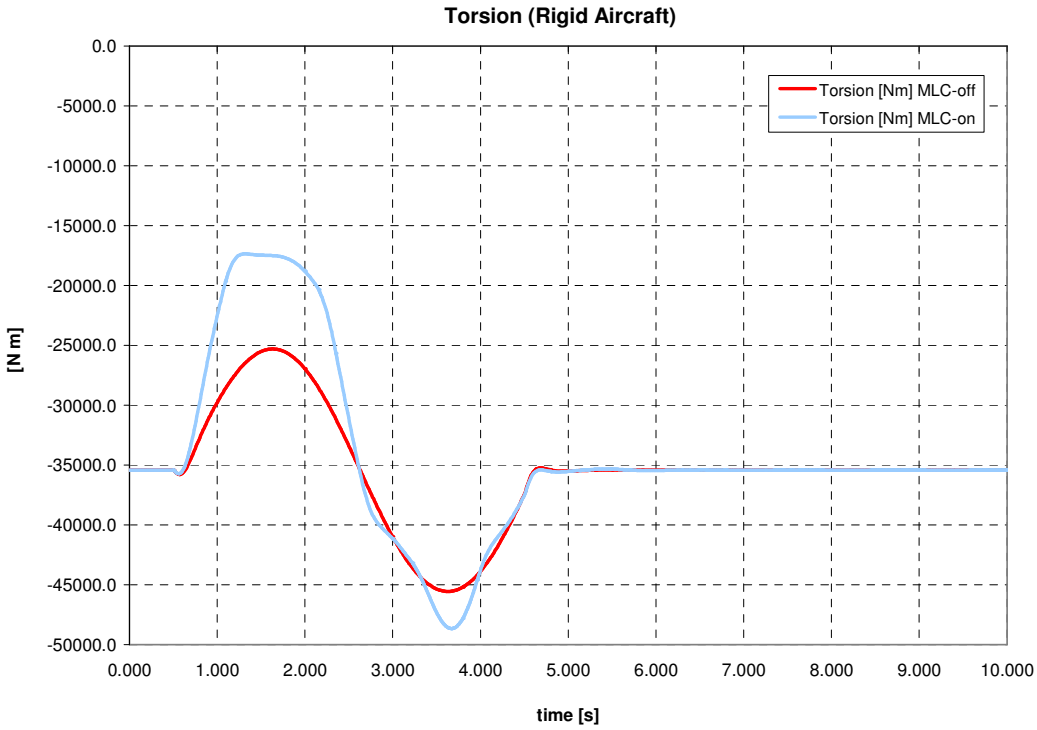

Fig. 76: Torsion at the wing root (WCS), Flight Case #2M3, Rigid aircraft.

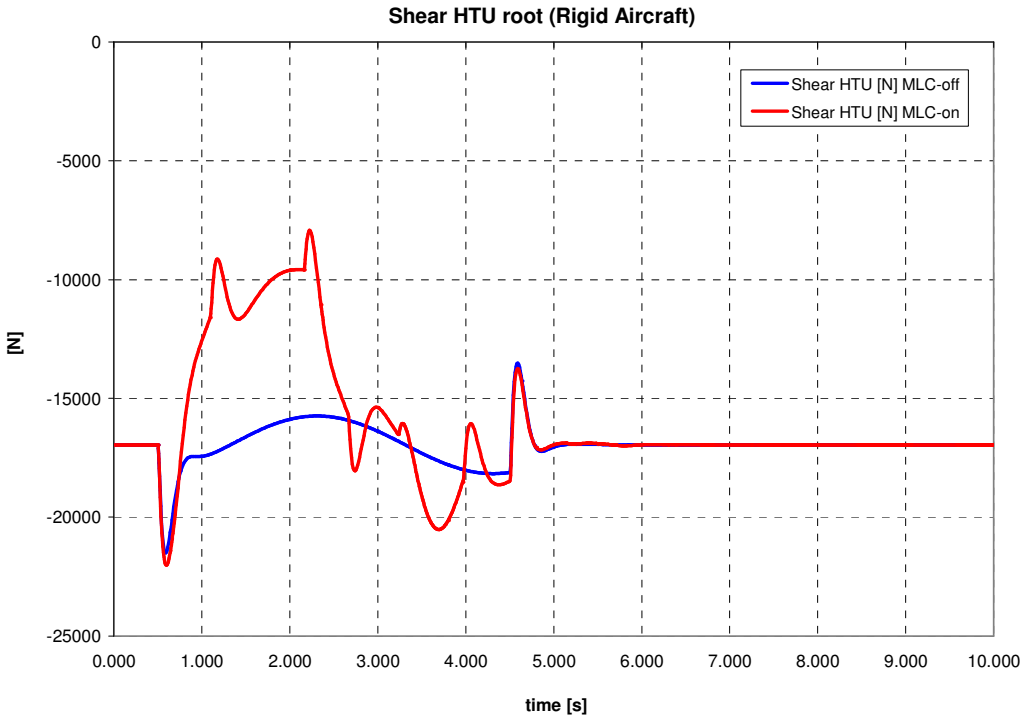

Fig. 77: Shear at the horizontal tail root, Flight Case #2M3, Rigid aircraft.

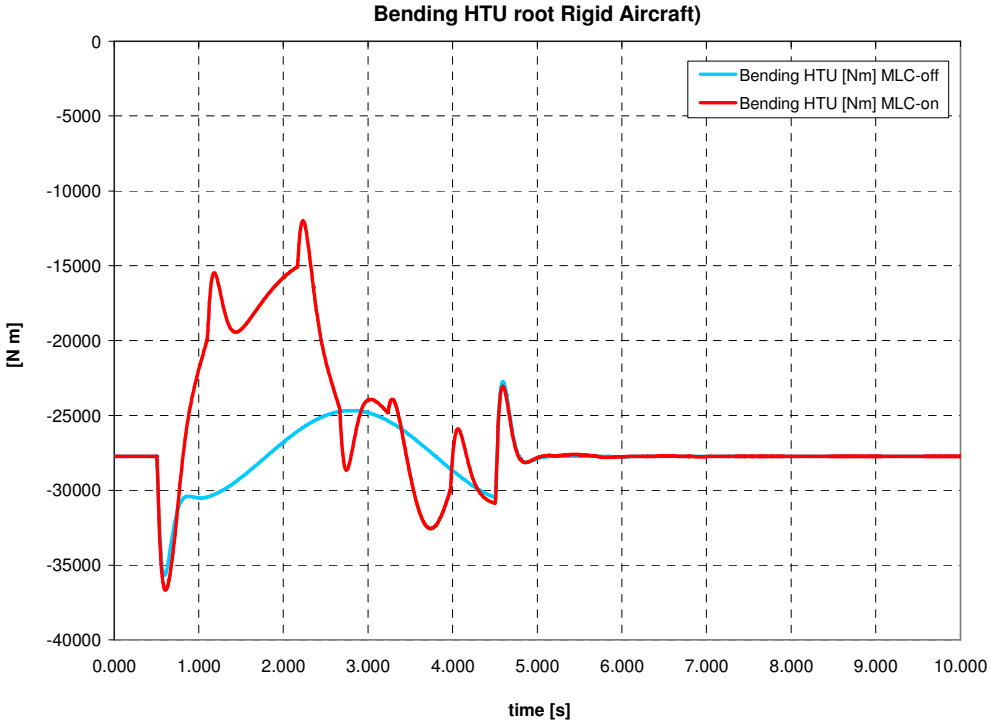

Fig. 78: Bending at the horizontal tail root, Flight Case #2M3, Rigid aircraft.

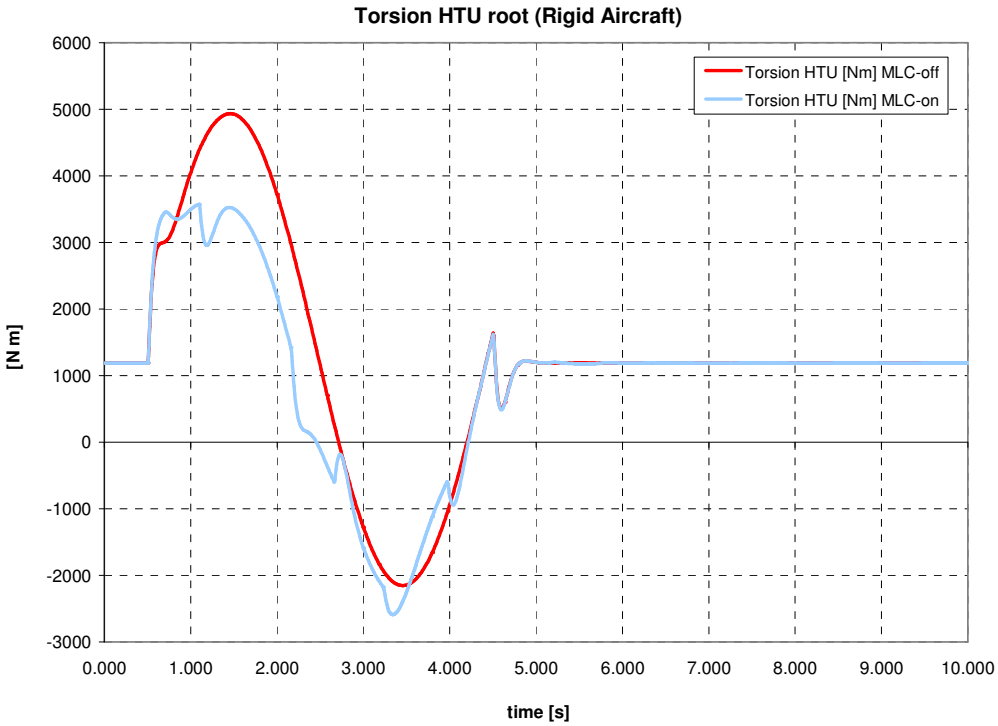

Fig. 79: Torsion at the horizontal tail root, Flight Case #2M3, Rigid aircraft.

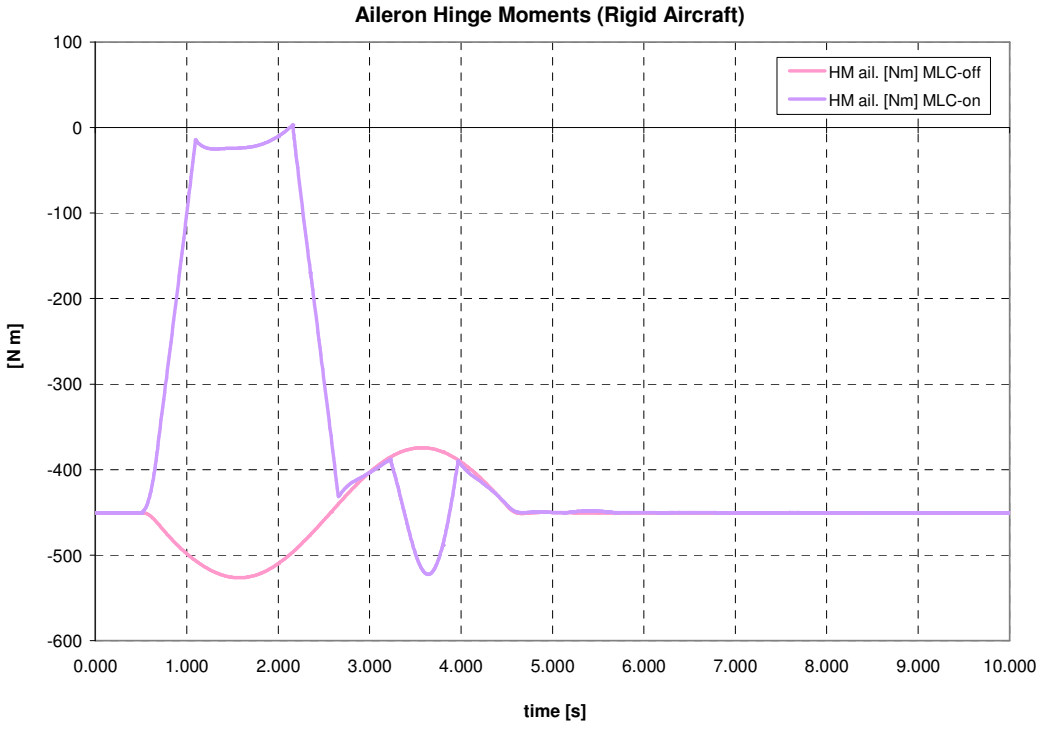

Fig. 80: Aileron Hinge Moments, Flight Case #2M3, Rigid aircraft.

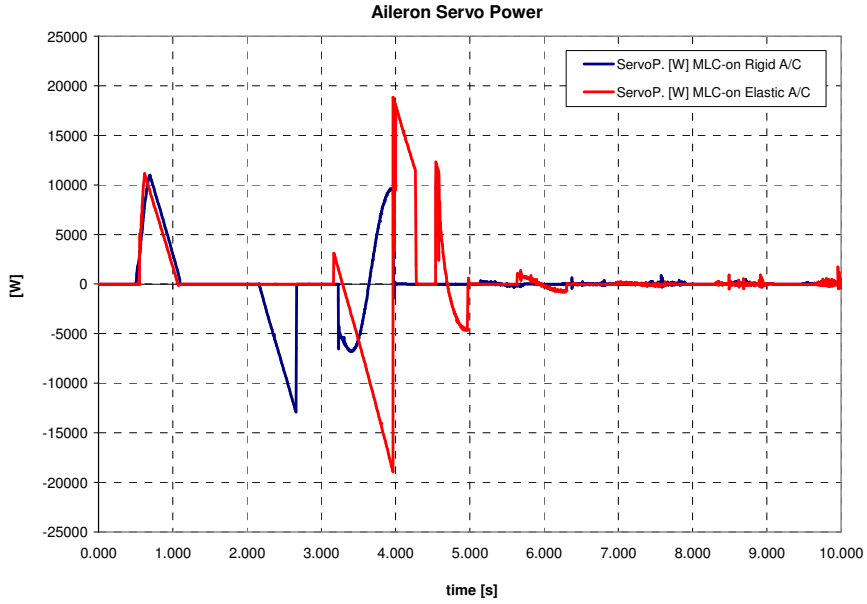

Fig. 81: Aileron Necessary Servo Power, Flight Case #2M3.

For reason of conciseness, only the Alleviation Factors AF coming from the development of the same maneuver for the other flight cases of Table 6 and Table 7 are following presented and discussed.

	Alleviation Factors					
ID	**AF elast**	**AF rig**	**AF elast**	**AF rig**	**AF elast**	**AF rig**
#1	19.99	30.63	18.29	26.42	16.21	23.23
#2	20.88	32.51	18.31	26.56	16.25	23.41
#3	20.32	33.41	18.06	26.52	16.17	23.59
#4	20.88	31.36	18.28	27.29	16.46	23.99
	Mass Condition M3		***Mass Condition M2***		***Mass Condition M1***	

Table 12: Alleviation Factor AF, dependency upon mass conditions.

	Alleviation Factors	
ID	**AF elast**	**AF rig**
	Sensitivity versus M	
#2SM0M3	21.12	30.45
#2M3	20.88	32.51
#2SM1M3	21.29	34.51
#2SM2M3	22.22	34.72
	Sensitivity versus q	
#2Sq0M3	22.36	33.86
#2M3	20.88	32.51
#2Sq1M3	19.42	28.38
#2Sq2M3	17.86	25.29

Table 13: Alleviation Factor AF, dependency upon Mach Number and Dynamic Pressure.

The dependencies of *AF* upon *M*, *q* and aircraft weight (fuel) are depicted in the following three figures for both rigid and elastic aircraft.

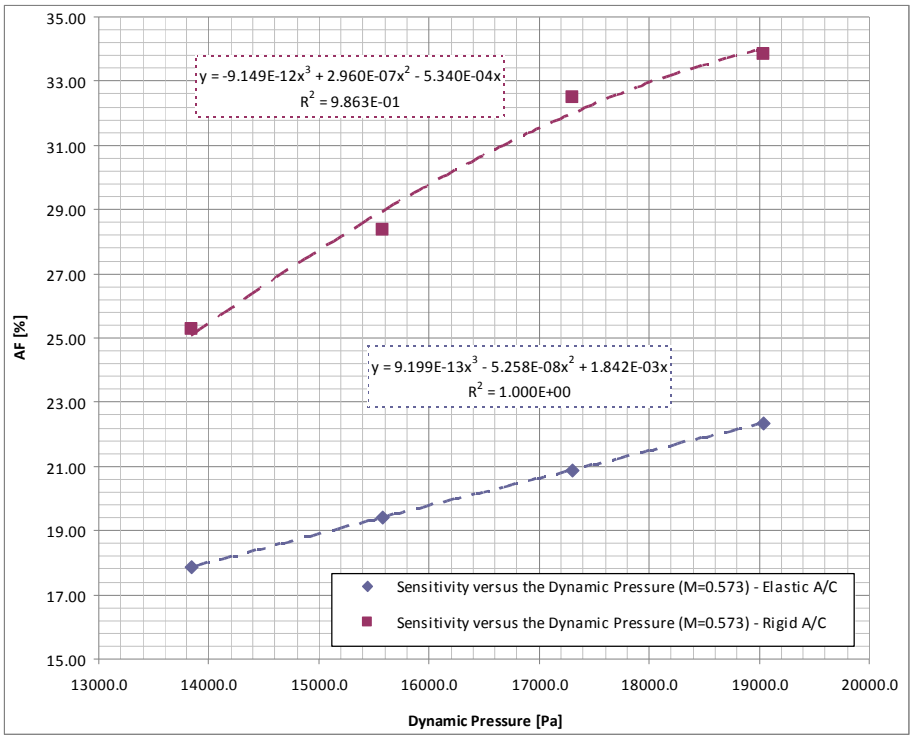

Fig. 82: Alleviation Factor AF, dependency upon the Dynamic Pressure.

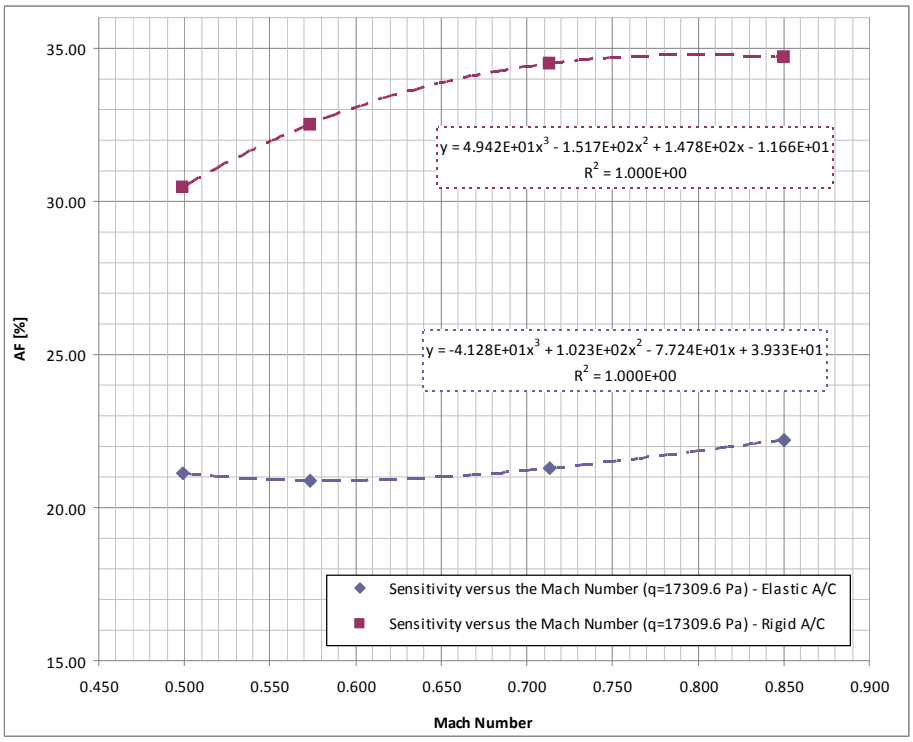

Fig. 83: Alleviation Factor AF, dependency upon the Mach Number.

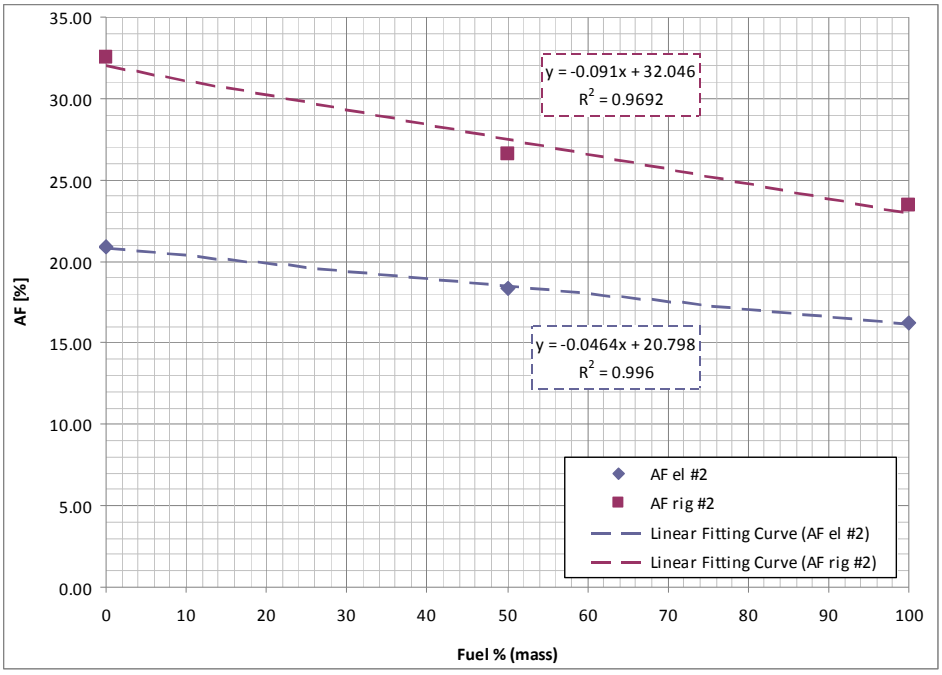

Fig. 84: Alleviation Factor AF, dependency upon mass conditions.

At fixed Mach number, greater the dynamic pressure, more effective the LAS (Fig. 82). The gap between rigid and elastic aircraft increases with the dynamic pressure.

The LAS effectiveness augmentation with Mach number is less marked than with the dynamic pressure (Fig. 83). In case of elastic aircraft, such a dependency becomes very slight.

Fig. 84 shows the dependency of AF upon mass conditions: the trend appears quite linear. This behavior repeats at different flight conditions (i.e. different Mach number and dynamic pressures).

An analytical model made of polynomial functions has been defined by using the data of Table 12 and Table 13 and the fitting curves of Fig. 82, Fig. 83 and Fig. 84. The analytical model so built is then used to recover the alleviation factors previously calculated for flight case #1M3, #2M3, #3M3 and #4M3.

Recovered values are reported in Table 14 together with percent errors. Notice that percent errors are relatively low so that this model can be considered sufficiently reliable to characterize the performance of the MLC system for a wide range of flight conditions in a conceptual design phase.

		Analitical model AF vs q, M		Err. %	
q [Pa]	M	AF Elastic	AF Rigid	Elastic	Rigid
17652.6	0.499	21.43	30.43	6.74	-0.67
17309.6	0.573	20.90	32.00	0.09	-1.62
16565.4	0.713	20.66	32.68	1.65	-2.22
15728.4	0.850	20.80	31.20	-0.39	-0.50

Table 14: Alleviation Factor AF, recovered value and percent errors (analytical model).

4.4. Conclusion Remarks

In this chapter, a conceptual design of an active control system for load alleviation during an unsteady longitudinal maneuvers is presented. An application to a business aircraft considered only as a test case-study has been performed.

The system has been conceived to be able to alleviate the wing bending moment at a wing section near the wing root but by following always the same imposed maneuvering load factor.

The LAS incorporates a Load Factor Feedback (LFF) to the elevators in order to perform a desired longitudinal maneuver by automatically acting on the elevators through a PID controller.

The MLC is accomplished by observing the bending on the wing root section and by symmetrically acting on the ailerons by means of a simple P controller in order to shift the wing center of pressure inboard, and thus to minimize the difference between measured bending moment and 1-g bending moment.

All numerical analyses aimed at simulating the aircraft behavior during maneuver with MLC-on or MLC-off are performed both by taking into account and by neglecting the flexibility of the aircraft. Indeed the synthesis of the controllers has been made by tuning the gains in either case, i.e. for rigid and elastic aircraft, in order to appreciate the different performance by keeping always the same limit gain and phase margins.

The study demonstrates how much is important to consider the effect of aeroelasticity early in the conceptual design of such a MLC system, hence by providing much more reliable indications about their effectiveness and also about the quality of flight mechanics in general.

Results of analyses performed for different dynamic pressures, Mach numbers and mass conditions, show attained wing bending reductions between 17% and 23% ,with minimum wing torsion and horizontal tail load augmentations (under 10%). Furthermore, the calculation of the necessary load alleviator servo power demonstrates also the possibility to adopt such a system with a relatively low dedicated power.

5. Fatigue Life Extension due to a MLC system

As often highlighted in the previous sections, the reduction in structural internal wing loads due to the adoption of a MLC system can be motivated by the requirement of reaching enhanced performance (aerodynamic efficiency growth due to a wing Aspect-Ratio augmentation or higher maneuver limit load factors for high performance aircraft), OEW reduction, or structural fatigue life extension.

The major limit of this kind of systems appears when it has to be installed on commercial transport aircraft for reduced OEW or augmented wing aspect-ratio. In this case extensive RAMS analyses and high redundancy of the MLC related sub-systems are required by the Certification Authority. Otherwise the structural design must be performed at system off. Thus the unique actual benefit to be gained from the adoption of a MLC system on a commercial transport is the fatigue life extension.

The present section is focused on the estimation of the fatigue life extension of a structural joint (wing lower skin-stringer) located close to the wing root. Analyses are carried-out by following the state-of-the-art method presented in [60], [61], and [62].

The application is performed to the same aircraft as sections 3 and 4, a business jet responding to the Part 25 of the EASA Certification Specification, for two kinds of mission: short and long range (see Table 15 and Table 16).

Flight Profile #1: Range 700 NM						
Segment	Pset or Thrust (per engine)	Segment Length (min)	Fuel burned [kg]	Init. Segment A/C Weight [Kg]	Altitude (ft)	Speed (KCAS/Mach)
Taxi	Ground Idle	10	25	13143	0	-
Takeoff	Takeoff	1	50	13118	0 - 1500	-
Climb	MCL	9.5	272.5	13068	1500 - 37000	275 / 0.75
Cruise	MCR	73	1020	12795.5	37000	0.82
Descent	Flight Idle	14	96	11775.5	37000 - 0	270-250
Approach	Flight Idle	2	21	11679.5	0	-
Taxi	Ground Idle	5	12.5	11658.5	0	-
				11646		

Table 15: Flight Profile #1, Short Range Mission – 700 Nautical Miles.

Flight Profile #2:Range 3000 NM						
Segment	Pset or Thrust (per engine)	Segment Length (min)	Fuel burned [kg]	Init. Segment A/C Weight [Kg]	Altitude (ft)	Speed (KCAS/Mach)
Taxi	Ground Idle	10	25	16693	0	-
Takeoff	Takeoff	1	50	16668	0 - 1500	-
Climb	MCL	21.5	497.6	16618	1500 - 43000	275 / 0.75
Cruise	MCR	360	4293	16120.4	43000	0.8
Descent	Flight Idle	19.5	149	11827.4	43000 - 0	270-250
Approach	Flight Idle	2	21	11678.4	0	-
Taxi	Ground Idle	5	12.5	11657.4	0	-
				11644.9		

Table 16: Flight Profile #2, Long Range Mission – 3000 Nautical Miles.

5.1.Analysis Strategy

Analyses are carried-out for both cases of MLC-on and MLC-off in order to appreciate the benefit of having an MLC system in terms of structural fatigue life improvement.

Hypotheses of this work are:

1. When MLC is switched on, the airplane is in level flight with a wing root bending alleviation of 10% (AF=0.1);

2. If a gust front is going to be encountered, the MLC is switched-off and load alleviators (control surfaces) are blocked to the last position for keeping the static load alleviation constant during the turbulence;

As regards the hypothesis No. 1, Appendix 1 reports calculations performed by following the method presented in section 2 and showing that this amount of alleviation is achievable with a load alleviator deflection of few degrees (about 3 degrees).

Indeed the hypothesis No. 2 is applicable since the aircraft is equipped with a cloud warning radar.

5.2.Determination of Cumulative Frequency Load Distributions

The fatigue life of civil aircraft wing structures is related to the variations in stress experienced under the following five main types of loading:

1. Gust Loads;
2. In-flight maneuver loads;
3. Ground maneuver loads;
4. The once-per-flight loads resulting from the difference between in-flight and on-ground load levels, usually termed the Ground-Air-Ground (GAG)-cycle;
5. Local loads such as those arising from flaps, undercarriages, etc.

The method to determine the cumulative frequency of occurrence of loads 1 and 2 are presented in [61] whereas for loads 3 in [62].

The GAG-cycle (load type 4) is derived from the in-flight gust and maneuver spectrum and the ground maneuver cumulative frequency distributions as described in [60].

Loads 5 are special cases not accounted for in the damage calculation presented herein.

5.2.1. Bending Moment vs Cumulative Frequency of Occurrence. Gust and In-Flight Maneuver Loads

Cumulative Frequency versus wing root bending moment due to flight loads is calculated for both missions, short and long range. The aircraft is assumed to carry a cloud warning radar.

Table 17 and Table 18 report detailed data of each flight plan together with gust parameters. The presented gust data are normalized with respect to the 10 *ft/s* (3.05 *m/s*) gust, as done in [61].

									Total Mission Time (min)=	99.5																	AF=	0.1	
Stage	Description	Length [min]	Fuel burned [kg]	Initial A/C Weight	Hp init [ft]	Hp end [ft]	Speed [KCAS]	Hp med. [ft]	σ (p/p_0)	Speed [KEAS]	Speed [KTAS]	q [Pa]	D [km]	W [kN]	M	$C_{L\alpha}$ rig (a)	$\frac{2W}{g\rho_0\sigma S a c}$	F_0	F_M/F_0	F_M	k	l_{10} [nmiles]	l_{10} [km]	D/ l_{10}	Δn_{10}	Mm [N m]	Mm MLC-on [N m]	ΔM(10) [N m]	ΔM(10) MLC-on [N m]
1	Takeoff	1	50	13118	0	1500	218	750	0.978	217.4	219.8	7662.8	6.8	128.4	0.333	5.716	32.3	0.792	0.972	0.770	2.417	9.5	17.6	0.386	0.357	2.11E+05	1.90E+05	7.53E+04	6.77E+04
2	Climb	9.5	272.5	13068	1500	37000	275	19250	0.547	269.1	364.0	11737.5	106.7	126.9	0.591	6.217	52.5	0.859	0.941	0.809	1.076	350.0	648.2	0.165	0.707	2.17E+05	1.95E+05	1.53E+05	1.38E+05
3	Cruise	73	1020	12795.5	37000	37000	267	37000	0.284	250.8	470.3	10196.1	1059.8	120.5	0.820	7.296	81.6	0.902	0.901	0.813	1.020	3500.0	6482.0	0.163	1.185	2.19E+05	1.97E+05	2.59E+05	2.33E+05
4	Descent	14	96	11775.5	37000	0	260	18500	0.560	255.2	340.9	10559.7	147.3	115.0	0.552	6.112	47.2	0.848	0.947	0.803	1.083	300.0	555.6	0.265	0.708	2.00E+05	1.80E+05	1.42E+05	1.28E+05
5	Approach	2	21	11679.5	0	0	-	0	1.000			D_{TOT}=	1320.6																

Table 17: Calculation of Flight Parameters – Flight Profile #1.

									Total Mission Time (min)=	404																	AF=	0.1	
Stage	Description	Length [min]	Fuel burned [kg]	Initial A/C Weight	Hp init [ft]	Hp end [ft]	Speed [KCAS]	Hp med. [ft]	σ (p/p_0)	Speed [KEAS]	Speed [KTAS]	q [Pa]	D [km]	W [kN]	M	$C_{L\alpha}$ rig (a)	$\frac{2W}{g\rho_0\sigma S a c}$	F_0	F_M/F_0	F_M	k	l_{10} [nmiles]	l_{10} [km]	D/ l_{10}	Δn_{10}	Mm [N m]	Mm MLC-on [N m]	ΔM(10) [N m]	ΔM(10) MLC-on [N m]
1	Takeoff	1	50	16668	0	1500	190	750	0.978	189.9	192.0	5848.6	5.9	163.3	0.291	5.670	41.4	0.830	0.976	0.810	2.417	9.5	17.6	0.337	0.255	2.49E+05	2.24E+05	6.37E+04	5.73E+04
2	Climb	21.5	497.6	16618	1500	43000	220	22250	0.493	216.1	307.7	7569.3	204.2	160.6	0.505	6.001	76.2	0.898	0.953	0.856	1.058	700.0	1296.4	0.157	0.476	2.56E+05	2.30E+05	1.22E+05	1.10E+05
3	Cruise	360	4293	16120.4	43000	43000	245	43000	0.213	227.6	493.1	8399.6	5479.3	137.1	0.860	7.613	118.7	0.926	0.893	0.826	1.020	6000.0	11112.0	0.493	1.169	2.61E+05	2.35E+05	3.06E+05	2.75E+05
4	Descent	19.5	149	11827.4	43000	0	220	21500	0.506	216.3	304.0	7583.4	183.0	115.3	0.498	5.986	53.5	0.862	0.954	0.822	1.061	500.0	926.0	0.198	0.627	2.00E+05	1.80E+05	1.25E+05	1.13E+05
5	Approach	2	21	11678.4	0	0	-	0	1.000			D_{TOT}=	5872.4																

Table 18: Calculation of Flight Parameters – Flight Profile #2.

To evaluate the Alleviating Factor F_M diagrams of Fig. 85 (extracted from [61]) are used. The calculation of $\frac{2W}{g\rho Sac}$, $\frac{\bar{c}}{d_e}$ and A are required, where a is the lift coefficient slope (corrected with the Mach Number influence), A is the aspect ratio and d_e is evaluated according to the expression $d_e = d + \frac{b}{2}\tan\Lambda$. d is the gust gradient distance for unswept wings (100 *ft*, 30.5 *m*) and Λ is the sweep angle.

The ratio of up-gusts to down-gusts k is determined by means of the diagram provided by [61], and reported in Fig. 86.

l_{10} is defined as the distance that the aircraft has to cover to meet a 10 *ft/s* (3.05 *m/s*) gust whereas Δn_{10} is the incremental normal load factor arising from such a gust, according to the formula $\Delta n = \frac{\rho_0 V_e S a F_0 v_e}{2W}$, where V_e is the EAS of the airplane and v_e is the EAS of the gust. l_{10} is obtained from Fig. 87, extracted from [61].

M_m is the wing root bending in trimmed flight at n=1 and ΔM_{10} is the incremental wing root bending due to the incremental normal load factor Δn_{10}, both bending values calculated for MLC-off and MLC-on (with AF=0.1).

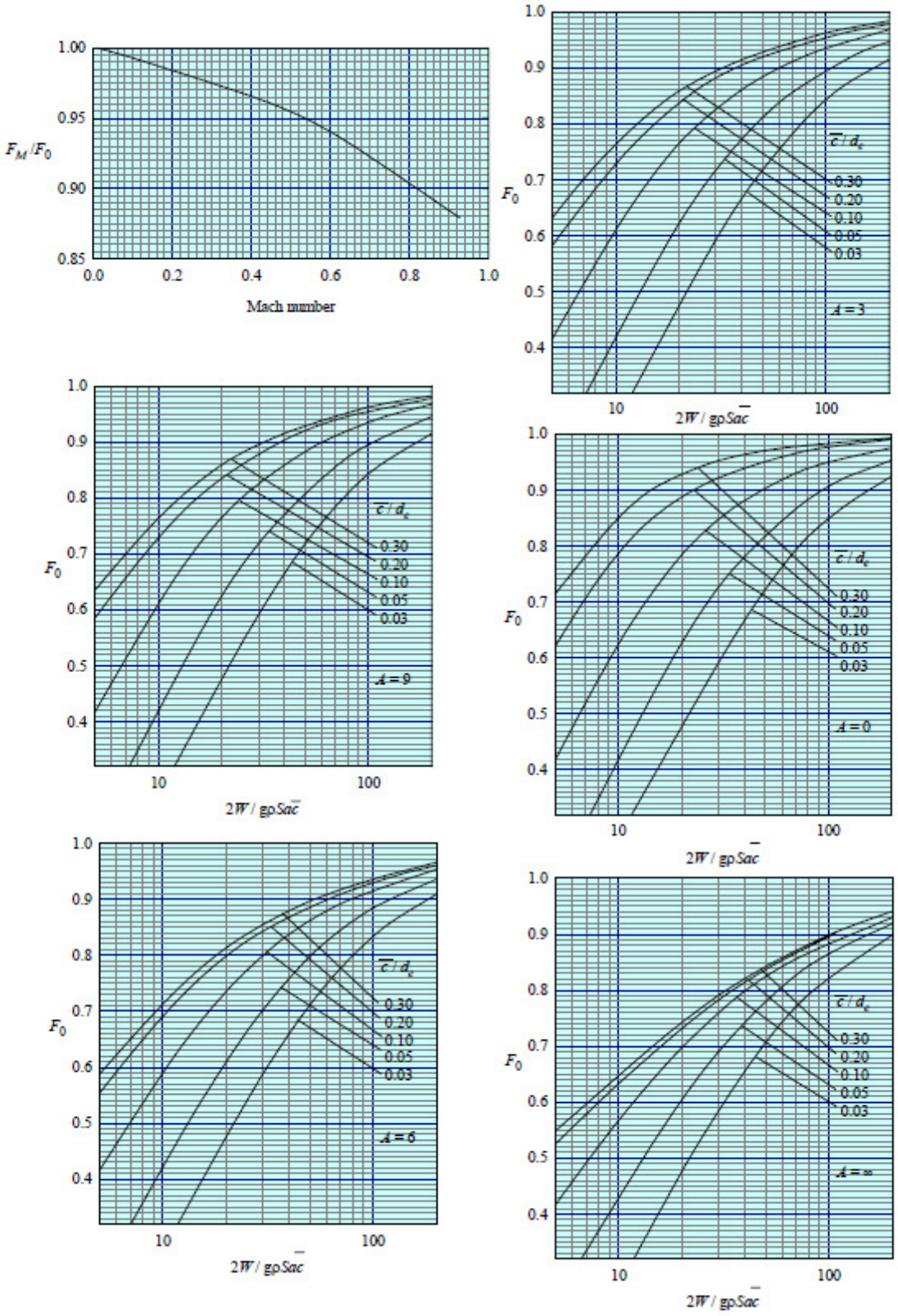

Fig. 85: Alleviating Factor for Vertical Gusts.

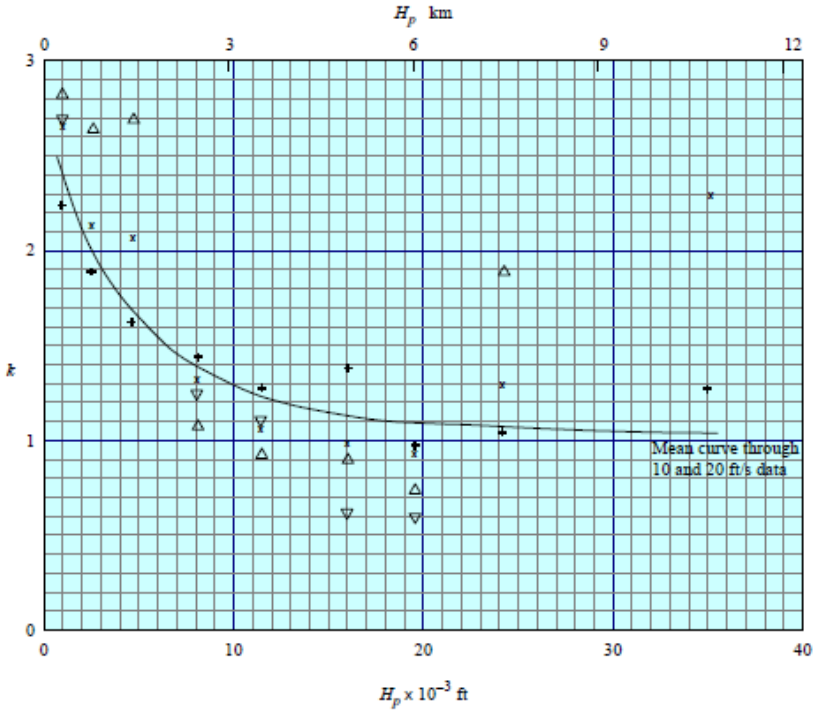

Fig. 86: Ratio of Up-gusts to Down-gusts.

The calculation of cumulative frequency versus wing root bending moment curves is done by choosing a value of M_{max} and a value of M_{min}, respectively greater than and smaller than M_m. Their differences ΔM is then calculated and the ratio $\frac{\Delta M}{\Delta M_{10}}$ used to factor the 10 *ft/s* gust and thus to estimate the gust velocity v_e.

The gust velocity v_e, for both up-gust and down-gust, is used to read the relative gust frequencies by means of Fig. 88, extracted from [61].

The cumulative frequencies of up-gust $(f_c)_u$ and down-gust $(f_c)_d$ are then calculated by factorizing with k according to the following expressions:

$$(f_c)_u = \left(\frac{D}{l_{10}}\right) r \frac{k}{1+k}, \tag{59}$$

$$(f_c)_d = \left(\frac{D}{l_{10}}\right) r \left(1 - \frac{k}{1+k}\right). \tag{60}$$

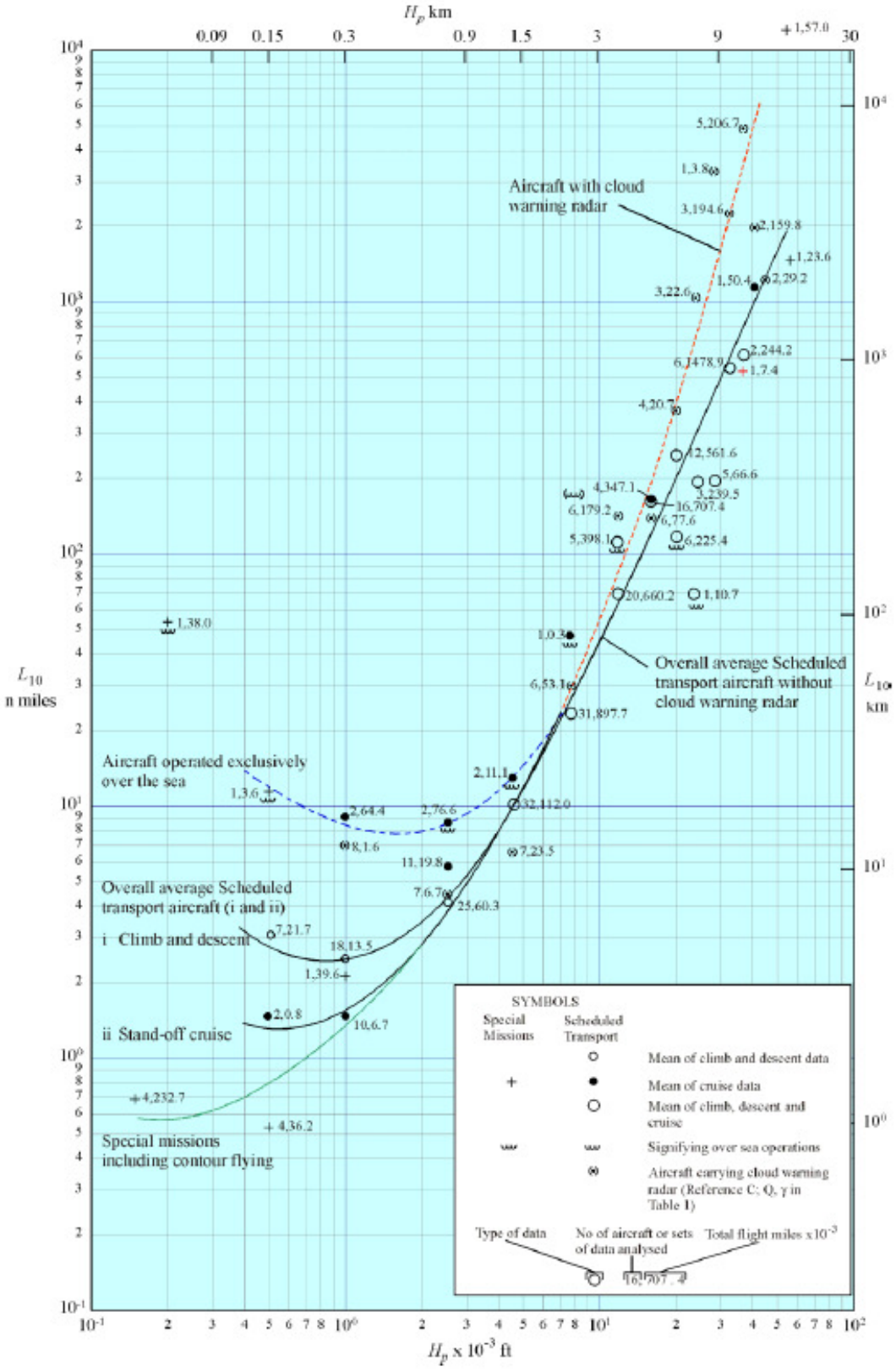

Fig. 87: Gust Frequencies, Overall Averages.

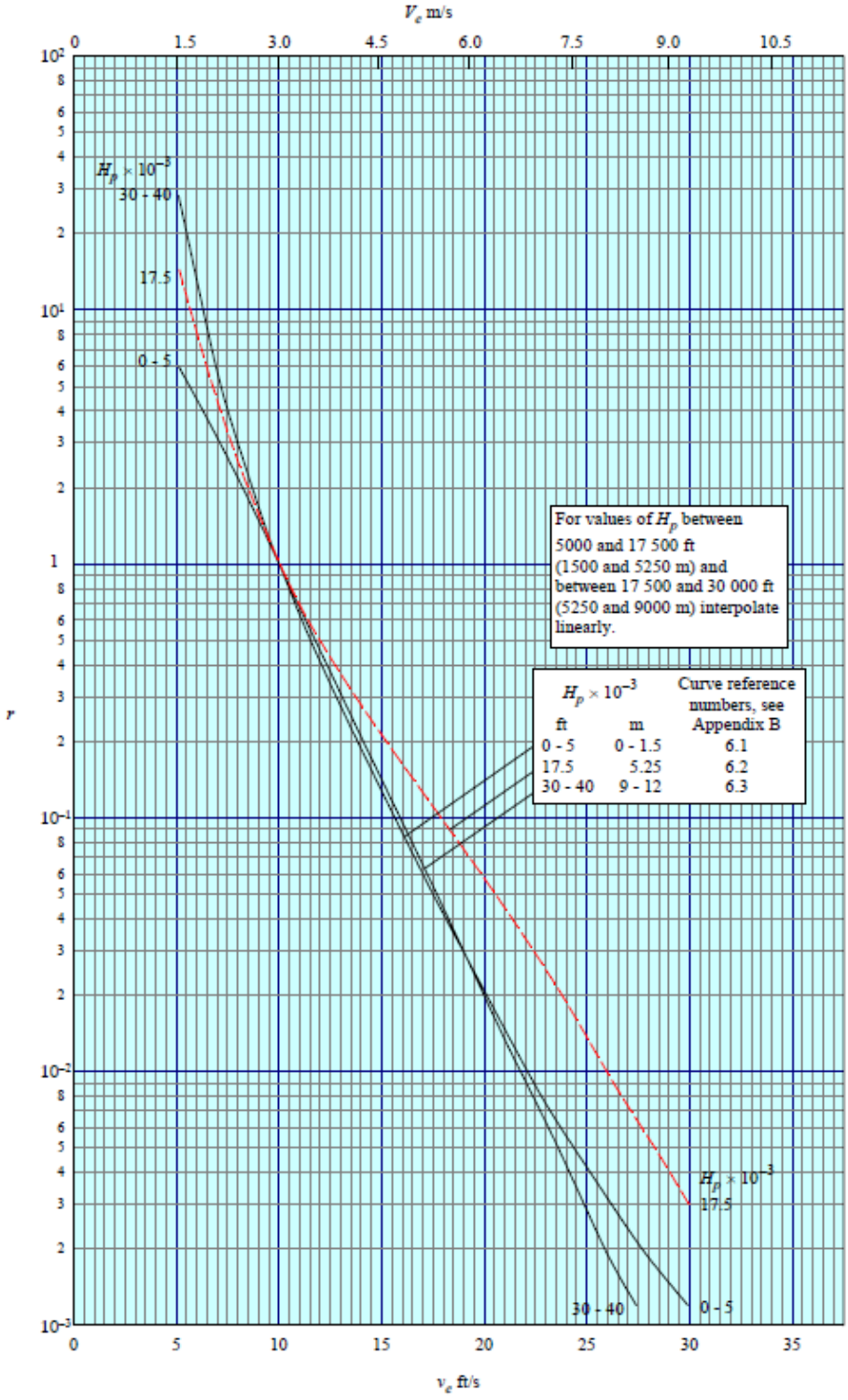

Fig. 88: Relative Gust Frequencies (Aircraft with Cloud Warning Radar).

Table 19 and Table 20 show the calculation of the cumulative frequency of occurrence of the bending moments M_{max}=350 *kN m* and M_{min}=45.0 *kN m*, for **Flight Profile #1**, respectively in case of MLC-off and MLC-on. Moments are in *N m*.

	M_{max}=	3.50E+05		M_{min}=	4.50E+04	
Flight Stage	$(v_e)_u$	r	$(f_c)_u$	$(v_e)_d$	r	$(f_c)_d$
1	5.64E+00	3.47E-02	9.47E-03	6.72E+00	1.06E-02	2.90E-03
2	2.66E+00	1.75E+00	1.49E-01	3.42E+00	6.35E-01	5.42E-02
3	1.54E+00	2.67E+01	2.20E+00	2.05E+00	7.03E+00	5.81E-01
4	3.22E+00	8.07E-01	1.11E-01	3.34E+00	6.97E-01	9.61E-02
		Σ=	2.47E+00		Σ=	7.34E-01

Table 19: Cumulative Frequency of Occurrence – M_{max}=350 kNm, M_{min}=45.0 kNm – MLC-off – Flight Profile #1.

	M_{max}=	3.50E+05		M_{min}=	4.50E+04	
Flight Stage	$(v_e)_u$	r	$(f_c)_u$	$(v_e)_d$	r	$(f_c)_d$
1	5.64E+00	3.47E-02	9.47E-03	6.72E+00	1.06E-02	2.90E-03
2	2.66E+00	1.75E+00	1.49E-01	3.42E+00	6.35E-01	5.42E-02
3	1.54E+00	2.67E+01	2.20E+00	2.05E+00	7.03E+00	5.81E-01
4	3.22E+00	8.07E-01	1.11E-01	3.34E+00	6.97E-01	9.61E-02
		Σ=	2.47E+00		Σ=	7.34E-01

Table 20: Cumulative Frequency of Occurrence – M_{max}=350 kNm, M_{min}=45.0 kNm – MLC-on – Flight Profile #1.

Cumulative frequencies obtained by repeating the procedure of Table 19 and Table 20 for a range of Bending Moments, for the flight stage 3 (cruise), are reported in Table 21 and Table 22, respectively for MLC-on and MLC-off.

Cumulative frequencies versus bending moments are also plotted in Fig. 89.

Cruise; MLC-off			
$(f_c)_u$	M_{max}	$(f_c)_d$	M_{min}
9.99E-04	7.73E+05	1.00E-03	-3.35E+05
3.00E-03	6.99E+05	3.00E-03	-2.61E+05
1.00E-02	6.18E+05	1.00E-02	-1.81E+05
3.00E-02	5.44E+05	3.00E-02	-1.07E+05
1.00E-01	4.67E+05	1.00E-01	-2.90E+04
3.00E-01	4.16E+05	3.00E-01	2.19E+04
1.00E+00	3.75E+05	1.00E+00	6.21E+04
3.00E+00	3.40E+05	3.00E+00	9.77E+04
1.00E+01	3.01E+05	1.00E+01	1.37E+05
3.00E+01	2.66E+05	3.00E+01	1.72E+05
1.00E+02	2.27E+05	1.00E+02	2.11E+05

Table 21: Cumulative Frequencies for a range of bending moments – MLC-off – Cruise (Flight Profile #1).

Cruise; MLC-on; AF=0.1			
$(f_c)_u$	M_{max}	$(f_c)_d$	M_{min}
9.99E-04	6.95E+05	1.00E-03	-3.01E+05
3.00E-03	6.29E+05	3.00E-03	-2.35E+05
1.00E-02	5.57E+05	1.00E-02	-1.63E+05
3.00E-02	4.90E+05	3.00E-02	-9.60E+04
1.00E-01	4.20E+05	1.00E-01	-2.61E+04
3.00E-01	3.74E+05	3.00E-01	1.97E+04
1.00E+00	3.38E+05	1.00E+00	5.59E+04
3.00E+00	3.06E+05	3.00E+00	8.80E+04
1.00E+01	2.71E+05	1.00E+01	1.23E+05
3.00E+01	2.39E+05	3.00E+01	1.55E+05
1.00E+02	2.04E+05	1.00E+02	1.90E+05

Table 22: Cumulative Frequencies for a range of bending moments – MLC-on – Cruise (Flight Profile #1).

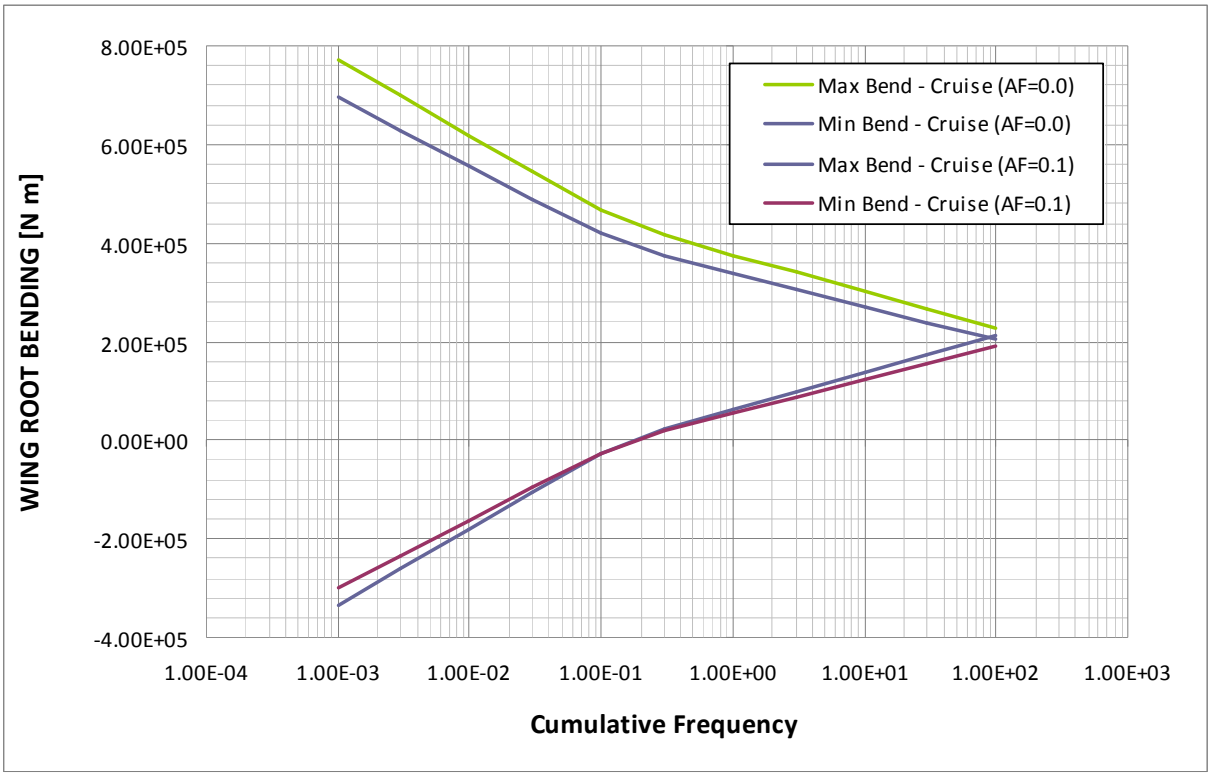

Fig. 89: Cumulative Frequencies versus bending moments – Cruise (Flight Profile #1)

Cumulative frequencies for the whole flight profile #1, are reported in Table 23 and Table 24, respectively for MLC-on and MLC-off.

Cumulative frequencies versus bending moments are also plotted in Fig. 90.

Flight Proflie #1; MLC-off			
$(f_c)_u$	M_{max}	$(f_c)_d$	M_{min}
9.99E-04	7.73E+05	1.00E-03	-3.35E+05
3.00E-03	7.01E+05	3.00E-03	-2.66E+05
1.00E-02	6.25E+05	1.00E-02	-1.91E+05
3.00E-02	5.55E+05	3.00E-02	-1.22E+05
1.00E-01	4.78E+05	1.00E-01	-4.58E+04
3.00E-01	4.23E+05	3.00E-01	1.10E+04
1.00E+00	3.80E+05	1.00E+00	5.52E+04
3.00E+00	3.44E+05	3.00E+00	9.06E+04
1.00E+01	3.06E+05	1.00E+01	1.26E+05
3.00E+01	2.73E+05	3.00E+01	1.55E+05
1.00E+02	2.41E+05	1.00E+02	1.83E+05

Table 23: Cumulative Frequencies for a range of bending moments – MLC-off – Flight Profile #1.

Flight Proflie #1; MLC-on; AF=0.1			
$(f_c)_u$	M_{max}	$(f_c)_d$	M_{min}
9.99E-04	6.95E+05	1.00E-03	-3.02E+05
3.00E-03	6.31E+05	3.00E-03	-2.39E+05
1.00E-02	5.63E+05	1.00E-02	-1.72E+05
3.00E-02	4.99E+05	3.00E-02	-1.10E+05
1.00E-01	4.30E+05	1.00E-01	-4.12E+04
3.00E-01	3.81E+05	3.00E-01	9.89E+03
1.00E+00	3.42E+05	1.00E+00	4.97E+04
3.00E+00	3.09E+05	3.00E+00	8.15E+04
1.00E+01	2.75E+05	1.00E+01	1.13E+05
3.00E+01	2.46E+05	3.00E+01	1.39E+05
1.00E+02	2.17E+05	1.00E+02	1.64E+05

Table 24: Cumulative Frequencies for a range of bending moments – MLC-on – Flight Profile #1.

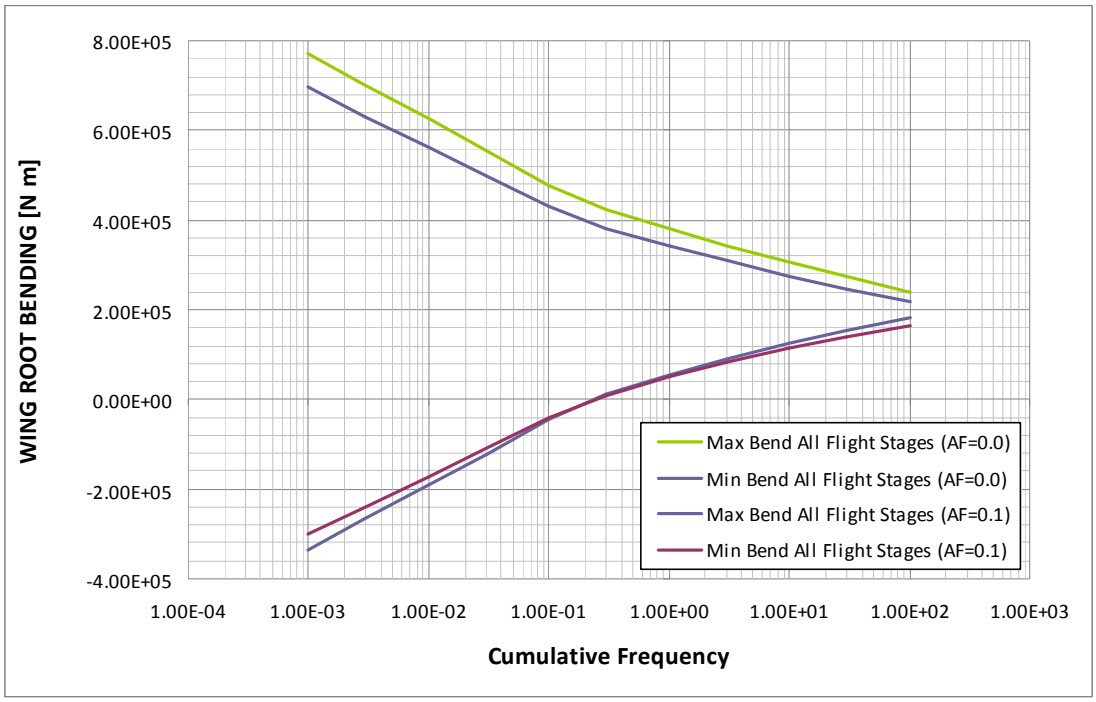

Fig. 90: Cumulative Frequencies versus bending moments – Flight Profile #1.

Table 25 and Table 26 show the calculation of the cumulative frequency of occurrence of the bending moments M_{max}=350 *kN m* and M_{min}=45.0 *kN m*, for **Flight Profile #2**, respectively in case of MLC-off and MLC-on. Moments are in *N m*.

	M_{max}=	3.50E+05		M_{min}=	4.50E+04	
Flight Stage	$(v_e)_u$	r	$(f_c)_u$	$(v_e)_d$	r	$(f_c)_d$
1	4.83E+00	9.12E-02	2.17E-02	9.79E+00	3.48E-04	8.28E-05
2	2.36E+00	3.03E+00	2.45E-01	5.28E+00	9.31E-02	7.54E-03
3	8.84E-01	1.51E+02	3.75E+01	2.16E+00	5.25E+00	1.31E+00
4	3.66E+00	4.80E-01	4.89E-02	3.77E+00	4.25E-01	4.32E-02
		Σ=	**3.78E+01**		**Σ=**	**1.36E+00**

Table 25: Cumulative Frequency of Occurrence – M_{max}=350 kNm, M_{min}=45.0 kNm – MLC-off – Flight Profile #2.

	M_{max}=	3.50E+05		M_{min}=	4.50E+04	
Flight Stage	$(v_e)_u$	r	$(f_c)_u$	$(v_e)_d$	r	$(f_c)_d$
1	6.69E+00	1.09E-02	2.61E-03	9.55E+00	6.36E-04	1.52E-04
2	3.33E+00	6.99E-01	5.66E-02	5.15E+00	1.05E-01	8.49E-03
3	1.27E+00	5.42E+01	1.35E+01	2.11E+00	5.95E+00	1.48E+00
4	4.60E+00	1.82E-01	1.86E-02	3.65E+00	4.86E-01	4.94E-02
		Σ=	**1.36E+01**		**Σ=**	**1.54E+00**

Table 26: Cumulative Frequency of Occurrence – M_{max}=350 kNm, M_{min}=45.0 kNm – MLC-on – Flight Profile #2.

Cumulative frequencies for cruise and for the whole flight profile #2, are reported in Table 27, Table 28, Table 29 and Table 30, for both cases of MLC-on and MLC-off.

Cumulative frequencies versus bending moments are also plotted in Fig. 91 and Fig. 92.

Cruise; MLC-off			
$(f_c)_u$	M_{max}	$(f_c)_d$	M_{min}
1.00E-03	1.01E+06	1.00E-03	-4.87E+05
3.00E-03	9.15E+05	3.00E-03	-3.92E+05
1.00E-02	8.20E+05	1.00E-02	-2.97E+05
3.00E-02	7.33E+05	3.00E-02	-2.10E+05
1.00E-01	6.37E+05	1.00E-01	-1.14E+05
3.00E-01	5.54E+05	3.00E-01	-3.11E+04
1.00E+00	4.89E+05	1.00E+00	3.37E+04
3.00E+00	4.46E+05	3.00E+00	7.66E+04
1.00E+01	4.00E+05	1.00E+01	1.23E+05
3.00E+01	3.59E+05	3.00E+01	1.64E+05
1.00E+02	3.13E+05	1.00E+02	2.10E+05

Table 27: Cumulative Frequencies for a range of bending moments – MLC-off – Cruise (Flight Profile #2).

Cruise; MLC-on; AF=0.1			
$(f_c)_u$	M_{max}	$(f_c)_d$	M_{min}
1.00E-03	9.09E+05	1.00E-03	-4.39E+05
3.00E-03	8.23E+05	3.00E-03	-3.53E+05
1.00E-02	7.38E+05	1.00E-02	-2.67E+05
3.00E-02	6.60E+05	3.00E-02	-1.89E+05
1.00E-01	5.73E+05	1.00E-01	-1.03E+05
3.00E-01	4.99E+05	3.00E-01	-2.80E+04
1.00E+00	4.40E+05	1.00E+00	3.03E+04
3.00E+00	4.02E+05	3.00E+00	6.89E+04
1.00E+01	3.60E+05	1.00E+01	1.10E+05
3.00E+01	3.23E+05	3.00E+01	1.48E+05
1.00E+02	2.81E+05	1.00E+02	1.89E+05

Table 28: Cumulative Frequencies for a range of bending moments – MLC-on – Cruise (Flight Profile #2).

Flight Proflie #1; MLC-off			
$(f_c)_u$	M_{max}	$(f_c)_d$	M_{min}
1.00E-03	1.01E+06	1.00E-03	-4.87E+05
3.00E-03	9.15E+05	3.00E-03	-3.92E+05
1.00E-02	8.20E+05	1.00E-02	-2.97E+05
3.00E-02	7.33E+05	3.00E-02	-2.10E+05
1.00E-01	6.37E+05	1.00E-01	-1.15E+05
3.00E-01	5.54E+05	3.00E-01	-3.29E+04
1.00E+00	4.89E+05	1.00E+00	3.21E+04
3.00E+00	4.46E+05	3.00E+00	7.51E+04
1.00E+01	4.01E+05	1.00E+01	1.19E+05
3.00E+01	3.59E+05	3.00E+01	1.55E+05
1.00E+02	3.14E+05	1.00E+02	1.86E+05

Table 29: Cumulative Frequencies for a range of bending moments – MLC-off – Flight Profile #2.

Flight Proflie #1; MLC-on; AF=0.1			
$(f_c)_u$	M_{max}	$(f_c)_d$	M_{min}
1.00E-03	9.09E+05	1.00E-03	-4.39E+05
3.00E-03	8.23E+05	3.00E-03	-3.53E+05
1.00E-02	7.38E+05	1.00E-02	-2.67E+05
3.00E-02	6.60E+05	3.00E-02	-1.89E+05
1.00E-01	5.73E+05	1.00E-01	-1.04E+05
3.00E-01	4.99E+05	3.00E-01	-2.96E+04
1.00E+00	4.40E+05	1.00E+00	2.89E+04
3.00E+00	4.02E+05	3.00E+00	6.76E+04
1.00E+01	3.60E+05	1.00E+01	1.08E+05
3.00E+01	3.23E+05	3.00E+01	1.40E+05
1.00E+02	2.82E+05	1.00E+02	1.68E+05

Table 30: Cumulative Frequencies for a range of bending moments – MLC-on – Flight Profile #2.

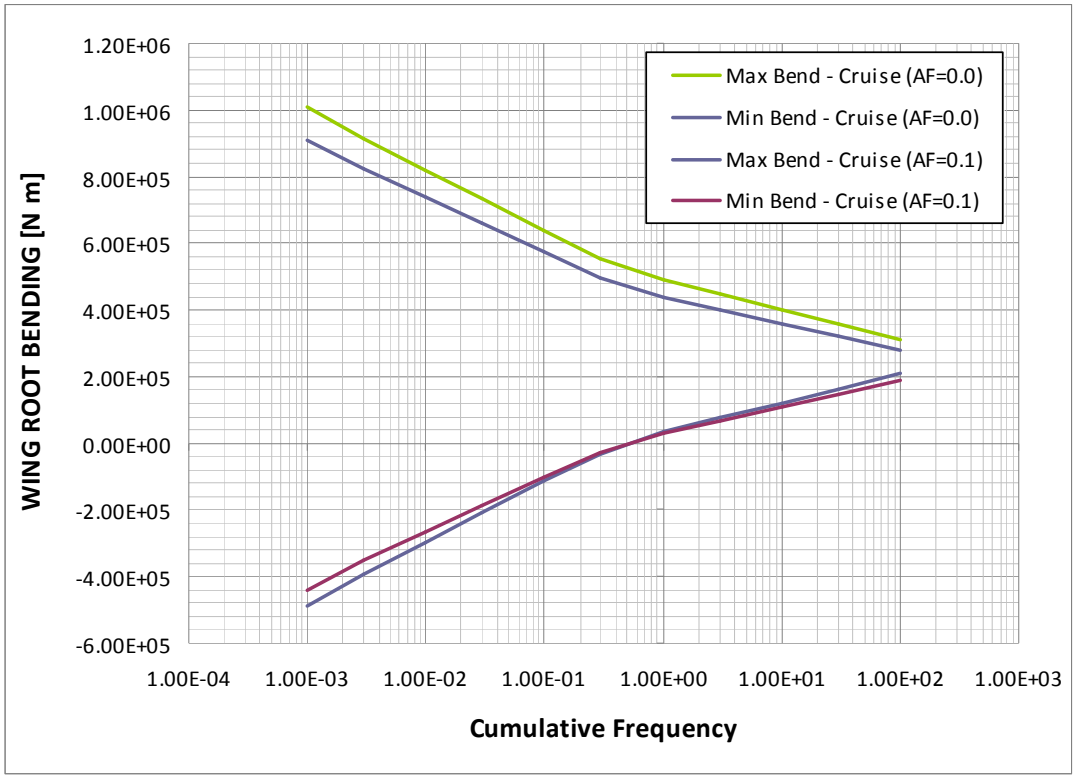

Fig. 91: Cumulative Frequencies versus bending moments – Cruise (Flight Profile #2).

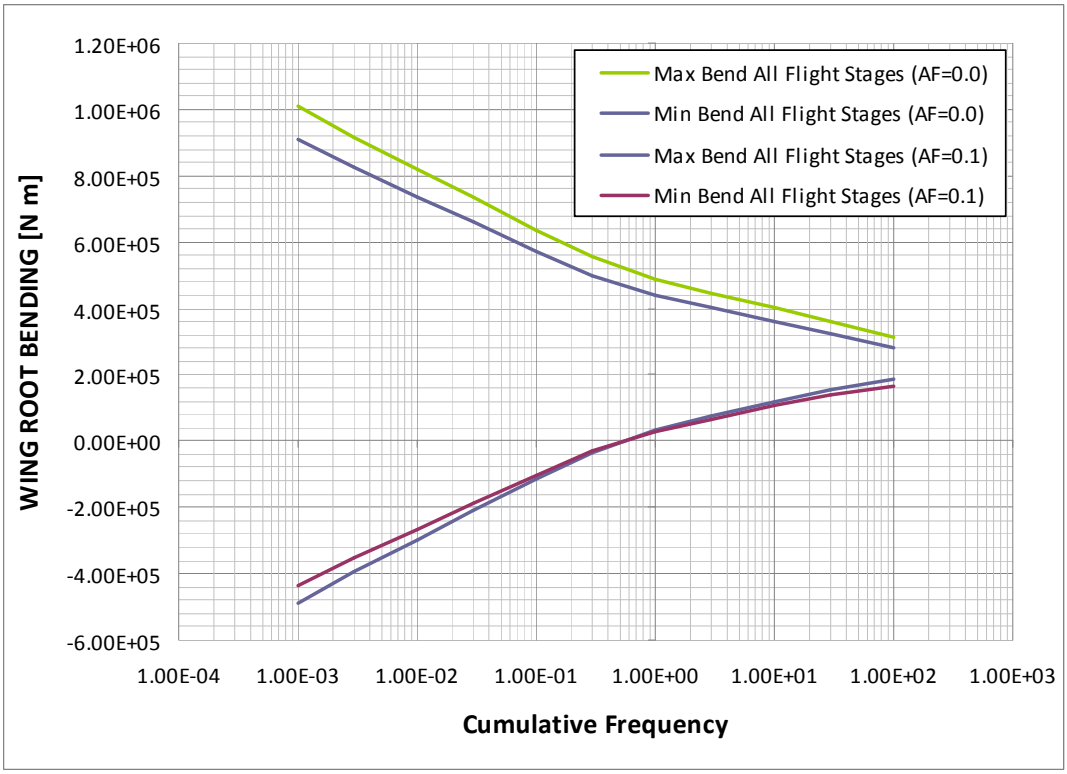

Fig. 92: Cumulative Frequencies versus bending moments – Flight Profile #2.

5.2.2. Bending Moment vs Cumulative Frequency of Occurrence. Ground Loads

The ground load spectrum, in terms of vertical load factors and thus of wing root bending moments, results from the data presented in [62].

Table 31 shows take-off and landing conditions with associated root bending moments for both mission profiles #1 and #2. Since the MLC system acts on aerodynamic loads, no benefit is gained from the adoption of such a system during ground operations.

	Mission Profile #1		Mission Profile #1	
	A/C Mass [kg]	M_m [N m]	A/C Mass [kg]	M_m [N m]
Take-off	13118.0	-38348.7	16668.0	-54291.0
Landing	11679.5	-34129.9	11678.4	-34127.1

Table 31: Take-Off and Landing Data – A/C Mass and Bending Moments.

Fig. 93 shows the wing root bending versus the aircraft mass, for inertia loads at $\Delta n_z=1$.

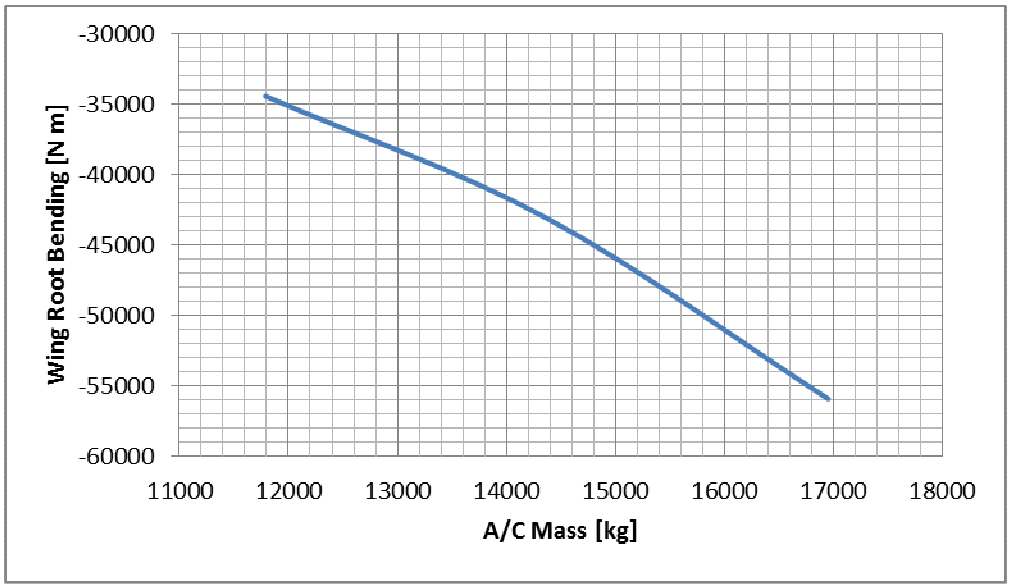

Fig. 93: Wing Root Bending versus A/C Mass – Inertia Loads at $\Delta n_z=1$.

Take-off and landing run curves of Fig. 94 (extracted from [62]) provide frequency of incremental load factors per flight for civil aircraft of the same category as the case-study aircraft.

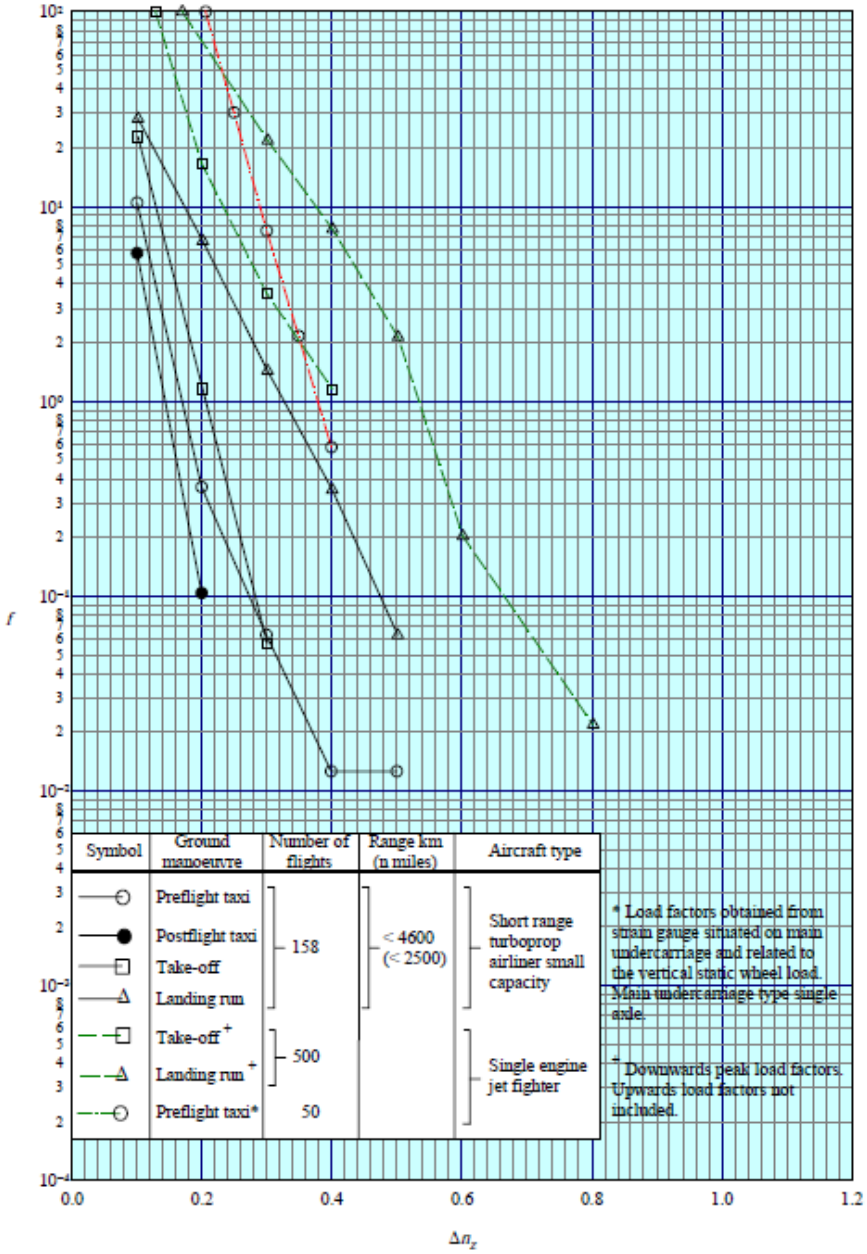

Fig. 94: Frequency of Incremental load factors per flight (12250 kg < Take-Off Mass < 22700 kg).

In the calculation of the cumulative frequency per flight presented in Fig. 94, the frequency of upward and downward values of Δn_z, of equal magnitude about the steady condition, have been combined without regard to their direction and this summation is divided by the number of flights so as to obtain the number of times per flight a load factor has been reached or exceeded [62].

Next tables list a range of load factors and, for take-off and landing, the associate bending moments, and increment load factors Δn_z. Data are separated into upward and downward

values by dividing into 53 percent upward acceleration values and 47 percent downward acceleration values, as provided by [62].

Calculations are performed for both mission profiles: Fig. 95 and Table 32 are related to mission profile #1 whereas Fig. 96 and Table 33 are related to mission profile #2.

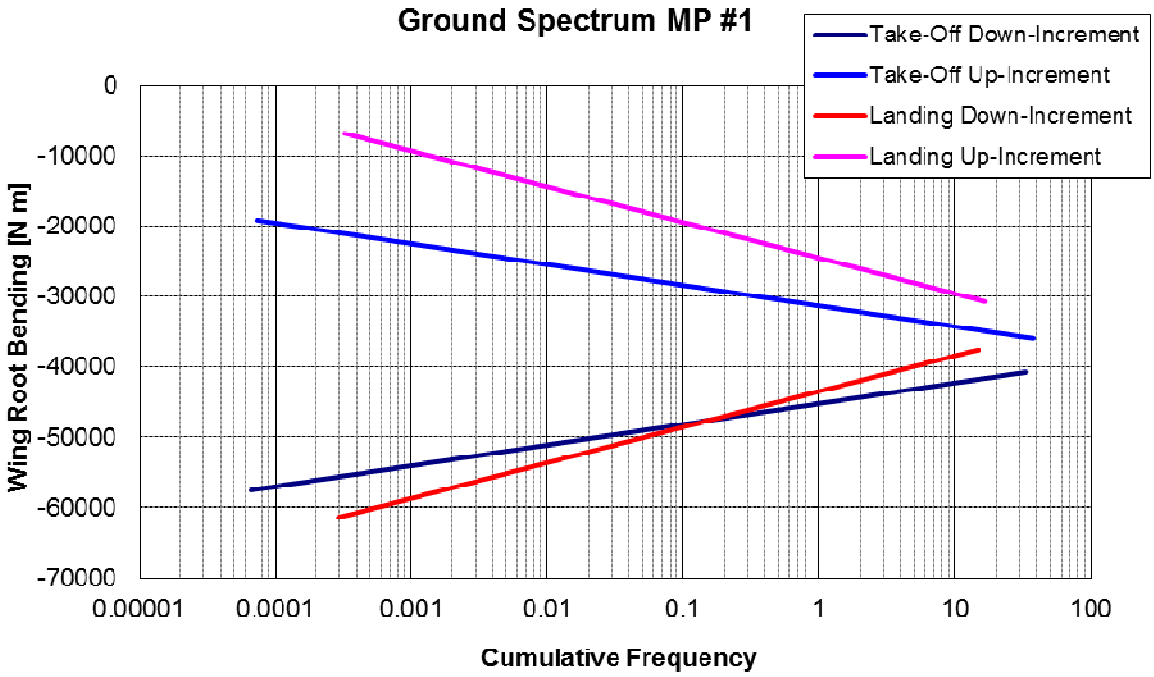

Fig. 95: Ground Spectrum – Mission Profile #1.

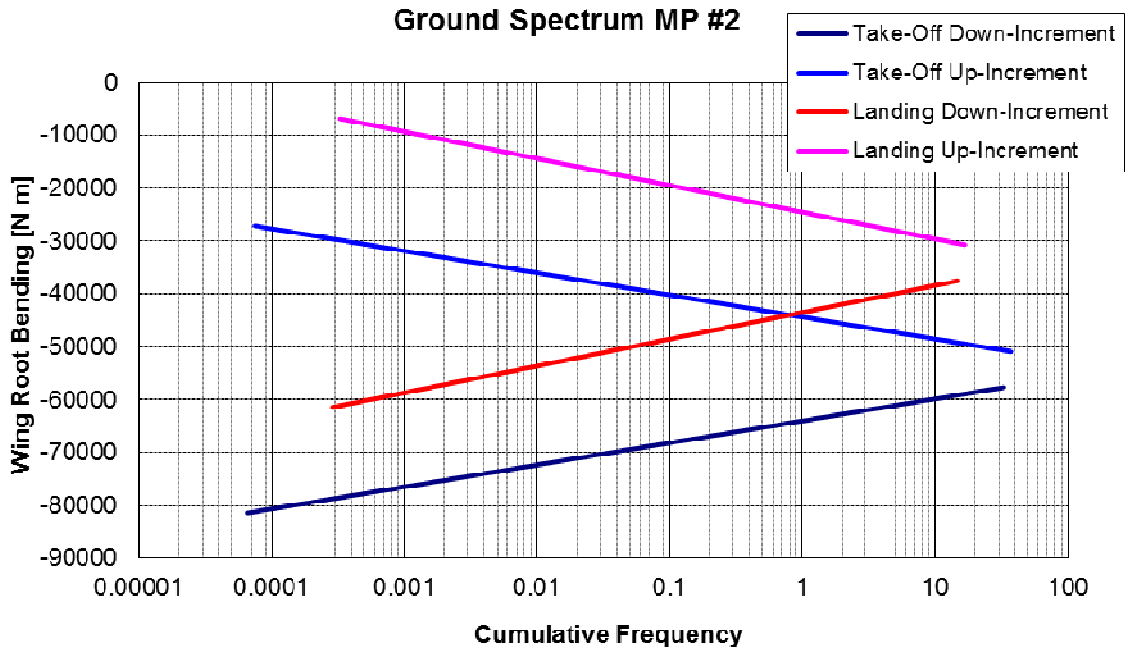

Fig. 96: Ground Spectrum – Mission Profile #2.

Take-Off					
n_z	Bending Moment	Δn_z	f	Downward Frequency	Upward Frequency
-1.500	-57523.0	0.500	1.40E-04	6.58E-05	
-1.438	-55126.2	0.438	9.13E-04	4.29E-04	
-1.375	-52729.4	0.375	5.96E-03	2.80E-03	
-1.313	-50332.6	0.313	3.88E-02	1.83E-02	
-1.250	-47935.8	0.250	2.53E-01	1.19E-01	
-1.188	-45539.0	0.188	1.65E+00	7.77E-01	
-1.125	-43142.2	0.125	1.08E+01	5.07E+00	
-1.063	-40745.4	0.063	7.03E+01	3.30E+01	
-1.000	-38348.7	0.000			
-0.938	-35951.9	0.063	7.03E+01		3.73E+01
-0.875	-33555.1	0.125	1.08E+01		5.71E+00
-0.813	-31158.3	0.188	1.65E+00		8.76E-01
-0.750	-28761.5	0.250	2.53E-01		1.34E-01
-0.688	-26364.7	0.313	3.88E-02		2.06E-02
-0.625	-23967.9	0.375	5.96E-03		3.16E-03
-0.563	-21571.1	0.438	9.13E-04		4.84E-04
-0.500	-19174.3	0.500	1.40E-04		7.42E-05
Landing					
n_z	Bending Moment	Δn_z	f	Downward Frequency	Upward Frequency
-1.800	-61433.8	0.80	6.14E-04	2.89E-04	
-1.700	-58020.8	0.70	2.89E-03	1.36E-03	
-1.600	-54607.8	0.60	1.36E-02	6.40E-03	
-1.500	-51194.8	0.50	6.41E-02	3.01E-02	
-1.400	-47781.8	0.40	3.02E-01	1.42E-01	
-1.300	-44368.8	0.30	1.42E+00	6.67E-01	
-1.200	-40955.9	0.20	6.68E+00	3.14E+00	
-1.100	-37542.9	0.10	3.14E+01	1.48E+01	
-1.000	-34129.9	0.00			
-0.900	-30716.9	0.10	3.14E+01		1.67E+01
-0.800	-27303.9	0.20	6.68E+00		3.54E+00
-0.700	-23890.9	0.30	1.42E+00		7.52E-01
-0.600	-20477.9	0.40	3.02E-01		1.60E-01
-0.500	-17064.9	0.50	6.41E-02		3.39E-02
-0.400	-13652.0	0.60	1.36E-02		7.21E-03
-0.300	-10239.0	0.70	2.89E-03		1.53E-03
-0.200	-6826.0	0.80	6.14E-04		3.25E-04

Table 32: Ground Spectrum Data – Mission Profile #1.

Take-Off					
n_z	Bending Moment	Δn_z	f	Downward Frequency	Upward Frequency
-1.500	-81436.5	0.500	1.40E-04	6.58E-05	
-1.438	-78043.3	0.438	9.13E-04	4.29E-04	
-1.375	-74650.1	0.375	5.96E-03	2.80E-03	
-1.313	-71256.9	0.313	3.88E-02	1.83E-02	
-1.250	-67863.7	0.250	2.53E-01	1.19E-01	
-1.188	-64470.5	0.188	1.65E+00	7.77E-01	
-1.125	-61077.4	0.125	1.08E+01	5.07E+00	
-1.063	-57684.2	0.063	7.03E+01	3.30E+01	
-1.000	-54291.0	0.000			
-0.938	-50897.8	0.063	7.03E+01		3.73E+01
-0.875	-47504.6	0.125	1.08E+01		5.71E+00
-0.813	-44111.4	0.188	1.65E+00		8.76E-01
-0.750	-40718.2	0.250	2.53E-01		1.34E-01
-0.688	-37325.1	0.313	3.88E-02		2.06E-02
-0.625	-33931.9	0.375	5.96E-03		3.16E-03
-0.563	-30538.7	0.438	9.13E-04		4.84E-04
-0.500	-27145.5	0.500	1.40E-04		7.42E-05
Landing					
n_z	Bending Moment	Δn_z	f	Downward Frequency	Upward Frequency
-1.800	-61428.9	0.80	6.14E-04	2.89E-04	
-1.700	-58016.1	0.70	2.89E-03	1.36E-03	
-1.600	-54603.4	0.60	1.36E-02	6.40E-03	
-1.500	-51190.7	0.50	6.41E-02	3.01E-02	
-1.400	-47778.0	0.40	3.02E-01	1.42E-01	
-1.300	-44365.3	0.30	1.42E+00	6.67E-01	
-1.200	-40952.6	0.20	6.68E+00	3.14E+00	
-1.100	-37539.9	0.10	3.14E+01	1.48E+01	
-1.000	-34127.1	0.00			
-0.900	-30714.4	0.10	3.14E+01		1.67E+01
-0.800	-27301.7	0.20	6.68E+00		3.54E+00
-0.700	-23889.0	0.30	1.42E+00		7.52E-01
-0.600	-20476.3	0.40	3.02E-01		1.60E-01
-0.500	-17063.6	0.50	6.41E-02		3.39E-02
-0.400	-13650.9	0.60	1.36E-02		7.21E-03
-0.300	-10238.1	0.70	2.89E-03		1.53E-03
-0.200	-6825.4	0.80	6.14E-04		3.25E-04

Table 33: Ground Spectrum Data – Mission Profile #2.

5.3.Definition of the GAG-Cycle

The GAG-cycle is usually the most damaging cycle in the wing loading spectrum, indeed it can account up to 90 percent of the total damage, depending upon aircraft type and flight profile.

The GAG-cycle is determined by calculating the cumulative frequency curve of the largest positive and largest negative loads that occur in each flight.

As regards the largest positive loads, the cumulative frequency curve is derived from the total gust and maneuver cumulative frequency curve of section 5.2.1 (see Fig. 90 for flight profile #1 and Fig. 92 for flight profile #2) from very low frequencies to f_c=1.0, by calculation of the maximum peak per flight cumulative frequency curve. A rather reliable estimation of this last curve is done by connecting the point at f_c=10^{-3} on the total gust and maneuver spectrum by a straight line to the point at f_c=1/3 at the same level as the total spectrum passes through the f_c=1.0 value. The sketch of Fig. 97 extracted from [60] clarifies the derivation procedure.

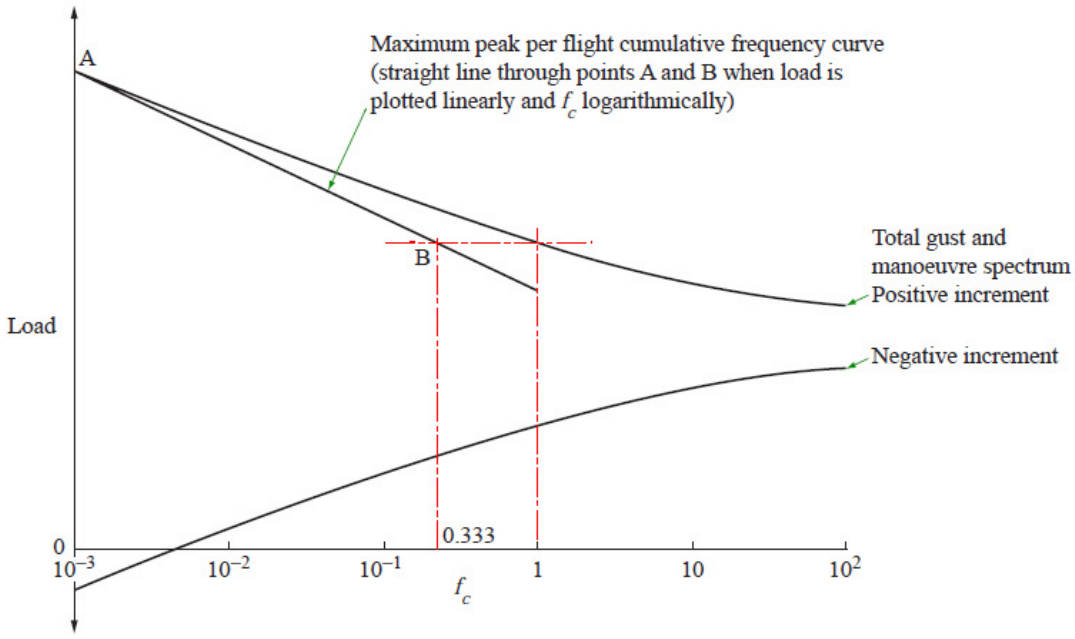

Fig. 97: Method to estimate the maximum peak per flight cumulative frequency curve.

The maximum peak per flight cumulative frequency curve follows the expression:

$$M_p = a + b \log_{10}(f_c)_p . \tag{61}$$

Coefficients *a* and *b* are reported in the following table for each flight profile for both MLC-on and off.

Flight Profile #1			
MLC-Off		MLC-On (AF=0.1)	
a=	305063.1	a=	274556.8
b=	-155878	b=	-140291
Flight Profile #2			
MLC-Off		MLC-On (AF=0.1)	
a=	390787.4	a=	351708.6
b=	-206470	b=	-185823

Table 34: Coefficients for the Maximum Peak per Flight cumulative frequency curve.

As concerning the largest negative loads occurring in each flight, the largest (negative) spectrum of ground maneuver is used for cumulative frequencies from 10^{-3} to 1.0.

Sketch of Fig. 98 shows the load spectrum generally used to define the GAG-cycle.

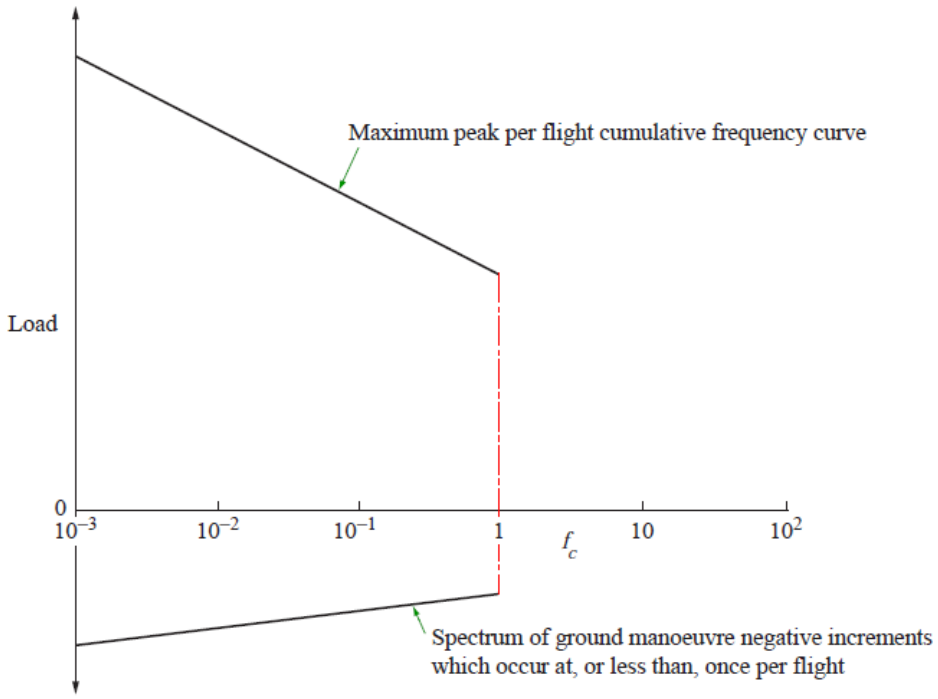

Fig. 98: Load spectrum used to define the GAG-cycle.

5.4.Definition of Remaining In-Flight Gust and Maneuver Loading Cycles

Reference [60] recommends to divide this cycle in two parts: a first part valid for f_c below the unity and a second part for f_c above the unity.

For values of f_c smaller than 1.0, the positive increment of the remaining in-flight gust and maneuver loading cycle is given by the difference between the total and the maximum peak per flight cumulative frequency spectra. This positive increment is usually termed the residual up-gust and maneuver spectrum. The negative increment is equal to that of the total spectrum at the same cumulative frequency range.

Rainflow analyses show that at high values of f_c (greater than the unity) it is incorrect to associate the change from the highest to the lowest mean load with every gust or maneuver [60], i.e. the pairing process has to be applied to the cumulative frequency spectra of the individual flight stages separately.

Fig. 99 summarizes the whole evaluation process for obtaining the remaining in-flight gust and maneuver loading cycles.

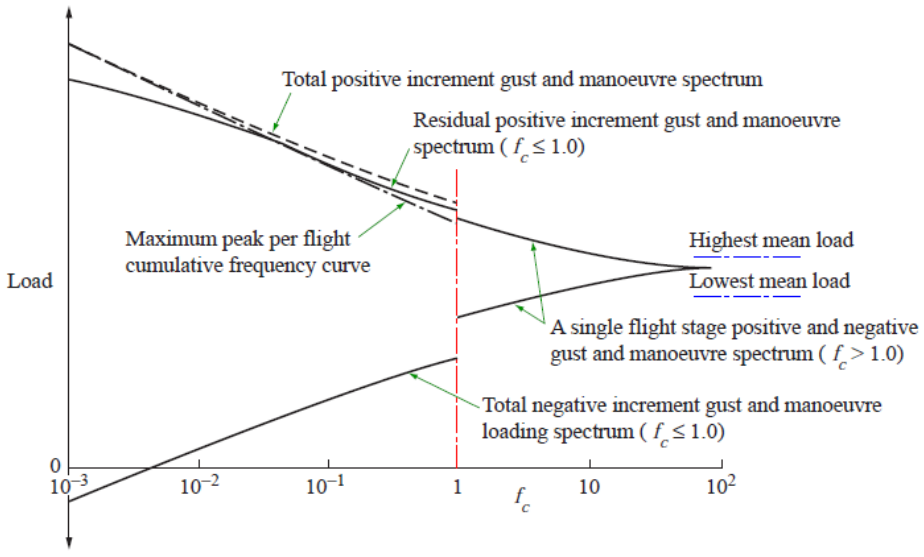

Fig. 99: Cumulative Frequency Spectra defining the Gust and Maneuver Loading Cycles.

Calculations related to the numerical application are presented later in section 5.5.2.

5.5. Contributions to the Cumulative Damage – Fatigue Life

The damage calculation is performed for a structural joint between a wing lower skin and a stringer located close to the root buttock line.

The main hypothesis on which this analysis is based is the univocal relationship between the stress in the joint and the bending moment at the wing root. The joint stress value is evaluated by FE analysis for a root bending moment of 1.0 *kN m*. It is equal to **0.2615** ***MPa***.

Since the entire work is focused on the life extension to be gained from the adoption of a MLC system, the S-N curve provided by [60] is used. It is depicted in Fig. 100.

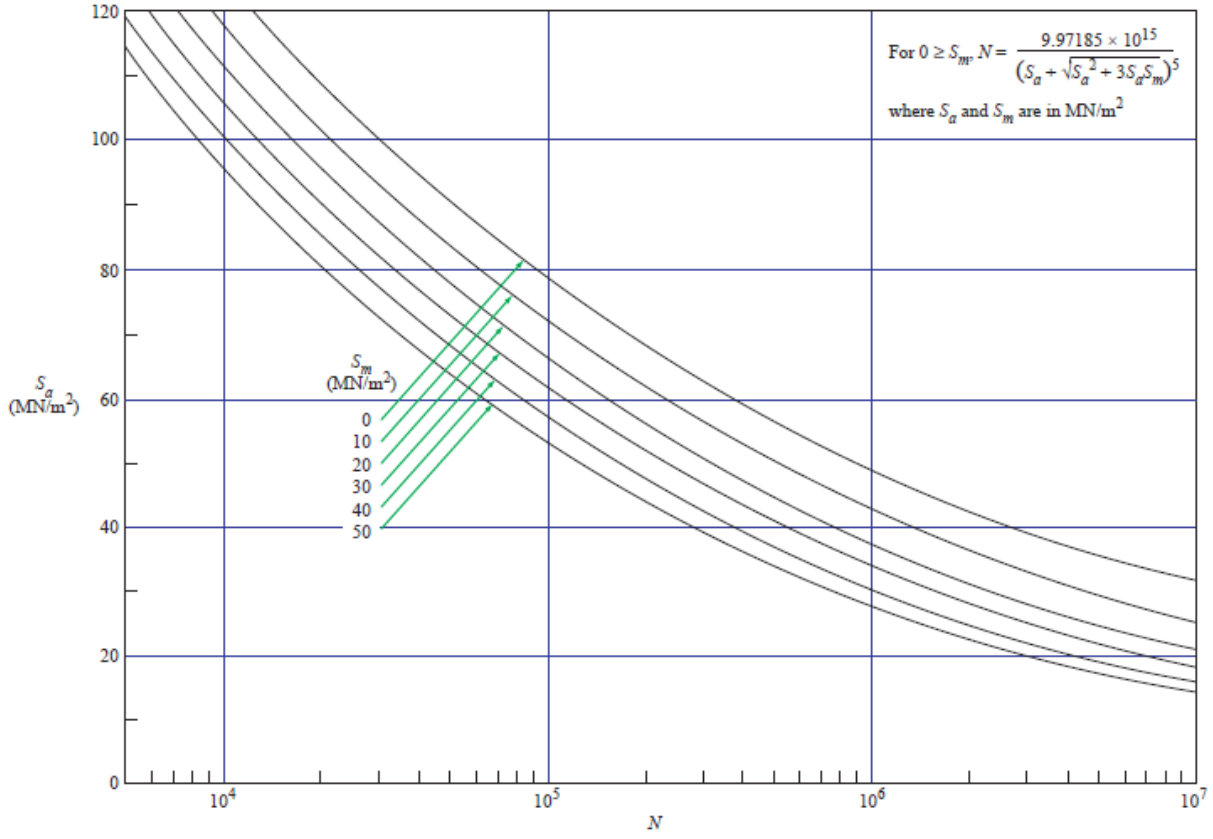

Fig. 100: Adopted S-N Curves.

5.5.1. Damage Resulting from GAG-Cycle

The GAG-cycle damage is obtained from the maximum peak per flight cumulative frequency curve and the lowest envelope of the ground maneuver spectrum.

In order to calculate the damage the spectrum is divided into a convenient number of segments. Table 35 and Table 36 list different values of frequencies (up to f_c=1.0) and bending moments with associated maximum and minimum stresses and resulting damage for both mission profiles #1 and #2. It is evident the diminution of the damage when the MLC system is operative.

Flight Profile #1 - 700 NM											
MLC-off											
$(f_c)_p$	M_p	Log-mean$(f_c)_p$	$\Delta(f_c)_p$	M_{max} [N m]	M_{min} [N m]	σ_{max} [Mpa]	σ_{min} [Mpa]	σ_a [Mpa]	σ_m [Mpa]	N	D=$\Delta(f_c)_p$/N
9.99E-04	7.73E+05										
		1.731E-03	2.00E-03	7.36E+05	-57100.3	192.379	-14.935	103.657	88.722	4141	4.83E-07
3.00E-03	6.98E+05										
		5.477E-03	7.00E-03	6.58E+05	-54889.0	171.989	-14.356	93.173	78.817	7156	9.78E-07
1.00E-02	6.17E+05										
		1.732E-02	2.00E-02	5.80E+05	-51583.1	151.604	-13.492	82.548	69.056	13282	1.51E-06
3.00E-02	5.42E+05										
		5.477E-02	7.00E-02	5.02E+05	-49021.0	131.218	-12.821	72.020	59.198	26816	2.61E-06
1.00E-01	4.61E+05										
		1.732E-01	2.00E-01	4.24E+05	-47044.0	110.833	-12.304	61.569	49.264	60576	3.30E-06
3.00E-01	3.87E+05										
		5.477E-01	7.00E-01	3.46E+05	-45632.7	90.448	-11.935	51.192	39.256	159971	4.38E-06
1.00E+00	3.05E+05										
										Σ=	**1.33E-05**
MLC-on (AF=0.1)											
$(f_c)_p$	M_p	Log-mean$(f_c)_p$	$\Delta(f_c)_p$	M_{max} [N m]	M_{min} [N m]	σ_{max} [Mpa]	σ_{min} [Mpa]	σ_a [Mpa]	σ_m [Mpa]	N	D=$\Delta(f_c)_p$/N
9.99E-04	6.95E+05										
		1.731E-03	2.00E-03	6.62E+05	-57100.3	173.141	-14.935	94.038	79.103	6878	2.91E-07
3.00E-03	6.28E+05										
		5.477E-03	7.00E-03	5.92E+05	-54889.0	154.790	-14.356	84.573	70.217	11870	5.90E-07
1.00E-02	5.55E+05										
		1.732E-02	2.00E-02	5.22E+05	-51583.1	136.443	-13.492	74.967	61.476	22003	9.09E-07
3.00E-02	4.88E+05										
		5.477E-02	7.00E-02	4.52E+05	-49021.0	118.096	-12.821	65.459	52.637	44340	1.58E-06
1.00E-01	4.15E+05										
		1.732E-01	2.00E-01	3.81E+05	-47044.0	99.750	-12.304	56.027	43.723	99880	2.00E-06
3.00E-01	3.48E+05										
		5.477E-01	7.00E-01	3.11E+05	-45632.7	81.403	-11.935	46.669	34.734	262656	2.67E-06
1.00E+00	2.75E+05										
										Σ=	**8.04E-06**

Table 35: GAG-Cycle Max and Min Stress, Frequency of Occurrence and Damage – Flight Profile #1.

Flight Profile #2 - 3000 NM											
MLC-off											
$(f_c)_p$	M_p	Log-mean$(f_c)_p$	$\Delta(f_c)_p$	M_{max} [N m]	M_{min} [N m]	σ_{max} [Mpa]	σ_{min} [Mpa]	σ_a [Mpa]	σ_m [Mpa]	N	$D=\Delta(f_c)_p/N$
1.00E-03	1.01E+06										
		1.732E-03	2.00E-03	9.61E+05	-74122.7	251.334	-19.387	135.361	115.974	1089	1.84E-06
3.00E-03	9.12E+05										
		5.477E-03	7.00E-03	8.58E+05	-72112.5	224.333	-18.861	121.597	102.736	1893	3.70E-06
1.00E-02	8.04E+05										
		1.732E-02	2.00E-02	7.54E+05	-70581.7	197.332	-18.461	107.896	89.436	3519	5.68E-06
3.00E-02	7.05E+05										
		5.477E-02	7.00E-02	6.51E+05	-68893.8	170.331	-18.019	94.175	76.156	7147	9.79E-06
1.00E-01	5.97E+05										
		1.732E-01	2.00E-01	5.48E+05	-67069.0	143.330	-17.542	80.436	62.894	16340	1.22E-05
3.00E-01	4.99E+05										
		5.477E-01	7.00E-01	4.45E+05	-65208.6	116.329	-17.055	66.692	49.637	44072	1.59E-05
1.00E+00	3.91E+05										
										Σ=	**4.91E-05**
MLC-on (AF=0.1)											
$(f_c)_p$	M_p	Log-mean$(f_c)_p$	$\Delta(f_c)_p$	M_{max} [N m]	M_{min} [N m]	σ_{max} [Mpa]	σ_{min} [Mpa]	σ_a [Mpa]	σ_m [Mpa]	N	$D=\Delta(f_c)_p/N$
1.00E-03	9.09E+05										
		1.732E-03	2.00E-03	8.65E+05	-74122.7	226.201	-19.387	122.794	103.407	1809	1.11E-06
3.00E-03	8.21E+05										
		5.477E-03	7.00E-03	7.72E+05	-72112.5	201.900	-18.861	110.380	91.519	3139	2.23E-06
1.00E-02	7.23E+05										
		1.732E-02	2.00E-02	6.79E+05	-70581.7	177.599	-18.461	98.030	79.569	5823	3.43E-06
3.00E-02	6.35E+05										
		5.477E-02	7.00E-02	5.86E+05	-68893.8	153.298	-18.019	85.659	67.639	11798	5.93E-06
1.00E-01	5.38E+05										
		1.732E-01	2.00E-01	4.93E+05	-67069.0	128.997	-17.542	73.269	55.727	26880	7.44E-06
3.00E-01	4.49E+05										
		5.477E-01	7.00E-01	4.00E+05	-65208.6	104.696	-17.055	60.876	43.820	72159	9.70E-06
1.00E+00	3.52E+05										
										Σ=	**2.98E-05**

Table 36: GAG-Cycle Max and Min Stress, Frequency of Occurrence and Damage – Flight Profile #2.

5.5.2. In-Flight Gust and Maneuver Damage

Following the procedure of section 5.4, the definition of cycles when $f_c \leq 1.0$ is different to that when $f_c > 1.0$. Table 37 and Table 38 deal with the region $f_c \leq 1.0$, respectively for mission profile #1 and #2.

Δf_c is the difference in log-mean(f_c) values, whereas $(f_c)_p$ is calculated by means of eq.(61) with M_t replacing M_p. f_c (residual) is equal to the difference between log-mean(f_c) and $(f_c)_p$.

Values in the column M_t (residual) are obtained by interpolating the curve M_{max} vs f_c (residual) on points log-mean(f_c). The resulting curve M_t (residual) versus f_c (residual) represents the remaining in-flight gust and maneuver loading cycle.

Flight Profile #1 - 700 NM													
MLC-off													
f_c	M_{max} [N m]	Log-mean(f_c)	Δf_c	$(f_c)_p$	f_c residual	M_t residual [N m]	M_{min} [N m]	σ_{max} [Mpa]	σ_{min} [Mpa]	σ_a [Mpa]	σ_m [Mpa]	N	D ($\Delta(f_c)$/N)
9.99E-04	7.73E+05												
		1.731E-03	2.00E-03	1.530E-03	2.018E-04	5.590E+05	-57100.3	146.196	-14.935	80.565	65.631	15467.55	1.293E-07
3.00E-03	7.01E+05												
		5.477E-03	7.00E-03	5.831E-03	3.538E-04	5.038E+05	-54889.0	131.775	-14.356	73.066	58.709	25612.61	2.733E-07
1.00E-02	6.25E+05												
		1.732E-02	2.00E-02	1.661E-02	7.134E-04	4.783E+05	-51583.1	125.107	-13.492	69.299	55.808	33285.91	6.009E-07
3.00E-02	5.55E+05												
		5.477E-02	7.00E-02	5.080E-02	3.975E-03	4.330E+05	-49021.0	113.249	-12.821	63.035	50.214	54123.68	1.293E-06
1.00E-01	4.78E+05												
		1.732E-01	2.00E-01	1.376E-01	3.556E-02	3.959E+05	-47044.0	103.549	-12.304	57.927	45.622	83664.89	2.390E-06
3.00E-01	4.23E+05												
		5.477E-01	7.00E-01	3.269E-01	2.208E-01	2.786E+05	-45632.7	72.875	-11.935	42.405	30.470	440817.20	1.588E-06
1.00E+00	3.80E+05												
												Σ=	**6.275E-06**
MLC-on (AF=0.1)													
f_c	M_{max} [N m]	Log-mean(f_c)	Δf_c	$(f_c)_p$	f_c residual	M_t residual [N m]	M_{min} [N m]	σ_{max} [Mpa]	σ_{min} [Mpa]	σ_a [Mpa]	σ_m [Mpa]	N	D ($\Delta(f_c)$/N)
9.99E-04	6.95E+05												
		1.731E-03	2.00E-03	1.480E-03	2.515E-04	5.961E+05	-57100.3	155.903	-14.935	85.419	70.484	11374.81	1.759E-07
3.00E-03	6.31E+05												
		5.477E-03	7.00E-03	4.273E-03	1.204E-03	5.347E+05	-54889.0	139.842	-14.356	77.099	62.743	19294.04	3.628E-07
1.00E-02	5.63E+05												
		1.732E-02	2.00E-02	1.291E-02	4.410E-03	4.750E+05	-51583.1	124.223	-13.492	68.857	55.366	34428.67	5.809E-07
3.00E-02	4.99E+05												
		5.477E-02	7.00E-02	3.751E-02	1.726E-02	4.290E+05	-49021.0	112.192	-12.821	62.507	49.685	56591.30	1.237E-06
1.00E-01	4.30E+05												
		1.732E-01	2.00E-01	1.047E-01	6.853E-02	3.939E+05	-47044.0	103.034	-12.304	57.669	45.365	85669.38	2.335E-06
3.00E-01	3.81E+05												
		5.477E-01	7.00E-01	2.186E-01	3.291E-01	3.293E+05	-45632.7	86.122	-11.935	49.028	37.093	201545.07	3.473E-06
1.00E+00	3.42E+05												
												Σ=	**8.164E-06**

Table 37: In-Flight Gust and Maneuver Damage $f_c \leq 1.0$ – Flight Profile #1.

Flight Profile #2 - 3000 NM													
MLC-off													
f_c	M_{max} [N m]	Log-mean(f_c)	Δf_c	$(f_c)_p$	f_c residual	M_t residual [N m]	M_{min} [N m]	σ_{max} [Mpa]	σ_{min} [Mpa]	σ_a [Mpa]	σ_m [Mpa]	N	D ($\Delta(f_c)$/N)
1.00E-03	1.01E+06												
		1.732E-03	2.00E-03	1.477E-03	2.551E-04	8.707E+05	-74122.7	227.725	-19.387	123.556	104.169	1751.94	1.142E-06
3.00E-03	9.15E+05												
		5.477E-03	7.00E-03	4.206E-03	1.271E-03	7.877E+05	-72112.5	206.030	-18.861	112.445	93.584	2848.92	2.457E-06
1.00E-02	8.20E+05												
		1.732E-02	2.00E-02	1.190E-02	5.424E-03	7.265E+05	-70581.7	190.007	-18.461	104.234	85.773	4217.43	4.742E-06
3.00E-02	7.33E+05												
		5.477E-02	7.00E-02	3.214E-02	2.263E-02	6.501E+05	-68893.8	170.038	-18.019	94.029	76.010	7206.32	9.714E-06
1.00E-01	6.37E+05												
		1.732E-01	2.00E-01	9.008E-02	8.312E-02	5.802E+05	-67069.0	151.747	-17.542	84.644	67.102	12465.80	1.604E-05
3.00E-01	5.54E+05												
		5.477E-01	7.00E-01	2.094E-01	3.384E-01	4.687E+05	-65208.6	122.586	-17.055	69.820	52.765	34453.88	2.032E-05
1.00E+00	4.89E+05												
												Σ=	5.442E-05
MLC-on (AF=0.1)													
f_c	M_{max} [N m]	Log-mean(f_c)	Δf_c	$(f_c)_p$	f_c residual	M_t residual [N m]	M_{min} [N m]	σ_{max} [Mpa]	σ_{min} [Mpa]	σ_a [Mpa]	σ_m [Mpa]	N	D ($\Delta(f_c)$/N)
1.00E-03	9.09E+05												
		1.732E-03	2.00E-03	1.480E-03	2.518E-04	7.834E+05	-74122.7	204.901	-19.387	112.144	92.757	2908.27	6.877E-07
3.00E-03	8.23E+05												
		5.477E-03	7.00E-03	4.223E-03	1.254E-03	7.088E+05	-72112.5	185.395	-18.861	102.128	83.267	4720.71	1.483E-06
1.00E-02	7.38E+05												
		1.732E-02	2.00E-02	1.188E-02	5.441E-03	6.538E+05	-70581.7	171.004	-18.461	94.732	76.272	6974.73	2.867E-06
3.00E-02	6.60E+05												
		5.477E-02	7.00E-02	3.211E-02	2.266E-02	5.849E+05	-68893.8	152.976	-18.019	85.498	67.478	11916.12	5.874E-06
1.00E-01	5.73E+05												
		1.732E-01	2.00E-01	9.013E-02	8.307E-02	5.220E+05	-67069.0	136.540	-17.542	77.041	59.499	20557.08	9.729E-06
3.00E-01	4.99E+05												
		5.477E-01	7.00E-01	2.088E-01	3.389E-01	4.225E+05	-65208.6	110.505	-17.055	63.780	46.725	56066.30	1.249E-05
1.00E+00	4.40E+05												
												Σ=	3.313E-05

Table 38: In-Flight Gust and Maneuver Damage $f_c \leq 1.0$ – Flight Profile #2.

As concerns the region f_c>1.0, the cycles are defined by using the cumulative frequency curves for each individual flight stage separately.

Just as an example, Table 39 and Table 40 show calculations for the cruise segment of respectively flight profiles #1 and #2.

M_{max} and M_{min} are read from positive and negative increments of the cruise stage given in Table 21 and Table 22 for flight profile #1, and Table 27 and Table 28 for flight profile #2, at log-mean(f_c).

CRUISE - Flight Profile #1 - 700 NM										
MLC-off										
f_c	M_{max} [N m]	M_{min} [N m]	Log-mean(f_c)	$\Delta(f_c)$	σ_{max} [Mpa]	σ_{min} [Mpa]	σ_a [Mpa]	σ_m [Mpa]	N	D $\Delta(f_c)$/N
1.00E+00	3.75E+05	6.21E+04								
			1.73E+00	2.00E+00	9.47E+01	1.97E+01	3.75E+01	5.72E+01	3.12E+05	6.41E-06
3.00E+00	3.40E+05	9.77E+04								
			5.48E+00	7.00E+00	8.53E+01	2.92E+01	2.81E+01	5.73E+01	8.62E+05	8.12E-06
1.00E+01	3.01E+05	1.37E+05								
			1.73E+01	2.00E+01	7.54E+01	3.92E+01	1.81E+01	5.73E+01	3.75E+06	5.33E-06
3.00E+01	2.66E+05	1.72E+05								
			5.48E+01	7.00E+01	6.60E+01	4.86E+01	8.68E+00	5.73E+01	3.80E+07	1.84E-06
1.00E+02	2.27E+05	2.11E+05								
									Σ=	**2.17E-05**
MLC-on (AF=0.1)										
f_c	M_{max} [N m]	M_{min} [N m]	Log-mean(f_c)	$\Delta(f_c)$	σ_{max} [Mpa]	σ_{min} [Mpa]	σ_a [Mpa]	σ_m [Mpa]	N	D $\Delta(f_c)$/N
1.00E+00	3.38E+05	5.59E+04								
			1.73E+00	2.00E+00	8.53E+01	1.77E+01	3.38E+01	5.15E+01	5.26E+05	3.80E-06
3.00E+00	3.06E+05	8.80E+04								
			5.48E+00	7.00E+00	7.68E+01	2.63E+01	2.53E+01	5.15E+01	1.46E+06	4.80E-06
1.00E+01	2.71E+05	1.23E+05								
			1.73E+01	2.00E+01	6.78E+01	3.52E+01	1.63E+01	5.15E+01	6.35E+06	3.15E-06
3.00E+01	2.39E+05	1.55E+05								
			5.48E+01	7.00E+01	5.93E+01	4.38E+01	7.75E+00	5.15E+01	6.62E+07	1.06E-06
1.00E+02	2.04E+05	1.90E+05								
									Σ=	**1.28E-05**

Table 39: In-Flight Gust and Maneuver Damage f_c>1.0 – Cruise, Flight Profile #1.

CRUISE - Flight Profile #2 - 3000 NM										
MLC-off										
f_c	M_{max} [N m]	M_{min} [N m]	Log-mean(f_c)	$\Delta(f_c)$	σ_{max} [Mpa]	σ_{min} [Mpa]	σ_a [Mpa]	σ_m [Mpa]	N	D $\Delta(f_c)$/N
1.00E+00	4.89E+05	3.37E+04								
			1.73E+00	2.00E+00	1.24E+02	1.29E+01	5.54E+01	6.84E+01	5.97E+04	3.35E-05
3.00E+00	4.46E+05	7.66E+04								
			5.48E+00	7.00E+00	1.12E+02	2.43E+01	4.40E+01	6.84E+01	1.37E+05	5.12E-05
1.00E+01	4.00E+05	1.23E+05								
			1.73E+01	2.00E+01	1.01E+02	3.61E+01	3.23E+01	6.84E+01	4.03E+05	4.97E-05
3.00E+01	3.59E+05	1.64E+05								
			5.48E+01	7.00E+01	8.96E+01	4.72E+01	2.12E+01	6.84E+01	1.63E+06	4.29E-05
1.00E+02	3.13E+05	2.10E+05								
									Σ=	**1.77E-04**
MLC-on (AF=0.1)										
f_c	M_{max} [N m]	M_{min} [N m]	Log-mean(f_c)	$\Delta(f_c)$	σ_{max} [Mpa]	σ_{min} [Mpa]	σ_a [Mpa]	σ_m [Mpa]	N	D $\Delta(f_c)$/N
1.00E+00	4.40E+05	3.03E+04								
			1.73E+00	2.00E+00	1.11E+02	1.16E+01	4.99E+01	6.15E+01	1.01E+05	1.98E-05
3.00E+00	4.02E+05	6.89E+04								
			5.48E+00	7.00E+00	1.01E+02	2.18E+01	3.97E+01	6.15E+01	2.30E+05	3.04E-05
1.00E+01	3.60E+05	1.10E+05								
			1.73E+01	2.00E+01	9.06E+01	3.24E+01	2.91E+01	6.15E+01	6.80E+05	2.94E-05
3.00E+01	3.23E+05	1.48E+05								
			5.48E+01	7.00E+01	8.06E+01	4.25E+01	1.90E+01	6.15E+01	2.80E+06	2.50E-05
1.00E+02	2.81E+05	1.89E+05								
									Σ=	**1.05E-04**

Table 40: In-Flight Gust and Maneuver Damage f_c>1.0 – Cruise, Flight Profile #2.

Table 41 reports the contribution of each flight stage for both flight profiles in either case of MLC-on and off.

	Flight Profile #1		Flight Profile #2	
	MLC-off	MLC-on	MLC-off	MLC-on
Climb	1.955E-06	1.156E-06	1.552E-06	9.127E-07
Cruise	2.170E-05	1.281E-05	1.771E-04	1.046E-04
Descent	2.322E-06	1.374E-06	1.357E-06	8.080E-07

Table 41: List of Gust and Maneuver Damage Sums for f_c>1.0.

5.6. Cumulative Damage Calculation – Fatigue Life Estimation

The total damage together with the estimated mean life are listed in Table 42 for flight profile #1 and in Table 43 for flight profile #2.

DAMAGE CALCULATION AND LIFE ESTIMATION - Flight Profile #1		
Contribute	**MLC-Off**	**MLC-On**
GAG-CYCLE	1.325E-05	8.036E-06
IN-FLIGHT GUST AND MANOEUVRE fc<1	6.275E-06	8.164E-06
IN-FLIGHT GUST AND MANOEUVRE fc>1	2.597E-05	1.534E-05
TOTAL DAMAGE	**4.550E-05**	**3.154E-05**
LIFE ESTIMATION (NUMBER OF FLIGHTS)	**2.198E+04**	**3.171E+04**
LIFE ESTIMATION (FLIGHT HOURS)	**3.645E+04**	**5.258E+04**
LIFE ESTIMATION (NAUTICAL MILES)	**1.567E+07**	**2.261E+07**
FLEF (Fatigue Life Extension Factor)	**1.443**	

Table 42: Damage Calculation and Life Estimation – Flight Profile #1.

DAMAGE CALCULATION AND LIFE ESTIMATION - Flight Profile #2		
Contribute	**MLC-Off**	**MLC-On**
GAG-CYCLE	4.913E-05	2.984E-05
IN-FLIGHT GUST AND MANOEUVRE fc<1	5.442E-05	3.313E-05
IN-FLIGHT GUST AND MANOEUVRE fc>1	1.801E-04	1.064E-04
TOTAL DAMAGE	**2.836E-04**	**1.693E-04**
LIFE ESTIMATION (NUMBER OF FLIGHTS)	**3.526E+03**	**5.905E+03**
LIFE ESTIMATION (FLIGHT HOURS)	**2.374E+04**	**3.976E+04**
LIFE ESTIMATION (NAUTICAL MILES)	**1.118E+07**	**1.872E+07**
FLEF (Fatigue Life Extension Factor)	**1.675**	

Table 43: Damage Calculation and Life Estimation – Flight Profile #2.

The life estimation, in number of flights, is calculated as the inverse of the total damage since it is assumed that the failure occurs when ΣD=1.0.

Notice that the fatigue life is longer in case of short range mission (flight profile #1) because the airplane flights carrying a very small amount of fuel if compared to the that of the long range mission.

The FLEFs (Fatigue Life Extension Factors) are in either case much greater than the unity, indicating a very good life extension, beyond the best expectations.

5.7. Conclusion Remarks

In this chapter, the estimation of the fatigue life extension of a wing lower skin joint located close to the wing root has been performed by using methods published by ESDU, ref. [60], [61], and [62]. The aim of the work is to demonstrate the effective fatigue life extension derived from the adoption of a MLC system. Thus analyses are performed for either case of MLC-on and off for two different mission profiles: a short range mission (see Table 15) and a long range mission (see Table 16).

The registered fatigue life extension factors are in either case much greater than the unity, indicating a very good life extension, well beyond the more positive previsions.

The better result is obtained for the long range mission. In this case flight loads are prominent with respect to the ground ones, thus the benefit of having a MLC system aboard becomes much more relevant as regards the fatigue life extension.

It should be noted that the impact on aircraft aerodynamic drag due to the activation of a LAS has been never accounted for in the present study. Indeed the load alleviators deflection produces a change in the spanwise aerodynamic distribution with consequent variation of the induced drag. Moreover if the load alleviation is carried-out by shifting the aerodynamic center of pressure inboard, the induced drag probably increases.

Furthermore the airfoil camber augmentation leads to a wake drag increase and also to a wave drag increase at high Mach numbers.

That being stated, it is opinion of the author that this phenomenon has to be investigated. In fact if a net aerodynamic drag augmentation occurs the increase in fuel consumption may affect the fatigue life estimation.

6. Thesis Summary and Future Work

This thesis is based on studies about the use of Load Alleviation Systems aimed at controlling the flight maneuver loads. The system has to be able to reduce the wing bending in a specific wing station in the neighborhood of the wing root by means of a symmetrical actuation of the ailerons or other dedicated control surfaces located close to the wing tip.

The load alleviator deflection is performed in order to rearrange the aerodynamic loads. The result is the shift of the wing center of pressure inboard and a consequent reduction of the bending moment close to the wing root. As discussed so far, this way to proceed is not new, but the purpose of this work is to offer a practical approach to quantify the Load Alleviation during longitudinal maneuvers and to provide methods and numerical procedures useful for designing and/or analyzing such systems, by giving always particular emphasis to the importance of the structure flexibility, to be taken into account since the early stage of design.

The whole work is made of four parts.

The **first part** deals with symmetric balanced maneuvers, providing a method to evaluate the load alleviation effectiveness in an effortless and linear manner. A desired value of the bending moment alleviation in a generic fixed wing station can be obtained by following this method, for which the aerodynamic and load derivatives of the airplane are required. A numerical procedure aimed at determining such derivatives also for an aircraft in an unconventional configuration such as a Joined-Wing one, using a modal approach and taking into account aeroelastic effects, has been presented.

A limitation of the method is its inapplicability in high lift conditions, such as those falling between the points V_S and V_A of the Maneuver Diagram, at the vertical limit load factor, in the case of a positive value of $C_{m\beta}$ (negative swept wing). In such a situation, with the aircraft at its maximum attitude, the activation of the load alleviation system may produce the aircraft stall. Another relevant limitation especially in case of a strongly unconventional configuration consists in the uncontrollability of the internal load far from WCS. Extensive calculations are needed in order to prevent a sudden load increase with consequent unexpected structural failures.

In the **second part** a method to estimate the control surface effectiveness when it is used as load alleviator is provided. An application to an EASA CS-25 Business Aircraft for two

different kinds of maneuver and by adopting the ailerons as load alleviators, show that for a generic climb start maneuver, the maximum bending reduction at the wing root is about 37 percent, with a maximum aileron deflection less than 12 degrees.

This results are obtained by means of open-loop calculations only and involves methods that lets take into account the aircraft flexibility together with plunge and pitch rigid-body motions by applying a modal approach.

The **third part** of the work is a conceptual design of a MLC system for longitudinal maneuver. The system, when switched on, is able to minimize the bending moment augmentation in a wing station near the wing root during an unsteady maneuver.

The system incorporates a Load Factor Feedback (LFF) to the elevators in order to perform a desired longitudinal maneuver by automatically acting on the elevators through a PID controller, whereas the Maneuver Load Control (MLC) is accomplished by observing the bending on the wing root section and by symmetrically acting on the ailerons by means of a simple P controller. The goal is to minimize the difference between measured bending moment and 1-g bending moment.

All numerical analyses aimed at simulating the aircraft behavior during maneuver with MLC-on or MLC-off are performed both by taking into account and by neglecting the flexibility of the aircraft. Indeed the synthesis of the controllers has been made by tuning the gains in either case, i.e. for rigid and elastic aircraft, in order to appreciate the different performance, with gain and phase margins kept constant.

The study demonstrates how much is important to consider the effect of aeroelasticity early in the conceptual design of such a MLC system, hence by providing much more reliable indications about their effectiveness and also about the quality of flight mechanics in general.

The **fourth part** is focused on the estimation of the fatigue life extension of a structural joint (wing lower skin joint) located close to the wing root. Analyses are carried-out for a business jet responding to the Part 25 of the EASA Certification Specification for two kinds of mission: short and long range.

Estimated fatigue life extensions result well beyond the most optimistic expectations, with life duration improvements up to 67.5 percent of the nominal fatigue life.

The better result is obtained for the long range mission for which flight loads are prominent with respect to the ground ones. Thus the benefit to carry a MLC system becomes much more important as regards the fatigue life improvement.

Future work will be focused on the load alleviation in a gust environment, for which a correlation of unsteady local accelerations with the load characteristic to be alleviated is the challenging issue.

Another relevant effort to be faced with is the introduction of the unsteady aerodynamics instead of the quasi-steady one. The adoption of the modal approach with subsequent Roger approximation of the unsteady generalized aerodynamic forces will introduce in the state-space system further equations related to the modeled aerodynamic delays. A method aimed at observing and controlling them, also from a practical viewpoint, is the main expected difficulty to be overcome.

Acknowledgments

This PhD work has been funded by the Italian Aerospace Research Center (CIRA scpa), through the company training plan.

Special thanks to my mentor Modesto Pecora ("u mast"). His friendship, in some cases also irrational and litigious (☺), but especially his contagious passion for aeronautics and aeroelasticity, together with his invaluable technical support actually represent a "lighthouse" for me and for everyone wants to approach the fascinating and complex world of aeroelasticity.

Many thanks also to my tutor Professor Leonardo Lecce, for his willingness and all precious advices provided during the development of each part of this work.

****

Ringraziamenti

Il presente lavoro di dottorato è stato finanziato dal Centro Italiano Ricerche Aerospaziali (CIRA scpa) e costituisce parte integrante del piano di formazione individuale dedicato ai dipendenti del Centro.

Un ringraziamento particolare va al mio mentore Modesto Pecora ("u mast"). La sua amicizia, in alcuni casi anche irrazionale e litigiosa (☺), ma soprattutto la sua passione contagiosa per l'aeronautica e aeroelasticità, insieme al suo prezioso supporto tecnico rappresentano un "faro" per me e per tutti quanti vogliano avvicinarsi all'affascinante e complesso mondo dell'aeroelasticità.

Molte grazie anche al mio relatore professor Leonardo Lecce, per la disponibilità, l'attenzione e i preziosi consigli che ha avuto per me durante lo svolgimento di questo lavoro.

Appendix 1

Calculations performed by following the method presented in section 2 for the case-study airplane of sections 3, 4, and 5, show that a wing root bending alleviation of 10% (AF=0.1) is achievable with load alleviator deflections of just few degrees.

The airplane is considered to be in level flight at V_C, in three different mass conditions (see Table 7), at different altitudes from sea level to about 30 kft (see Table 6).

Fig. 101 and Fig. 102 show dependencies of the load alleviator deflection respectively upon aircraft mass (fuel mass) and altitude.

Fig. 101: Load Alleviator Deflection vs A/C Mass (fuel mass).

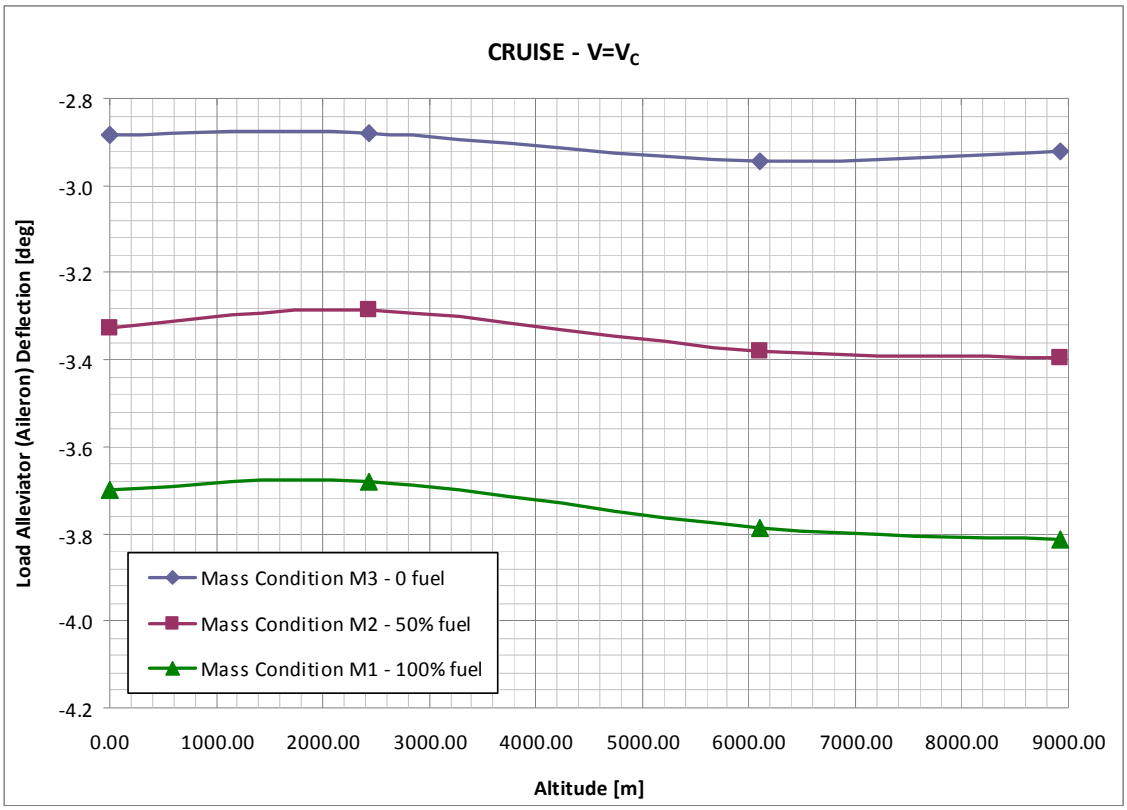

Fig. 102: Load Alleviator Deflection vs altitude

References

[1] Hahn, K.-U. Koenig, R., "ATTAS flight test and simulation results of the advanced gust management system LARS". AIAA Atmospheric Flight Mechanics Conference, Hilton Head Island, SC, Aug 10-12, 1992.

[2] Merat, R, "Study of a Direct Lift Control System Based on the A380 Aircraft", 46th AIAA Aerospace Sciences Meeting and Exhibit, 7 - 10 January 2008, Reno, Nevada.

[3] Wildschek, A., Maier, R., Hromcik, M., Hanis, T., Schirrer, A., Kozek, M., Westermayer, C. and Hemedi, M., "Hybrid Controller For Gust Load Alleviation And Ride Comfort Improvement Using Direct Lift Control Flaps", 3rd European Conference For Aerospace Sciences (EUCASS), Paris, July 6-9th 2009.

[4] Hecker, S., Hahn, K.-U., "Advanced Gust Load Alleviation System for Large Flexible Aircraft", 1st CEAS European Air & Space Conference, Berlin, Germany, 10.-13. September, 2007.

[5] O'Connell, R. F., "Design, Development and Implementation of an Active Control System for Load Alleviation for a Commercial Transport Airplane", AGARD-R-683.

[6] Ramsey, H. D., Lewolt, J. G., "Design Maneuver Loads for an Airplane with an Active Control System", AIAA Paper No. 79-0738.

[7] Bendixen, G. E., O'Connell, R. F. and Siegert, C. D., "Digital Active Control System for Load Alleviation for the Lockheed L-1011", Aeronautical Journal, Vol. 86, No. 849, November 1981.

[8] Pratt K. G., "A survey of Active Controls Benefits to Supersonic Transport", Symposium on Advanced Control Technology, Los Angeles, California, July 1974.

[9] Kurzhals, P. R., "Active controls in aircraft design. Executive summary", FMP Symposium on Stability and Control, Ottawa, Canada, Oct. 1978.

[10] Disney, T. E., "C5-A Active Load Alleviation System", Journal of Spacecraft, Vol. 14, No. 2, February 1977, pp. 81-86.

[11] Caplin, J., Ray, A., Joshi, S., "Damage-Mitigating Control of Aircraft for Enhanced Structural Durability", IEEE Transaction On Aerospace And Electronic Systems, Vol. 37, No. 3, July 2001.

[12] NASA Contractor Report 3164, "Selected Advanced Aerodynamics and Active Control Technology Concepts Development on a Derivative B-747 Aircraft", NASA Langley Research Center under Contract NAS1-14741 with The Boeing Commercial Airplane Company, July 1982.

[13] Thornton, S. V., "Reduction of Structural Loads using Maneuver Load Control on the Advanced Fighter Technology Integration (AFTI)/F-111 Mission Adaptive Wing", NASA Technical Memorandum 4526, NASA Dryden Research Facility, 1993.

[14] Paletta, N., Belardo, M., Pecora, M., "Load Alleviation on a Joined-Wing Unmanned Aircraft", Journal of Aircraft, Vol. 47, No. 6, November-December 2010.

[15] White, R. J., "Improving the Airplane Efficiency by Use of Wing Maneuver Load Alleviation", Journal of Aircraft, Vol. 8, No. 10, 1971, pp. 769, 775.

[16] J. A. Woods-Vedeler, A. S. Pototzky, S. T. Hoadley, "Rolling Maneuver Load Alleviation Using Active Controls", *Journal of Aircraft*, Vol. 32, No. 1, January-February 1995, pp. 68, 76.

[17] Harpoothian, E. and Oswald, W. B., "Use of Ailerons to Reduce Wing Loads", U.S. Pat. 2,742,245, 1949, Douglas Aircraft Co., Santa Monica, California.

[18] Rogers, J., T., Manning, K., J., R., "Wing Load Alleviation System Using Tabbed Aileron", U.S. Patent No. 4'479'620, The Boeing Company, Seattle, Wash., October, 30, 1984.

[19] Lewis, G., E., "Maneuver Load Alleviation System", U.S. Patent No. 4'796'192, The Boeing Company, Seattle, Wash., January, 3, 1989.

[20] G. Romeo, G. Frulla, E. Cestino, "Design of a high-altitude long-endurance solar-powered unmanned air vehicle for multi-payload and operations"; Proc. IMechE Vol. 221 Part G: J. Aerospace Engineering.

[21] Hall, D. W. and Hall, S. A. Structural sizing of a solar powered aircraft. NASA CR-172313, 1984.

[22] Colozza, A., Dolce, J. L., High-Altitude, Long-Endurance Airships for Coastal Surveillance, NASA/TM—2005-213427.

[23] Nickol, Craig L.; Guynn, Mark D.; Kohout, Lisa L.; Ozoroski, Thomas A, "High Altitude Long Endurance Air Vehicle Analysis of Alternatives and Technology Requirements Development", NASA Langley Research Center, Hampton, VA, USA, 45th AIAA Aerospace Sciences Meeting and Exhibit, 8-11 Jan. 2007, Reno, NV, USA.

[24] G. Romeo, G. Frulla, E. Cestino, G. Corsino, "HELIPLAT: Design, Aerodyna-mic, Structural Analysis of Long-Endurance Solar-Powered Stratospheric Platform", Journal of Aircraft Vol. 41, No. 6, November–December 2004.

[25] Patil, M. J., Hodges, D. H. and Cesnik, C. E. S., "Nonlinear Aeroelasticity and Flight Dynamics of High-Altitude Long- Endurance Aircraft," Journal of Aircraft, Vol. 38, No. 1, 2001, pp. 88-94.

[26] Patil, M. J. and Hodges, D. H., "Flight Dynamics of Highly Flexible Flying Wings," Journal of Aircraft, Vol. 43, No. 6, 2006, pp. 1790-1799.

[27] Raghavan, B. and Patil, M. J., "Flight Dynamics of High-Aspect-Ratio Flying Wings: Effect of Large Trim Deformation," Journal of Aircraft, Vol. 46, No. 5, 2009, pp. 1808-1812.

[28] Patil, M. J., "Nonlinear Gust Response of Highly Flexible Aircraft," 48th AIAA / ASME / ASCE / AHS / ASC Structures, Structural Dynamics, and Materials Conference, Honolulu, HI, Apr. 23-26, 2007.

[29] Shearer, C. M. and Cesnik, C. E. S., "Nonlinear Flight Dynamics of Very Flexible Aircraft," Journal of Aircraft, Vol. 44, No. 5, 2007, pp. 1528-1545.

[30] Patil M. J., "Nonlinear Aeroelastic Analysis of Joined-Wing Aircraft", 44th AIAA/ASME/ASCE/AHS/ASC Structures, Structural Dynamics & Materials Conference, Norfolk, Virginia, Apr. 7-10, 2003.

[31] J. Wolkovitch, "The Joined-Wing: An Overview", The AIAA 23rd Aerospace Sciences Meeting, Reno, NV, Jan. 14-17, 1986.

[32] J. W. Gallman, S. C. Smith, "Optimization of Joined Wing Aircraft", *Journal of Aircraft*, Vol. 30, No. 6, November-December 1993, pp. 897, 905.

[33] L. Di Palma, N. Paletta and M. Pecora, "Aeroelastic Desing of a Joined Wing UAV", SAE 2009 AeroTech Congress & Exhibition, November 10-12, 2009, Seattle, Washington, USA.

[34] A. Frediani, E. Rizzo, C. Bottoni, J. Scanu, and G. Iezzi, "The PrandtlPlane Aircraft Configuration" in Aeronautics Days, (Wien), Jun. 2006.

[35] A. Frediani, "The Prandtl Wing." Von Karman Institute, lecture series on Innovative Configuration and Advanced Concepts for Future Civil Aircraft, Jun. 2005.

[36] D. Dal Canto, N. Divoux, A. Frediani , G.L. Ghiringhelli, M. Terraneo, "Preliminary Design Against Flutter Of A Prandtlplane Lifting System", XX Congresso Nazionale AIDAA – Milano, 2009.

[37] G. Bindolino, G. Ghiringhelli, S. Ricci, and M. Terraneo "Multilevel Structural Optimization for Preliminary Wing-Box Weight Estimation", Journal of Aircraft, Vol. 47, No. 2, March-April 2010, pp. 475, 489.

[38] L. Demasi, E. Livne, "Exploratory Studies of Joined Wing Aeroelasticity", AIAA 2005-2172, 46th AIAA / ASME / ASCE / AHS / ASC Structures, Structural Dynamics, and Materials Conference, Austin, Texas, Apr. 18-21, 2005.

[39] L. Demasi, E. Livne, "Dynamic Aeroelasticity Coupling Full Order Geometrically Nonlinear Structures and Full Order Linear Unsteady Aerodynamics – The Joined Wing Case", AIAA 2008-1818, 49th AIAA / ASME / ASCE / AHS / ASC Structures, Structural Dynamics, and Materials Conference, Schaumburg, IL, Apr. 7-10, 2008.

[40] B. Imperatore, L. Vecchione, "A Flexible Wing Unmanned Aerial Research System", SAE 2009 AeroTech Congress & Exhibition, November 10-12, 2009, Seattle, Washington, USA.

[41] E. Albano, W. P. Rodden, "A Doublet-Lattice Method for Calculating Lift Distributions on Oscillating Surfaces in Subsonic Flows", AIAA *Journal*, Vol. 7, No. 2, February 1969, pp. 279, 285.

[42] R. L. Harden, R. N. Desmarais, "Interpolation Using Surface Splines", Journal of Aircraft, Volume 9, No. 2, February 1972.

[43] The MacNeal - Schwendler Corporation, "MSC/NASTRAN Version 70.5 – Quick Reference Guide", February 1998.

[44] Paletta, N., Belardo, M., Pecora, M., "Symmetric Quasi-Steady Maneuver Load Alleviation – A Method To Predict The Control Surface Efficiency When Used As Load Alleviator", 4th IC-SCCE, International Conference from Scientific Computing to Computational Engineering, Athens, Greece, July 2010.

[45] European Aviation Safety Agency (2009), "Certification Specifications for Large Aeroplanes CS-25", Amendment 7, October, 21st.

[46] Roskam, J., "Airplane Flight Dynamics and Automatic Flight Controls" Part I, book edited by DAR Corporation, Lawrence, Kansas, USA, 2009.

[47] Roskam, J., "Airplane Flight Dynamics and Automatic Flight Controls" Part II, book edited by DAR Corporation, Lawrence, Kansas, USA, 2009.

[48] W. S. Aiken, Jr., "Flight determination of wing and tail loads on a fighter-type airplane by means of strain-gage measurements", NACA TN n° 1729, October 1948.

[49] E. Rauscher, "Structural flight load measurement – Demonstration of structural integrity", Structural and Materials Panel – Specialist Meeting I, Siena, 1-6 April, 1984.

[50] L. Di Palma, M. Belardo, N. Paletta and M. Pecora, "USV1 In-Flight Loads Evaluation by means of strain gauges instrumentation – Part I", Proceedings of 4th CEAS, September 2007, Berlin.

[51] T.H. Skopinski, W. S. Aiken Jr and W. B Huston, "Calibration of strain-gage installation in aircraft structures for the measurements of flight loads", NASA Technical Report 1178, 1953.

[52] J. M. Jenkins and V. M. De Angelis "A summary of numerous strain-gage load calibrations on aircraft wings and tails in a technology format" NASA Technical Memorandum 4804 July 1997.

[53] W. A. Lokos, and R. Stauf "Strain gage loads calibration parametric study", NASA/TM-2004-212853, NASA Dryden Flight Research Center Edwards, California, August 2004.

[54] W. A. Lokos, C. D. Olney, T. Chen, N. D. Crawford, R. Stauf and E. Y. Reichenbach, "Strain gage loads calibration testing of the active aeroelastic wing F/A-18 Aircraft", NASA/TM-2002-210726, NASA Dryden Flight Research Center Edwards, California, May 2002.

[55] P. Bolzern, R. Scattolini, N. Schiavoni, "Fondamenti di Controlli Automatici", McGraw-Hill libri Italia srl, 1998.

[56] Dingyu Xue, Yang Quan Chen, and Derek P. Atherton, "Linear Feedback Control", book, Copyright ©2007 by the Society for Industrial and Applied Mathematics.

[57] Skogestad, S., "Probably the best simple PID Tuning rules in the world", AIChE Annual Meeting, Reno, Nevada, USA, 2001.

[58] Skogestad, S., "Simple analytical rules for model reduction and PID Controller Tuning", Journal of Process Control, No. 13, 2003, pp. 291-309.

[59] Skogestad, S., "Simple analytic rules for model reduction and PID Controller Tuning", Model, Identification and Control, Journal, 2004, No. 25, pp. 85-120.

[60] ESDU 79024, "Estimation of the Endurance of Civil Aircraft Wing Structures", ESDU International, ISBN 0 85679 272 1, October 1979.

[61] ESDU 69023, "Average Gust Frequencies Subsonic Transport Aircraft", ESDU International, ISBN 0 85679 259 4, Amendment A, B, C and D, March 1989.

[62] ESDU 75008, "Frequencies of Vertical and Lateral Load Factors resulting from Ground Manoeuvres of Aircraft", ESDU International, ISBN 0 85679 109-1, Amendment A and B, December 1994.

Web Sources

[63] http://en.wikipedia.org/wiki/State_space_(controls);

[64] http://en.wikipedia.org/wiki/Controllability;

[65] http://en.wikipedia.org/wiki/Observability.

[66] http://www.mathworks.com/help/toolbox/control/ref/sisotool.html.